



# ERNEST ORLANDO LAWRENCE BERKELEY NATIONAL LABORATORY

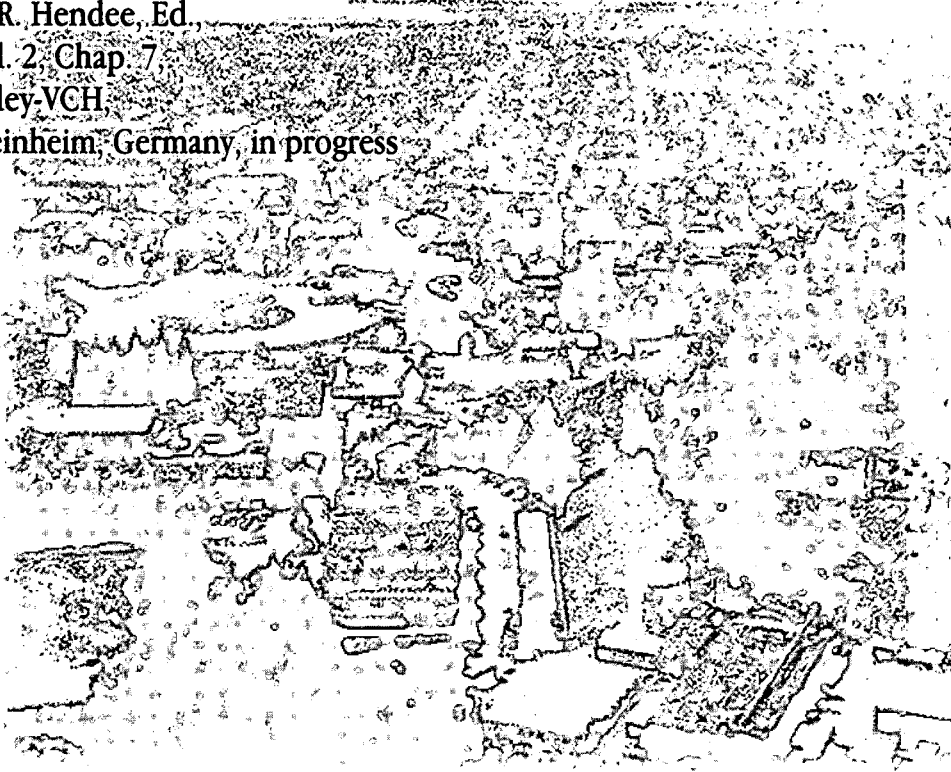
## Radiation Treatment Using Hadrons (Negative Pions, Neutrons, Proton, and Heavier Ions)

William T. Chu

Accelerator and Fusion  
Research Division

July 1997

To be published as  
a chapter in  
*Biomedical Uses of Radiation*,  
W.R. Hendee, Ed.,  
Vol. 2, Chap. 7,  
Wiley-VCH,  
Weinheim, Germany, in progress



Lawrence Berkeley National Laboratory  
Bldg. 50 Library - Ref.

REFERENCE COPY  
Does Not  
Circulate

## **DISCLAIMER**

This document was prepared as an account of work sponsored by the United States Government. While this document is believed to contain correct information, neither the United States Government nor any agency thereof, nor the Regents of the University of California, nor any of their employees, makes any warranty, express or implied, or assumes any legal responsibility for the accuracy, completeness, or usefulness of any information, apparatus, product, or process disclosed, or represents that its use would not infringe privately owned rights. Reference herein to any specific commercial product, process, or service by its trade name, trademark, manufacturer, or otherwise, does not necessarily constitute or imply its endorsement, recommendation, or favoring by the United States Government or any agency thereof, or the Regents of the University of California. The views and opinions of authors expressed herein do not necessarily state or reflect those of the United States Government or any agency thereof or the Regents of the University of California.

Volume 2, Chapter 7

Radiation Treatment Using Hadrons  
(Negative Pions, Neutrons, Proton, and Heavier Ions)\*

William T. Chu

Lawrence Berkeley National Laboratory  
University of California  
Berkeley, CA 94720

July 1997

\* This work was supported by the Director, Office of Energy Research, Energy Research Laboratory Technology Transfer Program, of the U.S. Department of Energy under Contract no. DE-AC03-76F00098

Outline for  
**Hadron Therapy**

<b>A. HADRON RADIATION</b>	<b>1</b>
<b>B. PHYSICAL AND BIOLOGICAL CHARACTERISTICS OF HEAVY CHARGED-PARTICLE BEAMS</b>	<b>4</b>
Bragg Peak and Distal Dose Falloff	4
Multiple Scattering and Lateral Dose Falloff (Penumbra)	6
Radiation Biology of Proton Beams	7
<b>C. PROTON RADIATION THERAPY</b>	<b>7</b>
Comparison of Photon and Proton Therapy Plans	9
On-Going Proton Radiation Therapy Trials	11
Planned Proton Beam Therapy at Existing Accelerators	11
<i>Clinical Requirements of Hospital-Based Proton Accelerator Facilities</i>	12
<i>Particle Beam Ranges, and Range Adjustment</i>	15
<i>Target Thickness and Range Modulation</i>	16
<i>Lateral Broadening of Beams, Penumbra, and Dose Uniformity</i>	18
<i>Beam Size, Divergence, and Emittance</i>	20
<i>Beam Optics</i>	22
<i>Control Systems for Medical Beams</i>	23
<b>Hospital-Based Proton Accelerator Facilities</b>	<b>23</b>
<i>First Medical Proton Facility in Loma Linda, California</i>	23
<i>Medical Proton Facility in Kashiwa, Japan</i>	24
<i>Northeast Proton Therapy Center (NPTC) in Boston</i>	25
<i>Other Planned Hospital-Based Proton Facilities</i>	26
<b>D. LIGHT AND HEAVY IONS FOR RADIATION THERAPY</b>	<b>27</b>

<b>Physics Considerations for Light and Heavy Ions</b>	27
<b>Biological Considerations for Light and Heavy Ions</b>	29
<b>Light and Heavy Ion Accelerator Facilities and Clinical Trials</b>	31
<i>Bevalac at LBNL in Berkeley, California</i>	31
<i>HIMAC at NIRS in Chiba, Japan</i>	31
<i>Clinical Beam at GSI in Darmstadt, Germany</i>	32
<i>Planned Light and Heavy Ion Facilities for Radiation Therapy</i>	32
<b>Clinical Results of Heavy Charged-Particle Beam Therapy</b>	33
<b>Future Development for Heavy Charged Particle Radiation Therapy</b>	35
<i>Three-Dimensional Conformal Therapy Delivery</i>	35
<b>E. FAST NEUTRON THERAPY</b>	38
<b>Rationale for Fast Neutron Therapy</b>	40
<i>Interactions of Fast Neutrons with Tissue</i>	40
<i>Biological Rationale</i>	42
<b>Clinical Trials Using Fast Neutrons</b>	43
<b>Clinical Results of Fast Neutron Trials</b>	47
<b>Future Development of Fast Neutron Therapy</b>	48
<b>F. NEUTRON CAPTURE THERAPY (NCT)</b>	49
<b>Early BNCT Clinical Trials</b>	50
<b>Renewed Interest in BNCT</b>	52
<b>Rationale for BNCT</b>	53
<b>Clinical Requirements</b>	54
<i>Basic Requirements</i>	55
<i>Background Dose Calculation</i>	57
<i>BNCT Dose Calculation</i>	59
<b>Progress in Borated Compounds</b>	60

<i>Boron Compounds Used in BNCT Clinical Trials</i>	60
<i>Development of New Boron Compounds for BNCT</i>	62
<i>Possible NCT Isotopes Other Than <sup>10</sup>B</i>	63
<b>Nuclear Reactor Sources of Epithermal Neutrons for BNCT</b>	64
<i>Reactor-Based Epithermal Neutron Sources</i>	64
<i>Reactors for BNCT</i>	66
<b>Alternative neutron sources for BNCT</b>	67
<i>Accelerator-Based BNCT</i>	68
<i>Comparison Between Epithermal Neutron Beams from Reactors and Accelerators</i>	69
<i>Accelerator Options for BNCT</i>	71
<i>Other Types of Accelerators for BNCT</i>	73
<b>Other Applications of BNCT</b>	73
<i>BNCT Enhanced Fast-Neutron Therapy</i>	73
<i>Boron Neutron Capture Synovectomy</i>	74
<b>Future Development of BNCT</b>	74
<b>G. OTHER HADRON BEAMS FOR RADIATION THERAPY</b>	75
<b>Negative Pions for Radiation Treatment</b>	75
<i>Physics Characteristics of <math>\pi^-</math></i>	76
<i>Negative Pion Biology</i>	78
<i>Negative Pion Clinical Trials</i>	79
<b>Antiproton Beams for Cancer Therapy</b>	80
<b>H. FUTURE OF HADRON THERAPY</b>	80
<b>ACKNOWLEDGMENTS</b>	82
<b>REFERENCES</b>	83

## Volume 2, Chapter 7

### **Hadron Therapy**

William T. Chu

Lawrence Berkeley National Laboratory

University of California, Berkeley

#### **A. HADRON RADIATION**

There occurs annually about 1.25 million new cancer patients in the U.S. alone, and about 50% get radiation therapy in the course of their treatments. Radiation oncologists now mainly rely on electron linacs (~10-25 MeV) as teletherapy radiation sources, which provide high-energy photon and electron beams for cancer treatment. These types of radiation are called *conventional radiation*. The energy deposited by photons is characterized by an exponentially decreasing dose with depth. Electrons, being light and therefore easily scattered, deposit their energy over a broad peak with gradually sloping distal edge. In treating a deep-seated tumor, the entrance dose is always larger than the target dose, which is followed by a very gradually decreasing exit dose. These shortcomings could be overcome to a certain extent by using newly developed treatment schemes, such as three-dimensional conformal therapy or tomotherapy, in which multiple ports of variable apertures and intensities are used to concentrate the dose inside an irregularly-shaped target volume, while spreading out, and thereby diluting, the entrance and exit doses over larger surrounding tissues.

In order to control tumors that do not respond well to these conventional radiation treatments, researchers have studied other types of radiations that provide superior dose localization characteristics and/or a better differential effect between tumor and normal cells. These radiations include beams of negative pions, neutrons, protons and heavier ions (e.g., helium, carbon, neon, silicon and argon nuclei). Collectively they are called *hadron* radiation, as these particles belong to the family of strongly interacting particles.

Hadrons are much more massive than either photons or electrons, and therefore the medical community sometimes calls them *heavy particles*. Proton and heavier-ion radiations are also called *heavy charged-particle* radiations, to distinguish them from electrically neutral neutrons. When they first became available for clinical use, nuclei heavier than protons were called *heavy ions*. More recently, nuclei with an atomic number equal to or smaller than that of neon nuclei ( $Z=10$ ) are called *light ions*, leaving the name *heavy ions* to heavier ones such as silicon and argon nuclei. Such a nomenclature convention is reflected in the naming of medical accelerator facilities: the Heavy Ion Medical Accelerator in Chiba (HIMAC) is the name for the medical synchrotron facility in Chiba, Japan which is capable of accelerating ions as heavy as argon, whereas, the once-planned Light Ion Biomedical Research Accelerator (LIBRA) and European Light Ion Medical Accelerator (EULIMA) were to accelerate ions only as heavy as carbon nuclei. Because of their greater mass, accelerating heavy charged particles is more difficult, and providing heavy charged-particle radiations in the clinic is generally more costly compared with conventional radiations.

Active clinical research is pursued worldwide using proton radiation to take advantage of its dose-localizing effect due to their well-defined range and the

Bragg peak (Fig. 7.1). Clinical trials using heavier ions are performed because these high-LET radiations exhibit potential biological advantages over conventional radiations as well as proton beams. Linear energy transfer (LET) is a measure of energy loss per unit path length of absorbing material (tissue), often expressed as an energy loss per unit thickness of water-equivalent material ( $\text{keV}/\mu\text{m}$ ). Clinical efficacy of negative pion beams was studied because of their Bragg peak and its enhancement by the 'nuclear star' formations resulting from the capture of the pions in tissue nuclei.

Fig. 7.1

Dose distributions of fast neutron beams are similar to those of high-energy photon beams, and neutrons do not have a dose localizing advantage. Clinical trials are underway using beams of fast neutrons with energies of tens of MeV exploiting their high-LET properties. Certain slowly-growing well-differentiated tumor cells are very sensitive to high-LET radiations (e.g., neutrons and heavy ions), thus fast neutrons could eradicate tumor cells while saving the neighboring healthy tissue. In boron neutron capture therapy (BNCT), the role of dose localization is relegated to tumor-concentrating boron ( $^{10}\text{B}$ ) compounds. When the whole area around the tumor is bathed with thermal neutrons, those cells with  $^{10}\text{B}$  atoms are preferentially eradicated by the fission fragments following boron neutron capture.

The use of antiproton beams for treatment of human cancer has been proposed; however, actual implementation of their clinical use has not yet materialized mainly due to the difficulty of producing clinically meaningful numbers of antiprotons.

There are many excellent monographs and review articles on the medical use of heavy charged particles<sup>1-8</sup>, fast neutron therapy<sup>9</sup>, and boron neutron capture therapy<sup>10-11</sup>.

## B. PHYSICAL AND BIOLOGICAL CHARACTERISTICS OF HEAVY CHARGED-PARTICLE BEAMS

### Bragg Peak and Distal Dose Falloff

The primary mechanism of energy loss by energetic heavy charged particles (protons and heavier ions) penetrating an absorbing medium is through Coulomb interactions with atomic electrons in the medium. In other words, heavy charged particles slow down primarily by losing their kinetic energy as they ionize atoms in the medium. The energy loss per unit path length (or specific energy loss by heavy charged particles or stopping power of the medium), is inversely proportional to the square of the velocity of the projectile particles. The energy loss of a heavy charged particle per unit length (usually expressed in keV/ $\mu\text{m}$  or, in tissue, keV/(g/cm<sup>2</sup>)) may be expressed by the Bohr-Bethe formula:

$$\frac{dE}{dx} = - \frac{4\pi e^4 z^2 n_e}{m_e v^2} \left[ \ln \left( \frac{2m_e v^2}{I} \right) \right] = f(E), \quad (7-1)$$

where  $n_e$  is the electron density of the absorbing medium,  $z$  is the effective charge of the projectile particle,  $I$  is the mean ionization potential, and  $v$  is the velocity of the projectile. In Eq. (7-1), relativistic terms and low energy correction terms are not included. The reciprocal dependency on  $v^2$  results in a rise to a sharp maximum in ionization near the end of the range where the projectile velocity approaches  $v=0$ . This rise is known as the Bragg peak<sup>12</sup>.

As shown in Fig. 7.2(a), when a beam of monoenergetic protons enters the body, the depth-dose distribution is characterized by a relatively low dose in the entrance region (plateau) near the skin and a sharply elevated dose in a narrow region at the end of the range (Bragg peak). It can easily be seen that the range can be modulated to place the Bragg-peak dose in the target volume as shown in Fig. 7.1. It is possible to irradiate a very small localized region within the body with a pristine beam with a narrow Bragg peak, while keeping the entrance dose lower than that in the peak region. The Bragg peak is often spread out to cover an extended target by modulating the energy of the incident particles. The combined ionization produces what is often called the 'spread-out Bragg peak' (SOBP), as shown in Fig. 7.2(b). The radiation dose abruptly decreases beyond the Bragg peak, sparing from unwanted radiation those critical organs and normal tissues that are located downstream from the target volume.

Traversing a uniform medium, monoenergetic heavy charged particles lose energy at the same rate, and all of them will stop at the same depth, called the *range* of the particle. The range  $R$  is obtained by integrating the inverse of  $f(E)$  in Eq. (7-1):

$$R = \int_E^0 \frac{dE'}{f(E')}, \quad (7-2)$$

In reality, because the ionization process is stochastic, there is a small dispersion in the path length distribution. For a particle of initial energy  $E$  and mean range  $R$ , proceeding in the direction of  $z$ , the range distribution is Gaussian<sup>13</sup>, and may be written as:

$$S(z) = \frac{1}{\sqrt{2\pi}\sigma_z} \exp\left(-\frac{(z-R)^2}{2\sigma_z^2}\right), \quad (7-3)$$

(6)

where  $\sigma_z$  is the variance in the path length distribution. The value of  $\sigma_z$  in water is given by:

$$\sigma_z(\text{water}) = 0.0120 \frac{R^{0.961}}{\sqrt{A}}. \quad (7-4)$$

The value of  $\sigma_z(\text{cm})$  is almost proportional to range,  $R(\text{cm})$ , and is inversely proportional to the square root of the particle mass number  $A$ . This formula is valid in the range of  $2 \leq R \leq 40$  cm. For example, for a range of 20 cm in water,  $\sigma_z = 0.2$  cm for protons, 0.1 cm for helium, 0.06 cm for carbon, and 0.046 cm for neon particles. This *straggling* endows a range dispersion of several mm in the proton range, and a narrower spread by a factor of about 4.5 in the neon-ion range (Fig. 7.3(a)).

Fig. 7.3

### Multiple Scattering and Lateral Dose Falloff (Penumbra)

While the scattering (Coulomb scattering) of heavy charged particles from the nuclei of atoms in the medium has little effect on energy loss, this multiple scattering results in lateral beam broadening. The magnitude of multiple scattering is often expressed in a projected angular distribution in a  $z$ - $y$  plane defined by the direction of the initial projectile direction  $z$  and a perpendicular axis  $y$ . At the range  $R$ , the projected deflection  $y$  of the projectile is given by:

$$P(y) = \frac{1}{\sqrt{2\pi}\sigma_y} \exp\left(-\frac{y^2}{2\sigma_y^2}\right), \quad (7-5)$$

and the variance  $\sigma_y$  in water is given by:

$$\sigma_y(\text{water}) = \frac{0.0294 R^{0.896}}{z^{0.207} A^{0.396}}, \quad (7-6)$$

where  $z$  is the projectile charge, and  $\sigma_y$  and  $R$  are expressed in units of cm.

Litton, Lyman and Tobias have presented the results of multiple scattering of

heavy charged particles pertinent to therapy applications<sup>14</sup>. As in the case of range dispersion, lateral dispersions from multiple scattering of heavier ions are less than for lighter species (Fig. 7.3b). Fig. 7.4 illustrates the relative increase in the penumbra (lateral dose falloff distance from the 90% to 10% level) due to multiple scattering in water and copper for proton, helium-ion, and neon-ion beams. The variance ( $\sigma$ ) of the lateral dose falloff is expressed in terms of the variance ( $\sigma_0$ ) at the entrance of the absorber, and the penetration depth in water-equivalent thickness. In practical applications, the width of the lateral dose falloff may be reduced by collimating the beam immediately before it enters the patient.

Fig. 7.4

### Radiation Biology of Proton Beams

Penetrating protons transfer their kinetic energy to the medium by kicking energetic secondary electrons ( $\delta$ -rays) out of the atoms of the medium, and by exciting atoms and molecules in the medium. The ionization density of a proton track is similar to those of high-energy photons, except at the very end of the proton range where the ionization becomes denser. Therefore it is not surprising that the relative biological effectiveness (RBE) of protons is similar to that of photons, except at the end of the range where the value is somewhat elevated (RBE $\approx$ 1.1). RBE is defined as the ratio of the dose needed by a particular radiation to produce a given biological endpoint to the dose needed by a reference radiation, (e.g.,  $^{60}\text{Co}$   $\gamma$  rays), to achieve the same endpoint. The same radiation may have a range of RBE values depending on the endpoints.

### C. PROTON RADIATION THERAPY

The superior dose localization capabilities of proton beams suggest the possibility of depositing a higher dose in the target volume while reducing unwanted radiation in surrounding critical tissues. This possibility leads to a clinical expectation of increased local control with a decrease in normal-tissue complications. In 1946, Robert R. Wilson published his seminal paper on the rationale for using accelerated proton beams, and heavier ion beams such as carbon ions, for radiotherapy of human cancer and other diseases<sup>15</sup>. A year later, when the 184-Inch Synchrocyclotron was completed by Ernest Orlando Lawrence and his associates at the Radiation Laboratory (now the Lawrence Berkeley National Laboratory (LBNL)) of the University of California, Berkeley), Cornelius A. Tobias and John H. Lawrence performed the first biological investigations with high-energy nuclei<sup>16</sup>. In 1954, Tobias and Lawrence performed pioneering work in the first therapeutic exposure of humans to proton beams<sup>17</sup>. In the 1970s, clinical trials with accelerated proton beams in the U. S.<sup>18</sup>, Sweden<sup>19</sup>, and Russia<sup>20</sup> to test their dose-localization advantages in treating human diseases began.

During the past half century, many clinical trials have been performed using proton and heavier-ion beams at accelerators originally developed for physics uses. There are at least sixteen physics laboratories worldwide where clinical trials using accelerated protons are now performed, and the number is growing each year. In recent years, there has been heightened interest in the medical community throughout the world to build medical accelerators for the dedicated purpose of treating human cancer patients in several clinical centers.

Various accelerator types, including synchrotrons, cyclotrons, and linacs, have been considered for hospital-based proton facilities dedicated to therapy<sup>21</sup>. The cost of the accelerator is only ~15–20% of the total construction cost. The

remaining cost is distributed over the beam transport system, the clinical beam delivery systems with dosimetry and control systems (patient treatment nozzles), rotating gantries, patient positioners, and other ancillary facilities.

### **Comparison of Photon and Proton Therapy Plans**

Consider a mono-energetic heavy charged particle (proton or heavier ion) beam, which has a sharp penumbrae and a definite range with a sharp Bragg peak followed by a well-defined distal dose falloff. By manipulating the energy (or range) of the beam, a tumoricidal dose can be placed inside an irregularly shaped target volume while sparing the surrounding healthy tissues and critical organs.

If a higher dose could be deposited inside the target than that possible with conventional radiation while keeping the doses in surrounding tissues the same, an enhanced tumor control may result. If the doses were reduced in surrounding tissues, reduced complications may result. Using proton beams, 10% or more higher dose inside a target can be placed without increasing the dose in surrounding tissues. Fig. 7.5 shows a simplified description of the situation.

Fig. 7.5

In conventional radiation therapy, as well as in heavy charged-particle therapy, dose distributions delivered to the patient represent a difficult compromise between delivering sufficient dose to the tumor to sterilize it, and avoiding overdosing adjacent tissues which could result in debilitating side effects of the treatment. For idealized treatments using conventional radiations, Fig. 7.5(a) represents the tumor control probability (TCP), and Fig. 7.5(b) the normal tissue complication probability (NTCP). For a given dose, the difference between (a) and (b) represents the probability of tumor control without complication. Typically, the displacement of (b) from (a) is only ~5% of the dose. The sharp penumbrae and

the sharp distal dose falloffs of protons help reducing the doses in surrounding critical organs, and move the NTCP curve from (b) to (c). Therefore, using a proton beam, one can achieve the same TCP with a smaller NTCP, or a larger TCP for a given NTCP than for conventional radiations. The expectation is that with protons one can achieve more tumor controls without complications compared to photon treatment. Here, the sharpnesses in penumbræ and distal dose falloffs are measured in millimeters, and a small improvement makes a big difference in achieving a greater probability of tumor control without complications.

The conclusion is that a therapy plan using a few (2 to 4) proton ports can produce a therapeutic effectiveness which is equal to, or better than, that of a three-dimensional conformal therapy plan employing a larger number of photon ports. This is an important point because radiotherapy delivery is labor intensive, especially in therapy planning and treatment beam delivery.

Often proton therapy turns out to be cost-effective when compared with three-dimensional conformal photon therapy. As an illustration, proton and photon dose distributions are compared for treating a prostate carcinoma patient. The illustrations are for dose distributions with 18 MV x-rays (Fig. 7.6(a)) and 230 MeV protons (Fig. 7.6(b)) obtained for six field conformal therapy planning on the central axial CT slice. The figures indicate that with the proton plan the isodose lines conform more closely to the tumor volume compared with the photon plan. With 18 MV x rays the 95% isodose line covers the tumor volume, whereas for protons the 100% isodose line covers the tumor volume. Some portions of the rectum are receiving a full dose. This is to be expected because the prostate gland is adjacent to the anterior wall of the rectum and the posterior wall of the bladder. With proton beams, however, a smaller portion of these structures gets a full

dose. In both treatment plans there is a gradient of dose across the hip. This is due to the sharp falloff of the dose.

Fig. 7.6

Fig. 7.7 illustrates that for six-field plans the fraction of rectum volume receiving at least 55% of prescribed dose is reduced from 62% (18 MV x-rays) to 19% (using protons). These comparative treatment plans indicate an advantage for proton treatment of carcinoma of the prostate. The results indicate that proton treatments may ultimately play an important role in the treatment of prostate cancer<sup>22</sup>.

Fig. 7.7

### **On-Going Proton Radiation Therapy Trials**

The on-going proton clinical trials conducted at accelerators originally built for physics research are summarized in Table 7.1. When treating deeply-seated tumors in the human body, it is necessary to accelerate protons to ~220–250 MeV. Many accelerators listed in Table 7.1 are of lower energies (<100 MeV), and are mainly used to treat lesions reachable by short range (<5 cm) beams. Among the patients listed, about a half had small benign lesions (pituitary tumors, arteriovenous malformation (AVM), and others) within the cranium, and a third were treated for ocular choroidal melanomas. The helium-ion trial results from LBNL (1975–1992) are included here as the biological and clinical effects of helium ions are similar to those for protons.

Table 7.1

### **Planned Proton Beam Therapy at Existing Accelerators**

Many more proton medical facilities are proposed at existing or future accelerators built for physics research. The Kernfysisch Versneller Instituut

(KVI) in Groningen, The Netherlands, which installed a superconducting cyclotron to accelerate 200 MeV protons, plans to build a radiotherapy facility with one isocentric gantry room and another fixed beam treatment room<sup>23</sup>. The AUSTRON project in Austria plans to build a proton/light ion accelerator, which will produce neutrons, protons and light ions (400 MeV per nucleon) that can be used for radiation therapy<sup>24</sup>. The VICKSI cyclotron at the Hahn-Meitner Inst., Berlin, Germany plans to use 72 MeV proton beams for eye treatment. A 75-MeV cyclotron will be built by the Joint Institute of Nuclear Research (JINR) in Dubna, Russia and commissioned the Slovak Institute of Metrology, Bratislava in 2000 for medical and physics uses. Other efforts are at the Laboratori Nazionali di Legnaro (LNL), Padova, Italy, the ITEP in Moscow, Russia, the TRITRON in Munich, Germany, the Laboratori Nazionali di Legnaro in Padova, Italy, the North Carolina Storage Ring Project (NC STAR) in Raleigh, NC, Krakow, Poland, and the Yerevan Physics Institute in Erevan, Armenia.

### **Clinical Requirements of Hospital-Based Proton Accelerator Facilities**

In the late 1980s, after four decades of proton therapy clinical trials at more than a dozen accelerator facilities which were originally built for physics research, the medical community throughout the world became increasingly interested in constructing *hospital-based* proton medical accelerators. In 1991 the Loma Linda University Medical Center commissioned the first-in-the-world hospital-based proton medical accelerator facility (with a 250-MeV proton synchrotron). The second hospital-based proton facility (with a 235-MeV proton cyclotron) was commissioned at the Higashi Hospital, Kashiwa (near Tokyo), Japan in 1997. The third dedicated proton medical facility (with a 231-MeV proton cyclotron) is now under construction at the Northeast Proton Therapy Center (NPTC) of the

Massachusetts General Hospital (MGH) in Boston, MA and scheduled to be commissioned in 1998. The fourth facility will be at the Proton Medical Research Center (PMRC) of the Tsukuba University Medical Center in Japan, which is building a 270-MeV synchrotron to be completed in 1998.

Clinical requirements that the medical community places on the performance of hospital-based proton facilities are discussed below. LBNL and the NPTC collaborated to produce a list of clinical requirements<sup>26</sup>; later NPTC used it as the basis for constructing a proton medical facility<sup>27</sup>. The list includes: depth and thickness of targets to be treated, maximum attainable port sizes, dose uniformity across ports, degree of precision in delivered dose, maximum dose rate, minimum dose rate that can be precisely controlled, allowable degradation in distal dose falloffs and lateral penumbrae, effective source-to-axis distance (SAD), treatment beam directions ( $4\pi$  steradians), and upgradability (to beam scanning) of the facility. The ramifications of these clinical requirements on technical specifications are discussed elsewhere<sup>25</sup>, and presented here only briefly.

Diverse clinical requirements with many competing specifications drive the design of a medical proton accelerator and its treatment beams. For example, a clinical requirement asks for a large treatment field, up to 40 cm x 40 cm. It may be satisfied by using a scattering method, which necessarily degrades beam divergence, and requires higher proton energy to compensate for the energy loss in the scatterers. Another clinical requirement is a sharp lateral dose falloff (penumbra) required at the boundary of the treatment field. One may try to achieve it by increasing the apparent source-to-axis distance (SAD), but this may be impractical for a treatment beam line mounted on a rotating gantry with a limited length of drift space. Beam spreading is usually performed downstream of the last bending magnet on the gantry because doing otherwise would entail

larger aperture magnets that increase the weight and the cost of the gantry. A medical accelerator system must be designed by weighing the many pros and cons of competing specifications, and finding the optimal solution that meets all of the clinical requirements.

An accelerator is of course designed to satisfy its user requirements. For high-energy physics accelerators the most important machine parameters may be the attainable particle energy (to explore new regions of interactions) and beam intensity (for higher luminosity). For a medical accelerator the capital cost, reliability, and maintainability rate highly as machine performance requirements. Cost, reliability, and maintainability are important for physics machines also, but the level of requirements for them may not be as stringent as those for medical machines. Reliability here stands for availability of specified clinical beams within an acceptable time window. A reliability of 85% may be considered excellent for a physics facility, but such a reliability is not even acceptable for a medical facility, which would require a reliability better than 99%. Typically a patient receives ~30 exposure fractions for a course of treatments. If 1000 patients are treated per year at a given accelerator facility, it must provide ~30,000 fractions per year. Clinicians do not want to see more than one unscheduled interruption of treatment per month, because such an interruption forces changes in the prescription of subsequent treatment doses and schedules, or worse, such interruption may render the patient data ineligible for inclusion in a clinical trial. The fact that fewer than 12 interruptions are allowed per year for 30,000 fractions represents a better than 99.96% reliability of the treatment facility. The inflexibility and immediacy of meeting the requirements for the clinical beams are indeed stringent. If an accelerator or a detector malfunctions in a physics experiment, the measurement can be repeated, or the bad data may be

later discarded during the analysis. In clinical situations, however, once a part of a treatment dose is deposited in a patient, it cannot be discarded for any reason, and the treatment must be completed with an verifiable dosimetry provided. Ensuring the safety of the patient precedes all other clinical requirements.

In the sections, the clinical requirements as specified by the LBNL and the NPTC collaboration<sup>26</sup>, and their ramifications on technical specifications are discussed.

### ***Particle Beam Ranges, and Range Adjustment***

One of the clinical requirements is that the beam range in the patient should be available for values between  $3.5 \text{ g/cm}^2 - 32 \text{ g/cm}^2$  for fields up to  $22 \text{ cm} \times 22 \text{ cm}$ . The desired dose uniformity ( $\pm 2.5\%$ ) across the maximum port size determines the thickness of the scatterers. The field size is specified indicating that if the beam is laterally broadened using scatterers, the energy loss in the scatterers must be included in estimating the energy of an extracted beam. The required energy of the extracted protons is 285 MeV if a scattering system is used, and 235 MeV if a magnetic spreading system is employed.

Another clinical requirement specifies that the beam range adjustment should be in steps of  $0.1 \text{ g/cm}^2$  for ranges  $\geq 5 \text{ cm}$ , and in steps of  $0.05 \text{ g/cm}^2$  for ranges  $< 5 \text{ g/cm}^2$  between and during treatments. To provide various ranges, either a beam with an appropriate energy must be extracted (*e.g.*, from synchrotrons) or an extracted fixed-energy beam must be degraded using absorbers (*e.g.*, from cyclotrons or linacs). For a synchrotron, the protons may be extracted at different energies, and transported to the patient. Here,  $0.1 \text{ g/cm}^2$  step size in the full range of  $30 \text{ g/cm}^2$  means controlling the energy to  $\sim 1$  part in 300, and a 10% accuracy in attaining the step size implies controlling to  $\sim 1$  part in 3000. this requirement approaches the control accuracy limits of a dynamic magnet ( $\sim 1$  part

in 5000). It also implies tracking of all transport magnets throughout the transport system including the gantry optics. For a cyclotron, the beam will be extracted at full energy, degraded to an appropriate energy, and momentum analyzed (to reduce the energy spread in the beam) before transported to the patient. The resulting energy spread due to straggling in the absorbers may be then reduced by magnetic analysis and collimators. The magnet tracking requirements for the beam transport system are the same as for synchrotrons because the degrader is placed near the cyclotron, far away from treatment rooms to reduce background radiation.

Finer energy adjustments, called for in clinical requirements, may be achieved more readily by placing a mechanical range shifter in the treatment nozzle close to the patient. A *binary filter* or a *set of two wedges* may be used as a range shifter. A binary filter adjusts the range of a beam by means of a set of metal or plastic plates of various thicknesses. In a double-wedge system, the two wedges may be placed in opposing directions and moved in such a way that the particles in a finite beam spot traverse an adjustable yet uniform-thickness absorbing material. Most of the instruments discussed are described in detail in a recent review article<sup>28</sup>, and their discussion in this paper is kept to minimum.

### ***Target Thickness and Range Modulation***

Energy spread plus range straggling of incident particles in the absorbing material, including the patient, located along the beam path up to the stopping region, contributes to the finite width of the Bragg peak. The width of a Bragg peak of a mono-energetic proton beam extracted from an accelerator and stopped in water (or tissue) originates from the energy straggling in the absorbing medium and from the energy spread,  $\Delta E/E$ , of the extracted beam. For example, a

truly mono-energetic 150-MeV proton beam will show a dispersion due to energy straggling of 1.6 mm of stopping region at the end of a 15-cm range in water. If a beam is extracted from a typical synchrotron, the energy spread in one extraction pulse is  $\Delta E/E \approx 10^{-4}$ , which represents a 0.015-mm spread in water, negligible compared to the dispersion due to straggling. The energy spread among several pulses (a treatment requires always many pulses) is  $\Delta E/E \approx 10^{-3}$ , which represents a 0.15-mm spread in water or 10% of the straggling width. In this case, the energy straggling in the absorbing medium (the patient) is the major contributor to broadening the width of the Bragg peak. The particle beams from cyclotrons have about an order of magnitude larger  $\Delta E/E$  than those for synchrotron pulses. Energy spread among several extracted pulses of  $\Delta E/E \approx 10^{-2}$  will contribute a comparable range spread as the range straggling inside the absorbing medium. The particle beams from a cyclotron are extracted at full energy, and subsequently degraded to obtain lower energies. Therefore, to satisfy the clinical requirement that the distal dose falloff be not to exceed the straggling in water by more than 1 mm, it is important to momentum-analyze an energy-degraded beam and select those beams in a desired energy spread to obtain a smaller  $\Delta E/E < 10^{-3}$ .

The resulting Bragg peak is narrower than the clinical target thickness, typically 0.5 cm–16 cm, and the beam range must be modulated in order to cover the extent of the target thickness with the Bragg-peak dose. The energy spread and range straggling also contribute to deterioration of the steepness of the distal dose falloff of the spread-out Bragg peak (SOBP). The width of the Bragg peak may be spread out by a *range-modulating propeller*. The propeller is a fan-shaped stepped absorber, which is made to rotate in the beam so that the appropriate thickness of the propeller 'blades' intercept the beam. The profiles of the blades are designed in such a way that, when the beam traverses the propeller rotating at a

predetermined rate, a constant *biological dose* is imparted across the entire SOBP width. Instead of a range-modulating propeller, a wheel with several concentric annular tracks, divided into various absorber thicknesses, may be used to make different widths and slopes of spread-out peaks (Fig. 7.8). The desired results are achieved by rotating the wheel and turning the beams on and off synchronously with the angular position of the wheel. For a cyclotron the beam gating with a 50  $\mu$ sec time constant can be provided by turning the ion source current on and off.

Fig. 7.8

### *Lateral Broadening of Beams, Penumbra, and Dose Uniformity*

The next clinical requirement to satisfy for medical beams is making large radiation fields, up to 40 cm x 40 cm, with a dose uniformity of better than  $\pm 2.5\%$  over the entire treatment field. In the simplest *passive* method, it is accomplished using scatterers. A narrow pencil beam scattered by a thin scatterer produces an approximately 2-dimensional Gaussian dose distribution at isocenter. Here a scatterer is called thin when the kinetic energy of the particle does not change significantly by traversing it. The dose distribution as a function of the radial distance,  $r$ , from the central axis is

$$D(r) = \frac{1}{\pi \bar{a}^2} e^{-\left(\frac{r^2}{2\bar{a}^2}\right)}, \quad (7-7)$$

where  $\bar{a}$  is the rms radius of multiple scattering, and is related to the scattering angle and the drift-space from the scatterer to the isocenter. The resulting Gaussian-like beam traverses a *contoured scatterer*<sup>29</sup>, which is shown in Fig. 7.9 as an example of lateral beam-spreading devices. For this contoured scatterer, the energy absorbing power is constant at all radial distances. However, the beam particles traversing it near the central axis encounter more high-Z material,

whereas those at larger radial distances encounter more low-Z material. Thus, the central rays are scattered out more than the peripheral rays, flattening the Gaussian-like dose profile, and making it into a larger uniform-dose field. For a scattering method, the beam-tuning requirements are stringent as the beam must enter the device at its dead-center and parallel to its axis to produce the desired uniform dose distribution.

Fig. 7.9

A wobbler system is a simple magnetic beam spreading system that flattens the dose profile without resorting to scattering materials. Its use relaxes the stringent beam-tuning requirements encountered with the scattering methods. A wobbler system consists of two dipole magnets placed in tandem with their magnetic field directions orthogonal to one another and to the beam direction. The magnets are energized in saw-tooth fashion or sinusoidally with fixed frequencies, with a certain phase shift between the currents in two magnets. A beam entering a wobbler system along its axis emerges from it with the beam direction wobbling around the original beam direction to 'paint' a large area of uniform dose. At LBNL a wobbler system<sup>30</sup> was used to treat more than 7000 ports from 1986 to 1992. A wobbler system has also been used in patient treatments at the National Institute for Radiological Sciences (NIRS) in Chiba, Japan. The NPTC facility will initially use a wobbler system for beam spreading.

Next, techniques to achieve sharp lateral dose falloffs (penumbrae) are examined. In order to take full advantage of the dose localization properties of heavy charged-particle beams, great care must be taken to minimize the width of the lateral dose falloff. The apparent source size of the radiation field causes a penumbra, which contributes to broadening of the width of the lateral dose falloff. In order to minimize the apparent source size, the diameter of the beam has to be small

where the beam traverses material. This can be accomplished by placing any scattering and range-shifting material upstream of where the beam begins to spread transversely. However, any amount of material in the beam introduces an additional beam divergence due to multiple scattering. Positioning the material far upstream of the isocenter may lead to an intolerable increase in beam spot size at the target, which, if collimated, results in a reduction in the dose rate. Also, often the beam-line length (drift space) is limited on the treatment nozzle mounted on a rotating gantry. On the other hand, placing the scattering material close to the target volume reduces the scattering effect on low-velocity particles and preserves the modulated Bragg peak shape. For this reason the patient compensator is usually placed as closely as possible to the patient body. The unavoidable multiple scattering inside the patient body and other materials in the beam path, especially those near the patient such as the compensator, also contributes to the broadening of the width of lateral dose falloff<sup>31</sup>.

The amount of material used for scattering and for energy degradation also affects neutron production and projectile fragmentation for heavier ions, which in turn affects the peak-to-plateau ratio of the spread-out Bragg peak. The ratio is enhanced when the material is placed far upstream of the target, as a large portion of the neutrons and fragments will diverge out of the main beam. Above analyses show that the design of the scatterers and their locations in the beam line affect the physics and biology of the beam that enters the patient body, and consequently influences therapeutic effects.

### ***Beam Size, Divergence, and Emittance***

In treating a small target, such as an arteriovenous malformation (AVM), a heavy charged-particle beam with a small cross-section and small divergence is

needed. For example, in treating an AVM of  $5 \times 5 \times 5 \text{ mm}^3$  at a depth of 10 cm, multiple scattering in the patient alone spreads out the beam laterally by  $\sigma_y=0.23$  mm. This translates to a requirement that the emittance  $\epsilon$  of an 'ideal' pencil beam should be limited to  $\epsilon \approx 1.2 \times 10^2$  mm-mrad. A typical transverse emittance of a 200-MeV proton beam obtained through resonant extraction from a synchrotron, measured at the accelerator exit, is  $\epsilon \approx 5\pi$  mm-mrad unnormalized. Such an emittance is an order of magnitude smaller than the scattering effect inside the patient body, and is therefore acceptable. The typical emittance of a proton beam extracted from a cyclotron is bigger by a factor  $\sim 10$  than that from a synchrotron. As the beam fluence rate (number of protons/cm<sup>2</sup>/sec) needed for such a small-target treatment is only a very small fraction of a typical synchrotron or cyclotron output current, it allows the beam emittance to be made arbitrarily small through collimations as needed. On the contrary, for treating large areas up to 40 cm  $\times$  40 cm, a treatment time limit of two minutes prohibits throwing beam particles away by collimation. Even for large fields, the small beam emittance must be preserved if the field is produced using, for example, a pencil-beam scanning system.

The beam emittance determines the gap sizes of the transport magnets. This implication becomes acute for magnets on an isocentric gantry, because the total weight of the magnets determines the gantry structure and therefore its cost. An  $\text{H}^-$  synchrotron has been seriously considered for radiation therapy because its transverse emittance of the beam obtained through charge-exchange extractions is small,  $\epsilon \approx 0.1\pi$  mm-mrad<sup>32</sup>. The idea was dropped mainly because of expected difficulties in maintaining the required high vacuum ( $<10^{-10}$  torr) needed for a  $\text{H}^-$  synchrotron in a hospital setting.

### *Beam Optics*

A rotating gantry must satisfy the clinical requirement for isocentric treatments that the treatment beams can be brought into the patient, usually in a horizontal position, from any angle ( $4\pi$  steradians). The beam optics of a gantry takes a horizontally transported beam and bends it 180, 270, or even 360 degrees depending on the gantry design (see the gantry descriptions in Ref. 33). When the gantry is rotated, the x- and y-axes of the beam optics are also rotated and mixed. As the clinical beam delivery system on the gantry demands a circularly symmetric beam (emittance  $\epsilon_x'=\epsilon_y'$ ), the beam focusing elements on the gantry should be designed to preserve the circular beam spot of the incident beam ( $\epsilon_x=\epsilon_y$ ) at any gantry angle and proton energy.

For the above-mentioned 'contoured scatterers' to work properly, the beam must be tuned so that the beam spot is circular ( $\epsilon_x=\epsilon_y$ ) and centered on the filter axis, and the beam direction is parallel to the filter axis. An off-axis misalignment of 1-mm will result in an unacceptable lateral variation of dose to  $\pm 7\%$ . Instruments should be provided on treatment nozzles to verify the correct tuning of the beam for its spot size, shape, position, and angular orientation.

A dynamic beam delivery system, *e.g.*, beam wobbler or scanner, overcomes the undesirable need for scattering materials in the beam path. But the real benefit is their insensitivity to small misalignments of the beam. If the beam is misaligned, say, by 1 mm, the entire scanned field will be shifted by 1 mm, which will have insignificant consequences if the port is defined by a patient collimator. As long as the incident beam into the scanner does not wander during a scan cycle (typically ~1 second long), the desired uniformity can be achieved.

### ***Control Systems for Medical Beams***

To deliver accurate doses reliably, many instruments have been developed for *beam modification* and *beam measurement*. A well-developed treatment control system must oversee each treatment by controlling the beam modification and beam measurement procedures for correct treatment delivery. There should be no room for compromise in patient safety. Recently a thorough discussion on the rationale and structure of control systems for heavy charged-particle radiotherapy facilities has been presented<sup>34</sup>.

### **Hospital-Based Proton Accelerator Facilities**

The promising clinical results obtained with proton beams have led to plans to build hospital-based proton medical accelerator facilities. The trend is to construct the proton accelerator facilities that are capable of treating all sites from ocular melanomas to deep-seated large tumors by supplying proton beams of energy from 70 MeV to 250 MeV. These new facilities feature modern equipment designed to optimize the efficacy of proton radiation therapy. They will expand the patient treatment capacity and hence the range of potential proton treatments in an environment conducive to modern patient care, providing a level of comfort, efficiency, and proximity to other medical support facilities. Each of these facility plans to treat at least 1000 patients per year.

### ***First Medical Proton Facility in Loma Linda, California***

One notable initiative in proton therapy is the 1991 commissioning of the proton accelerator facility at the Loma Linda University Medical Center in Loma Linda, California. It is the *first* dedicated proton accelerator facility built for a hospital.

A 250-MeV zero-gradient synchrotron design was chosen for its compactness (20-m circumference) and its weak-focusing and large momentum-dispersion characteristics that allow a high space charge limit ( $10^{11}$  protons per pulse) to produce maximum intensity per unit circumference of the ring. The ion source delivers 37-keV protons to a short 1.6-meter radiofrequency quadrupole (RFQ), which in turn accelerates the protons to 2 MeV and injects them into the synchrotron. The accelerated protons are extracted at any desired energy between 70 and 250 MeV through resonant extraction using a small trim quadrupole magnet in the ring. The typical intensity of the extracted beam is  $3 \times 10^{10}$  protons per pulse at 27 pulses per minute. This translates to a dose rate of  $\sim 100$  cGy per minute for 20-cm diameter ports, resulting in typical treatment times of two minutes. To satisfy the clinical interest in treating field sizes up to 40-cm diameter without increasing the treatment time, there is an ongoing effort to improve the proton intensity<sup>35</sup>. The proton facility has three rotating-gantry rooms, two fixed horizontal beam-line rooms, one room for small-field treatments (eye and brain) and large-field treatments, and another room for research (Fig. 7.10). The first patient was treated with the eye beam in October 1990, and full patient treatments began in June 1991 using the isocentric gantry beam delivery system.

Fig. 7.10

### *Medical Proton Facility in Kashiwa, Japan*

The construction of an improved version of the NCPT proton facility (see below) has been completed at the National Cancer Center (NCC) East Hospital, Kashiwa, Japan. (This location is also referred to as the NCC-Higashi Hospital, as it is located at the Higashi (east) side of Tokyo). Patient treatments will start in early 1998. This NCC facility is funded by the Japanese Ministry of Health and Welfare.

The facility includes a 235-MeV isochronous cyclotron, two isocentric gantry rooms and a fixed beam treatment room<sup>36</sup>. The performance of the facility is similar to the NPTC facility described below.

### *Northeast Proton Therapy Center (NPTC) in Boston*

Another new hospital-based proton facility is in Boston, where the Massachusetts General Hospital (MGH) is constructing a facility at the Northeast Proton Therapy Center (NPTC)<sup>37</sup>. It aims to provide a unique regional resource in clinical research activities to the New England area. The accelerator is a 235-MeV isochronous cyclotron, able to deliver up to 1200 nA but hardware-limited at 300 nA in order to limit the maximum possible dose rate to the patient. The output current is adjustable to one part in 6500. The beam on-off time is 30  $\mu$ sec. The facility provides an 'energy select system,' a beam transport and switching system, two 'large-throw, in the plane,' isocentric gantries, a fixed horizontal beam line, two robotic patient positioning systems, an integral control system and a safety system (Fig. 7.11). The energy select system degrades the proton beam extracted at full energy, and collimates and momentum selects the beam before sending it down the beam transfer line. This system will be able to change the beam range in patients from 4 cm to 32.8 cm with a reproducibility  $<0.01$  cm. The measured distal falloff is 4.8 mm at full range, and 0.9 mm at 4-cm range. Energy switching will take 1.3–1.5 sec. The isocentric gantries, together with their robotic patient positioners, allow the proton beam to be directed at a patient from any angle, thereby ensuring the greatest possible ability to avoid critical organs in the course of irradiating the tumor. Each of the gantries includes a beam delivery system with both a passive beam spreader (scattering system) and an active beam wobbling system that can 'paint' large uniform fields without

resorting to scattering. The facility will consume electric power of 400 kW. NPTC plans to treat its first patient in the fall of 1998.

Fig. 7.11

### *Other Planned Hospital-Based Proton Facilities*

We have discussed synchrotrons and cyclotrons for proton therapy. Linacs are also considered for proton therapy, but the time structure of extracted pulses from linacs are not well suited for beam scanning and linacs may not find applications in future proton therapy. There is an interesting development in the area of superconducting cyclotrons. Recently a 238-MeV three-sector superconducting cyclotron design for use in radiation therapy was presented<sup>38</sup>. The advantages of such a machine are its compactness (the cyclotron outer radius is 1.6 m and the height is 2 m), inherent stability, and ease of operation. Combined with a cyclotron's high beam intensity, this capability naturally accommodates beam scanning. To take full advantage of the small footprint of the cyclotron, a supertwist gantry (270° total bend angle) is proposed which, when compared with a corkscrew gantry, gives more room for the patient and decreases the outside diameter of the gantry.

Today the most active construction activities for proton medical facilities are found in Japan. The Japanese Ministry of Health and Welfare, which has already built a proton facility in Tokyo, is deciding (in 1997) whether to build another proton facility in Shizuoka. The construction of a 270-MeV synchrotron at the Tsukuba University Medical Center will be completed in 1998 as already mentioned. It will be funded by the Japanese Ministry of Education. The Hyogo Prefecture government, with the help of the Japanese national government, is funding the construction of a carbon (420 MeV per nucleon) and proton (250 MeV)

medical facility. It will be a synchrotron within a synchrotron design, and will provide two isocentric gantry rooms, one horizontal fixed beam, one fixed vertical beam, and one 45-degree fixed beam rooms. The construction may start in early 1998. There are less delineated plans to construct proton facilities in Osaka, Kyoto and elsewhere.

The ADROTERAPIA collaboration is a group of scientists and clinicians in Italy concerned with developing a hadron therapy accelerator. They are studying the feasibility of building an  $H^-$  synchrotron (60-250 MeV), which may be upgraded to a heavier-ion machine later for therapy, as well as for boron neutron capture therapy and isotope production<sup>39,40</sup>. ITEP in Moscow, Russia is designing a negative hydrogen ion ( $H^-$ ) synchrotron facility with 2 isocentric gantry rooms, 1 fixed beam treatment room, and another room for experimental use. A very compact synchrotron, accelerating protons to 200 MeV is being designed at the Institute of Nuclear Physics (INS) in Novosibirsk<sup>41</sup>. There are proposals to install a hospital-based proton therapy center in Beijing, China<sup>42</sup>, Regensburg, Germany, and Antwerp, Belgium. The Proton Therapy Corporation of America (PTCA) in New York has plans to build several dedicated proton medical accelerator facilities. Proton Development N. A. Inc. of Chicago has similar plans for building proton accelerator facilities for radiotherapy as well as for lithography applications.

#### **D. LIGHT AND HEAVY IONS FOR RADIATION THERAPY**

##### **Physics Considerations for Light and Heavy Ions**

Range straggling and multiple scattering of penetrating heavy charged particles (protons and heavier ions) are discussed in Sec. B. The variance of these

quantities,  $\sigma_z$  (Eq. (7-4)) for straggling and  $\sigma_y$  (Eq. (7-6)) for multiple scattering are smaller for heavier projectiles. A physical advantage of heavier ions, compared with lighter ions, is that they suffer significantly less multiple scattering while penetrating an absorbing medium. The result is that heavier ion beams exhibit sharper lateral dose falloffs at the field boundary. This is an important property to be exploited in clinical applications as many tumors are immediately adjacent to critical organs that must be spared from radiation as much as possible.

For heavier ions, which are totally stripped nuclei with higher charges, the LET is greater than the LET of either protons or photons. The ionization is approximately proportional to the square of the charge and inversely proportional to the square of the velocity of the projectile particles, as discussed with Eq. (7-1). If the Bragg peak is spread out to cover an extended target by modulating the energy of the particles, the ratio of peak-to-plateau decreases; however, the *biologically effective* dose in the spread-out peak can still be much greater than the entrance dose as the slower ions have higher RBE values. For penetrating heavier ions, nuclear fragmentations result from nuclear interactions between the projectile nuclei and the nuclei in the medium, causing a reduction in the number of projectile particles with increasing depth. The secondaries, being lighter and less charged than the primaries, travel farther than the primaries and contribute a 'tail' dose beyond the Bragg peak (Fig. 7.12). The tail dose is on the order of 10–20 % of the entrance dose, and falls off relatively slowly with depth. Longer range beams have a smaller peak-to-plateau dose ratio than shorter range beams because of the increased loss of primaries. For the same reason, the plateau dose decreases slowly with depth for heavier ions.

## Biological Considerations for Light and Heavy Ions

The failure in local control of tumors treated with conventional radiation is often due to the inability of the radiation to completely eradicate anoxic (deprived of dissolved gaseous oxygen) tumor cells which are resistant to low-LET radiation. Regrowth of the cells in the anoxic core of the tumor results in the failure of local control. In 1967, Tobias and Todd gave the scientific justification for utilizing light and heavy ion beams to reduce this radiobiological oxygen effect<sup>43</sup>. Ions with higher atomic charges ( $Z$ ) produce higher LET, and particle beams having higher LET exhibit the biological advantages of lower oxygen effect. Such particle beams are able to eradicate radioresistant cells, which survive irradiation using low-LET radiations.

Fig. 7.13

Biology experiments performed first at LBNL, and later at NIRS and the Gesellschaft für Schwerionenforschung (GSI), Darmstadt, Germany, show that the RBE of a heavy charged-particle beam is not a simple function of LET<sup>44</sup> (see Fig. 7.13). In general, the values of RBE and the degrees of dose localization increase as the mass of the projectile particle increases from protons to silicon ions. Radiobiology experiments demonstrate the following results: (a) The high resistance of hypoxic cells relative to oxic cells is reduced when irradiated with high-LET radiation. In other words, the oxygen enhancement ratio (OER) is lower for higher-LET radiation, where the OER is defined as the ratio of the absorbed dose of a given radiation required to produce a given level of biological effect under anoxic conditions to the dose required to give the same level of effect under oxic conditions. In the case where the endpoint is the inability of cells to form colonies, for example, the value of the OER defines how much more radiation is required to render anoxic cells (usually found in tumor cores) unable

to form colonies compared with well oxygenated cells (usually found in healthy tissues surrounding the tumor volumes). (b) Slowly proliferating cells (in  $G_0$  or long  $G_1$  phase of the cell cycle) show an increase in sensitivity with higher LET values. (c) Overall treatment time with high-LET radiation can be shortened since fewer fractions of larger doses may be used instead of multiple fractions of small doses, since the surrounding normal tissue damage in a few fractions can be kept comparable to that of multiple standard low-LET fractions. Decreasing the number of treatments also benefits individual patients as well as the management of the clinic. It is considered advantageous to treat tumors with high-LET radiation if they have the following properties<sup>45</sup>: high intracellular repair, poor cell cycle redistribution, poor reoxygenation during treatment, and rapid proliferation in tumors.

The steep dose falloff at the distal edge of the spread-out Bragg peak is important in sparing normal tissues located distal to the target. Treatment doses are often limited by normal tissue complications. Therefore, sharp dose falloff is an important factor that influences the success and failure of treatments. As shown in Fig. 7.14, the distal part of the spread-out Bragg peak is composed largely of the Bragg peak of the most penetrating particles in the beam. This is deliberately done to keep the slope of the distal edge as steep as that of the pristine peak. As the RBE value of an ion beam varies across different parts of the Bragg ionization curve, the physical dose distribution must be adjusted to achieve a biologically uniform dose across the target region. The physical dose distribution of SOBP is sloped down with the depth of penetration as the distal part of the SOBP is composed of mostly high-LET Bragg peak doses whereas the proximal part contains mostly plateau doses of the particles that penetrate farther (Fig. 7.15).

Fig. 7.14
-----------

Fig. 7.15
-----------

## Light and Heavy Ion Accelerator Facilities and Clinical Trials

### *Bevalac at LBNL in Berkeley, California*

With advances in accelerator design in the early 1970s, it became possible to examine the biological effects of high-energy light and heavy ions. Synchrotrons at Berkeley and Princeton accelerated ions with atomic numbers between 6 and 18, at energies that permitted the initiation of several biological studies. The higher RBE values of these high-Z particle beams suggested a high likelihood of an enhanced therapeutic potential when compared with lower-Z particle beams.

The construction of the Bevalac accelerator complex at LBNL, in which the SuperHILAC injects heavy-ion beams into the Bevatron, expanded the opportunity for medical studies with heavy charged-particle beams (Fig. 7.16). Clinical trials<sup>46-48</sup> treating approximately 300 cancer patients using heavier-ion (mostly neon) beams took place at the LBNL Bevalac since 1977 until 1992 prior to the closure of the Bevalac in 1993.

Fig. 7.16

### *HIMAC at NIRS in Chiba, Japan*

The National Institute of Radiological Sciences (NIRS) commissioned the Heavy Ion Medical Accelerator in Chiba (HIMAC) in 1993. HIMAC has dual synchrotrons, each capable of producing ion beams from  $^4\text{He}$  to  $^{40}\text{Ar}$  up to a maximum energy per nucleon of 800 MeV<sup>49</sup>. There are two treatment rooms, one with both a horizontal and a vertical beam, and the other with only a vertical beam. There are also a secondary (radioactive) beam room, a biology experimental room, and a physics experimental room, all equipped with horizontal beam lines. All beam lines are of the fixed beam type, in contrast to rotating gantries for proton facilities (Fig. 7.17). For heavier ions, which have stiff

magnetic rigidity, it is impractical to build isocentric gantries. A 200-bed hospital is built adjacent to the HIMAC. In 1994 NIRS began clinical studies with carbon ions, initially focusing on head and neck, brain and lung tumors, and more than 270 patients have been treated by the summer of 1997.

Fig. 7.17

### *Clinical Beam at GSI in Darmstadt, Germany*

Preclinical studies to determine clinically important disease sites for heavy-ion beams have been started at GSI using the heavy ion accelerator (SIS), in collaboration with the University Clinic of Radiology, Heidelberg, and the German Cancer Research Center (DKFZ). The first carbon beams were introduced in the medical irradiation room in 1995, and clinical trials with carbon ions are slated to begin in 1997<sup>48</sup>. It is planned to provide intensity-controlled beams of the energy per nucleon between 80 MeV and 430 MeV suitable for delivery using a raster scanning system.

### *Planned Light and Heavy Ion Facilities for Radiation Therapy*

There is a move by the Japanese Science and Technology Agency, which funded the construction of HIMAC, to build another medical accelerator facility in Aomori, probably starting construction in 1999. The Hyogo Prefecture government, with the help of the Japanese national government, is funding the construction of a carbon (420 MeV per nucleon) and proton (250 MeV) medical facility, as already mentioned. It will be a synchrotron within a synchrotron design. The construction may start in early 1998.

In Italy, the above-mentioned ADROTERAPIA collaboration has plans to construct an  $H^-$  synchrotron, and convert it to a heavier-ion (probably up to  $^{20}Ne$ )

machine later. At the INFN-Laboratori Nazionali di Legnaro (LNL), Padova, Italy, low energy (in the range of energy per nucleon of 10 MeV) radiobiology experiments of protons and various ions have been conducted since 1984. Now a superconducting post-accelerator (ALPI) is being built for the existing TANDEM-XTU, and there is a proposal to use the ALPI as an injector for a synchrotron (ADRIA), and use the light and heavy ions, such as  $^{12}\text{C}$ ,  $^{20}\text{Ne}$ ,  $^{28}\text{Si}$ , and  $^{40}\text{Ar}$  with an energy per nucleon from 100 to 1000 MeV for radiotherapy trials.

In 1991 the European Community (EC) completed a feasibility study of constructing the European Light Ion Medical Accelerator (EULIMA)<sup>50</sup>. A tandem cyclotron for accelerating light ions, from  $^4\text{He}$  to  $^{20}\text{Ne}$ , to a maximum energy per nucleon of 500 MeV, as well as a synchrotron, were considered. A synchrotron design considering specific site conditions of a Heidelberg site has been also proposed. Biomedical research using heavy charged-particle beams is also under active consideration in Russia. A design study has been performed at ITEP to accelerate light ions from  $^{12}\text{C}$  to  $^{20}\text{Ne}$  with energy per nucleon up to 500 MeV, and bring the light-ion beams to the treatment rooms to be constructed for the  $\text{H}^-$  accelerator discussed above.

### **Clinical Results of Heavy Charged-Particle Beam Therapy**

Clinical evidence has demonstrated that protons (and helium ions) have the ability to deliver higher tumor doses while preserving adjacent critical normal tissues. Rates of long-term local control and survival ranged from 60-95% depending on tumor site and were higher than obtained with standard megavoltage x ray techniques. Notable examples in which proton beam therapy is highly effective are unresectable tumors in critical locations such as the orbit, eyes, skull base, juxtaspinal area, retroperitoneum or pelvis. The best results

were seen in treatment of skull-based tumors<sup>51</sup>. Chordomas and chondrosarcomas of the base of skull, which are a pair of formerly hard to cure rather uncommon tumors whose cure rates (five year survival rates) appear to have been approximately doubled with proton therapy. Local control rates at 5 years appear to be 91% for tumors in the base of skull, and 65% for those in the region adjacent to the cervical spine. Local control rates for choroidal melanoma is ~96%, and the five-year survival rate for patients is ~85%. Loma Linda has recently reported its clinical data on treating locally advanced carcinoma of the prostate<sup>52</sup>. Other diseases being considered for proton treatments include: head and neck tumors including nasopharynx, base of tongue, glottis, and salivary gland, thoracic and lumbar spine tumors, urinary bladder carcinoma, retroperitoneal sarcomas, cancer of the uterine cervix, carcinoma of the rectum, soft tissue sarcomas of the extremities, medulloblastomas, craniopharyngiomas, para-aortic lymph node disease, carcinoma of the bile duct, pediatric tumors, pituitary lesions, brain metastases, etc. Proton beam therapy has also been shown to be very effective in stereotactic radiosurgery of arteriovenous malformation (AVM)<sup>53</sup>. At Berkeley, treatments of pituitary patients using helium ions were also tried for over 36 years<sup>54</sup>. For an unbiased comparison, the proton results obtained at hospital-based proton facilities should be compared to those of dynamic 3-D conformal photon therapy.

In the LBNL clinical trial high-LET charged particles such as  $^{12}\text{C}$ ,  $^{20}\text{Ne}$  or  $^{28}\text{Si}$  ions were used in about 300 patients. However, the statistics are insufficient to prove or disprove the merits of heavier ions in clinical therapy. Neon ions, while giving promising initial results in some sites such as unresectable bone and soft tissue, salivary gland, biliary tract and prostate tumors, have had significant late effects on normal tissues<sup>47</sup>. The use of carbon ions may obviate this problem by

providing better equivalent-dose localization, more sparing of normal tissues and sufficient high-LET deposition for optimal results. In 1994 NIRS began clinical studies with carbon ions, initially focusing on head and neck, brain and lung tumors; in 1997 GSI started a clinical trial using carbon ions.

### **Future Development for Heavy Charged Particle Radiation Therapy**

Very exciting and strong proton-beam clinical trials to treat human cancer are in progress all over the world. Hospital-based proton accelerator facilities are continuously being built. Light- and heavy-ion beam therapy clinical trials are conducted in Japan and Germany.

In order to compare the clinical efficacy of heavy charged-particle beam therapy to what can be achieved by a modern three-dimensional conformal therapy using multiple, intensity-modulated photon beams, it is important to fully exploit the dose localizing advantage of heavy charged-particle beams. One must develop technologies to deliver optimum radiation dose distributions, *i.e.*, delivering a maximum dose to the tumor, and at the same time, minimizing the radiation dose delivered to surrounding sensitive, normal structures of the body. It can be achieved with three-dimensional conformal therapy delivery using pencil beam scanning technology. Beam scanning imposes stringent requirements on the accelerator facility performance and its control system in order to ensure patient safety. Clinically effective, operationally reliable and cost-effective proton therapy systems must be developed.

### ***Three-Dimensional Conformal Therapy Delivery***

In the currently used *fixed-modulation beam delivery* method a fixed width of a spread-out Bragg peak, which is wide enough to cover the thickest part of the

target, is used to treat the entire irregular target volume (Fig. 7.18). A compensator (bolus) is used to conform the dose falloff region (*i.e.*, distal edge of the Bragg peak dose region) with the distal surface of the target volume. This method produces a cylindrical treatment volume (hatched area in the figure), and normal tissues upstream of the target are unnecessarily irradiated. Analogous to conformal photon treatments, multiport treatment plans can reduce the unwanted dose below the tolerable levels.

Fig. 7.18
Fig. 7.19

A variable-modulation beam delivery (Fig. 7.19) may be achieved using a beam scanning system<sup>55</sup>. The raster scanning method requires controlled modulation not only the scan speeds, but also the beam energy and the beam fluence rate. A raster scanner system developed for the heavy ion program at LBNL was used for more than 50 patients since 1992 until the closure of Bevalac<sup>56</sup>. A three-dimensional dynamic conformal therapy delivery system, an integrated system that brought together the modulating the scan speed of a raster scanner, automatic controlling of a multileaf collimator, and modulation of the extraction intensity from a synchrotron, was successfully tested before the closure of the Bevalac in 1993. For beam scanning application at the Heavy Ion Synchrotron (SIS) of GSI, it has already been demonstrated that carbon ion beam's energy per nucleon can be varied from 80 MeV to 430 MeV (corresponding to 20–300 mm water-equivalent ranges) in 253 energy steps. The fluence-rate can be varied in 15 steps from  $1 \times 10^6$  to  $1 \times 10^8$  ions/spill in a reliable and reproducible way by applying a variable deflecting voltage to the chopper in the high-charge injection section. For all energies and fluence rates, the beam position at the patient will be accurately controlled in order to produce the desired dose distributions. The GSI system is currently readied for the clinical use<sup>57</sup>. A uniform extraction of proton

beams from a medical synchrotron has been also studied at Loma Linda proton facility<sup>58</sup>. A large field of an arbitrarily specified dose distribution can also be obtained by moving a beam spot across the field in discrete steps. A predetermined amount of radiation is deposited after positioning a beam spot at a given location in the target volume. The spot is then moved to the next position, and the process is repeated. This spot scanning approach has been adopted at PSI for proton therapy<sup>59</sup> (Fig. 7.20).

Fig. 7.20

Advantages of beam scanning for three-dimensional dynamic conformal therapy delivery have been discussed extensively<sup>56</sup>. A beam scanning system is employed to produce a prescribed dose distribution,  $D$ , in three dimensions as a convolution of the beam-profile function,  $p$ , and an occupation function,  $F$ :

$$D = F \otimes p . \quad (7-8)$$

Here,  $D$  may be a biological- or therapeutic-effect function specified inside and outside the target volume. For a particle beam traveling in z-direction, the beam-profile function,  $p$ , is given by the Bragg curve in z-direction, and multiple scattering in x- and y-directions. When  $D$  is specified and  $p$  known, the occupation function  $F$  (which is related to the beam-scanning pattern) may be found. One method is through iterations, viz.,

$$F_{n+1} = C [F_n + \alpha (D_0 - F_n \otimes p)] , \quad (7-9)$$

where  $F_0$  is the initial guess of the occupation function,  $C$  is a positive definite operator that allows only non-negative solutions, and  $\alpha$  is a convergence parameter<sup>60</sup>. Significant fluctuations, and therefore gradients, in  $F$  result in order to place uniform dose inside the target volume and sharp dose falloffs at its

edges<sup>59</sup> (Fig. 7.21). In actual beam scanning, the desired  $F$  is achieved through either modulating the extracted beam intensities or varying the scan speed, or both.  $F$  is related to an inverse of the slew rate for variable-velocity beam scanning using uniform beam intensities. Modeling of the beam-profile function  $p$  for pencil beams inside the patient body must include small-angle scattering, energy straggling, losses due to nuclear interactions, as well as the heterogeneity of the penetrating media. Beam scanning imposes stringent requirements on the accelerator facility performance, such as beam-energy variability, energy step size and switching time, beam emittance, beam position and angular precision and stability, duty factor of the beam spills, beam intensity control as a function of time, uncontrolled intensity fluctuations, and control systems, in order to assure patient safety.

Fig. 7.21

## E. FAST NEUTRON THERAPY

Approximately half of everyday matter is made of neutrons, but the fact that they are bound in nuclei with the strong force and are electrically neutral made it difficult to discover these particles. James Chadwick deduced the existence of neutrons in early 1932 by observing recoil protons produced by fast neutrons in paraffin. Only six years after this discovery Robert Stone at the Radiation Laboratory in Berkeley, California attempted the first use of neutrons to treat human cancer<sup>61</sup>. Using neutrons produced first at the 30-Inch Cyclotron, then at the 60-Inch Crocker Medical Cyclotron (built by Ernest Orlando Lawrence with

funds supplied by the National Cancer Institute), Stone treated 226 patients with various advanced malignancies to high doses. Stone reported his clinical observations after World War II, and concluded, "Neutron therapy as administered by us has resulted in such bad late sequelae in proportion to the few good results that it should not be continued"<sup>62</sup>. The failure was initially thought to be due to an increased relative biological effectiveness (RBE) of fast neutrons for late effect<sup>62</sup>. The RBE of the neutron beam had been measured in animals at large single doses, while the patients had been treated with fractionated therapy. Later it was realized that for neutrons the RBE for large single doses is much lower than for smaller fractionated doses (by a factor of about 2), and therefore, Stone's patients had been severely overdosed<sup>63</sup>.

In the late 1960s Mary Catterall at Hammersmith Hospital, London rekindled interest in fast neutron therapy by demonstrating that patients tolerated the neutron treatments well if the neutron therapy was delivered with appropriate fractionation based on new biological measurements<sup>64</sup>. The positive results of Catterall and her associates removed the stigma on fast neutrons and prompted further clinical trials in Europe<sup>65</sup>, Japan<sup>66</sup>, and the U.S.<sup>67</sup>. However, the results were ambiguous, in large part because of inadequacies in the neutron therapy equipment used in the trials. Many machines were originally built for nuclear physics research and hastily converted for clinical use. They often had less than optimal penetration, poor reliability, poor collimation, and low dose rate which severely compromised the delivery of treatment. In addition, the delivery of multiple beams to a recumbent patient was often not possible or practical. More recent clinical trials using fast neutrons from higher energy machines gave more consistent and encouraging results, and many studies are in progress today.

## Rationale for Fast Neutron Therapy

### *Interactions of fast neutrons with tissue*

The penetration characteristics of fast neutrons are similar to those of high-energy photons used in therapy. The depth dose distribution due to the primary neutrons is approximately exponential; scattered radiation and inelastic processes modify the depth dose characteristics. For example, the depth dose distribution due to the 14.1 MeV neutrons from a d-T generator is similar to, but slightly less penetrating than, that of  $^{60}\text{Co}$   $\gamma$  rays. For a 10 cm x 10 cm neutron field at a source-to-skin distance (SSD) of 80 cm, the depth of  $D_0$  is approximately 9.5 cm, while that for  $^{60}\text{Co}$   $\gamma$  rays is approximately 11.5 cm. On the other hand, fast neutrons (mean energy  $\approx 20$  MeV) from high energy proton reactions have a depth dose distribution like that of 6 MeV x rays (Fig. 7.22). Because of the larger number of scattering reactions and the larger average angle of scattering, the lateral dose falloff is less sharp for neutrons than for megavoltage x rays.

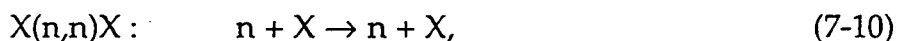
Fig. 7.22

The advantages of producing neutrons with a d-T generator are that the energy of the deuteron beam can be quite low ( $\sim 250$  keV), and a compact generator can be constructed, which can be mounted on a rotating gantry. However, with the available technology d-T generators can not produce clinically desirable neutron intensity. Increasing the target size and decreasing the distance from the target to patient (SSD), to increase the dose rate, broadens the neutron beam penumbra and degrades the beam quality. Also, at a low incident energy of the deuteron beam, the neutrons are emitted almost isotropically, requiring extensive shielding. The d-T generators used for clinical trials in the '70s and '80s typically produced only 10–15 cGy/minute at an SSD of 80–100 cm. Modern clinical trials

have thus moved toward producing fast neutrons through the (p,n) or (d,n) reaction on Be targets.

When fast neutrons penetrate tissue, ionization and dose deposition are through recoil protons produced by neutron collisions with hydrogen nuclei, and, to a lesser degree, recoil ions. The biological effects of fast neutrons are mediated by the energy transfer mechanisms of these recoil particles. Therefore, even though neutrons are electrically neutral, neutron beams behave as high-LET radiation since these low-energy protons and heavier ions lose their energy over short distances. This process is fundamentally different from low-LET photon radiation, which produces secondary electrons that are in turn also low-LET radiation. To fully describe neutron interactions, detailed knowledge of the atomic composition of tissue is necessary. In photon interactions, it is sufficient to know the electron density of the irradiated material, since all the basic interactions (photoelectric effect, Compton scattering and pair production) occur between photons and electrons, and the secondary particles resulting from these interactions are electrons.

In fast neutron therapy, neutrons penetrating tissue predominantly undergo elastic scattering interactions of the type



where X is the target nucleus (H, C, N, or O, the basic constituents of human tissue), and the energies and directions of the scattered neutron and recoil nucleus X are determined by the reaction kinematics. Below 10 MeV, about 90% of the tissue dose results from elastic scattering from hydrogen, and it steadily decreases as neutron energy increases<sup>3</sup>. For 15 MeV neutrons interacting with muscle tissue, for example, 97.8% of neutron interactions are elastic scattering, which include 84.1% of neutrons interacting with <sup>1</sup>H, 10.3% with <sup>16</sup>O, 2.4% with

$^{12}\text{C}$ , and 0.93% with  $^{14}\text{N}$ . The remainder are inelastic interactions with the most significant ones being  $^{16}\text{O}(n,n')\alpha$ ,  $^{16}\text{O}(n,n')$ ,  $^1\text{H}(n,\gamma)$ , and  $^{16}\text{O}(n,\alpha)$ .

A significant number of inelastic or particle emission interactions occur in which the neutron is absorbed in the target nucleus X to form an excited nucleus  $X^*$ , which eventually emits an energetic particle b (which may be a proton, neutron, deuteron,  $\alpha$  particle, etc.) in its transition to a product Y:



The principal secondary particles resulting from fast neutron interactions in tissue are recoil nuclei of p,  $\alpha$ ,  $^{12}\text{C}$ ,  $^{14}\text{N}$ , and  $^{16}\text{O}$ . These recoil nuclei have high LET, in comparison with low-LET electrons which result from photon interactions with tissue, and are important in radiation therapy as their reactions with cells exhibit elevated values of RBE, as discussed below. Based on their sheer numbers, the most significant dose components result from recoil protons (with LET in the range of 1–100 keV/ $\mu\text{m}$ ) and recoil  $\alpha$ -particles (100–300 keV/ $\mu\text{m}$ ).

### ***Biological Rationale***

The primary rationale for using fast neutron therapy was thought to be an ability of the radiation to overcome the adverse effects of hypoxia in tumors. It is well known that mammalian cells respond differently to radiation depending on the degree of tissue oxygenation. In general, cells are more resistant to radiation under poorly oxygenated conditions. For example, V79 Chinese hamster ovary cells irradiated by 250 keV x-rays exhibit  $\text{OER} \approx 3.2$  at the 10% survival level. For fast neutron beams the same cell line exhibits the value of  $\text{OER} \approx 1.6$ . Therefore, if tumors contain viable hypoxic cells, and if normal tissues are well oxygenated, there should be a therapeutic advantage of irradiating such tumors with fast

neutrons provided the mechanism of reoxygenation of hypoxic cells between fractionations can be understood and controlled.

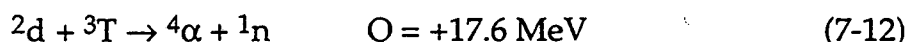
Fast neutrons have been shown to have a wide range of RBE values for tumors exceeding the range of RBE values for normal tissues. The RBE for slowly growing well-differentiated tumors was found to be much higher than for fast-growing poorly-differentiated tumors. Thus, applied to selected tumors, fast neutron beams would exhibit correspondingly high therapeutic advantage when compared with photon treatment<sup>68</sup>. These conclusions equally apply to other high-LET radiations, such as heavy ions. Another advantage of neutron therapy is the reduced variation in radiosensitivity throughout the cell cycle.

Another possible advantage for fast neutrons is in tumors which exhibit a high capacity for repair of sublethal and potentially lethal damage. These phenomena manifest themselves in cell survival curves as large shoulders on the curves at low doses under low-LET irradiation, e.g., photon treatment. Cells irradiated with fast neutrons result in survival curves with minimal shoulders, indicating that repair of sublethal and potentially lethal damage is greatly reduced after neutron irradiation. Melanomas, for example, are known to possess a high capacity for repair and, hence, neutron therapy may be advantageous in these cancers.

### **Clinical Trials Using Fast Neutrons**

Most fast-neutron radiotherapy facilities were initially developed by modifying existing particle accelerators (cyclotrons and linacs). These facilities were limited in their ability to deliver acceptable dose distributions. There was also a big interest in developing medically dedicated d-T generators for fast neutron

therapy as such machines operated at relatively low voltages (200–500 keV) are compact and inexpensive. In a d-T generator, usually deuterons ( $^2\text{H}$  nuclei) are accelerated and made to bombard tritium atoms ( $^3\text{H}$ ) placed on the surface of a metallic substrate such as titanium to produce neutrons, viz.,



The Q-value of +17.6 MeV is shared between the  $\alpha$  particle and the neutron and a d-T generator produces neutrons with an energy ~14 MeV with penetration characteristics similar to  $^{60}\text{Co}$   $\gamma$  rays. However, there are many drawbacks for this approach. Handling large quantities of tritium in the hospital environment is hazardous; sealed d-T generator tubes suffer from a short half-life of approximately 500 hours of operation; and making a practical and safe tritium gas target is difficult.

Aside from these technical difficulties, it is now widely accepted that d-T generators are unsuitable for fast neutron therapy because of their poor penetration and low neutron outputs. In 1986 a retrospective analysis was made on the complications observed in two groups of patients (330 head and neck cases and 128 pelvic cases) treated with fast neutrons<sup>67</sup>. The patients were stratified into four categories: those treated with low, intermediate, and high energy accelerator produced neutrons, and those treated with d-T generator produced neutrons. The observed complication rates decreased as the energy of the neutron beam increased. All of the clinical trials using d-T generators have been terminated.

There are currently more than ten facilities where modern clinical trials using fast neutrons are in progress. In these studies fast neutrons are produced by bombarding a beryllium target with accelerated proton or deuteron beams.

The usual neutron producing reactions for fast neutron therapy are:



where  $D/Q$  is the dose per accelerated charge (in Gy/C), and their values are obtained from the empirical expressions given by Wooton<sup>69</sup> for calculating the neutron dose rates achieved by these reactions at different energies of bombarding protons or deuterons ( $E_p$  or  $E_d$  in MeV). For the d-Be reaction, the neutron yield per  $\mu\text{C}$  of incident beam is approximately six times greater than for the p-Be reaction. Detailed design and performance specifications of cyclotron-based facilities have been described by Wooton<sup>69</sup>.

The locations of operating fast neutron radiotherapy centers in 1997 are listed in Table 7.2. In Table 7.2, an abbreviated notation for neutron production by accelerated particles are used: for example, the production of fast neutrons by 50 MeV protons on a Be target is abbreviated as p(50)Be. Among this list, Seattle, Seoul, and Faure have their proton beams transported to the targets mounted on isocentric gantries; whereas, in Detroit a superconducting cyclotron is mounted on an isocentric gantry.

Table 7.2
-----------

One of the notable fast neutron facilities is the superconducting cyclotron at the Gershenson Radiation Oncology Center of Harper Hospital in Detroit, Michigan<sup>70,71</sup> (Fig. 7.23). It is a 48 MeV deuteron cyclotron, which produces neutrons through the d(48)Be interaction in an internal thick Be target. Approximately flattened neutron fields of the size from 0 cm x 0 cm (collimator fully closed) to 26.5 cm x 30 cm (collimator fully open) are available. A deuteron beam current on target of 10  $\mu\text{A}$  produces a dose rate of ~32 cGy/minute at the

isocenter and at the depth of maximum dose (0.9 cm) for a 10 cm x 10 cm field. Deuteron beam currents of 12.5  $\mu\text{A}$  are routinely obtained to produce ~40 cGy/minute. The cyclotron rotates around the patient through 360° with a source-to-axis distance of 182.9 cm (6 feet). The depth at which 50% of maximum dose is obtained in water for a 10 cm x 10 cm field is  $D_0=13.4$  cm (Fig. 7.22). The surface dose for a 10 cm x 10 cm field is ~42% of the maximum dose. The isocentric mounting of the cyclotron and use of an internal target delivers clinical neutron beam into the patient without the need for beam extraction, beam transport and a bending magnet gantry to provide isocentric beam capability. This feature has the advantages of reducing cost and complexity. The simplified operation is expected to lead to increased reliability. The added complexity is maintaining the superconducting coil at liquid helium temperature in a hospital environment. A gantry-mounted cyclotron is restricted in supplying neutron beams to a patient on the treatment table at the rotation center of the gantry, and it is unable to channel the beams to other treatment rooms.

Fig. 7.23

Fig. 7.24 illustrates the medical facility setup at the National Accelerator Centre (NAC), Faure, South Africa, showing the fast neutron treatment area and proton therapy area. Here the beam from an accelerator is shared between two different treatment modalities, as well as with the nuclear physics users. The NAC facility is interesting that both fast neutron therapy and proton therapy are in one facility, and therefore more meaningful comparisons of clinical results from two modalities are expected.

Fig. 7.24

## Clinical Results of Fast Neutron Trials

The most recent comprehensive reviews of fast neutron radiotherapy are available in the papers by Griffin<sup>9</sup> and Wambersie<sup>65</sup>.

Earlier clinical trials from the early 1970s to the early 1980s found that the most promising sites for fast neutrons were salivary gland tumors, adenocarcinoma of the prostate, and soft tissue and bone sarcomas. Results of the treatment of squamous cell carcinoma of the head and neck and non-small cell lung cancer were equivocal, while in the treatment of brain, esophagus, pancreas, cervix and bladder tumors there was found to be no advantage over photon treatments.

Results from modern clinical trials conducted since 1984 show that fast neutrons are particularly effective in the treatment of adenoid cystic carcinoma of the salivary glands, a particularly slow growing tumor. Adenoid cystic carcinomas have been shown to have RBE values as high as 8.0 for neutron beams, whereas the RBE of normal tissues is ~3.0–3.2<sup>9</sup>. This implies that a 20 Gy dose of neutrons is equivalent to 160 Gy of conventional photons, which means a substantial therapeutic gain factor of ~2.5–2.7. The clinical results of fast neutron therapy for advanced unresectable salivary gland tumors demonstrate that it is highly effective (with a local control rate of ~67% compared to 24% for photon treatment) and should be regarded as the treatment of choice. Fast neutrons are also beneficial in the treatment of slowly growing well-differentiated soft tissue, osteogenic, and chondro sarcomas, and locally extended prostatic adenocarcinoma. In the treatment of bone sarcomas, neutron therapy is also regarded by some as a viable alternative to surgery involving limb amputation.

At Faure in South Africa there has been considerable interest in treating advanced breast cancer with neutron therapy, and a prospective trial comparing

neutrons with photons is now being planned<sup>72</sup>. The Faure group also reported encouraging results in the treatment of tumors of the maxillary antrum and paranasal sinuses in agreement with the results of Errington<sup>73</sup>. Fast neutrons have also been used in the treatment of unresectable malignant melanoma<sup>74</sup>.

Recent results in the treatment of non-small cell lung cancer have also suggested that patients with squamous cell histologies may benefit from fast neutron therapy and many neutron therapy centers have developed protocols for the treatment of lung cancer patients.

### **Future Development in Fast Neutron Therapy**

Fast neutron radiation therapy technology has evolved over the years to the point where it is now a reimbursable modality of choice for inoperable salivary gland tumors. On the basis of recent research data, it is emerging as a promising alternate modality for prostate adenocarcinoma, and soft-tissue and bone sarcomas. There is some evidence that squamous carcinoma of the lung, melanomas and paranasal sinus tumors may also be good prospects for fast neutron therapy in the future.

It would be a conservative estimate that ~5% of patients who at present receive conventional radiation treatments would benefit by fast neutron therapy. As there are ~0.5 million per year new cancer patients in the U.S. who receive conventional radiation therapy, ~100 fast neutron facilities will be needed to treat 25,000 patients.

In the past, many of the fast neutron therapy clinical trials were performed under severely disadvantageous conditions when compared with resources available in modern conventional therapy. To test the true efficacy of fast neutrons, the future

clinical trials must be performed with neutrons whose penetration and penumbra characteristics are as good as those of x rays from a modern linac. The clinical neutron beams should be isocentric, and the irregular ports should be defined by variable collimators.

#### F. NEUTRON CAPTURE THERAPY (NCT)

In 1936 Gordon Locher, a biophysicist working at the Franklin Institute of University of Pennsylvania, introduced a new form of cancer therapy using neutrons<sup>75</sup> only four years after the discovery of the particle by James Chadwick. Soon after, Gerald Kruger at University of Illinois also proposed a similar idea. The idea was to kill cancer cells by the  $\alpha$ -particles emitted as fission products after neutron captures by  $^{10}\text{B}$  nuclei. Using neutrons produced by a cyclotron at the Radiation Laboratory of the University of California, Berkeley, Kruger experimentally demonstrated his method<sup>76</sup>. This modality is now known as Neutron Capture Therapy (NCT), and when boron is used for the capture agent it is called Boron Neutron Capture Therapy (BNCT).

In proton and heavier ion radiation therapy, as well as in conventional therapy, attempts are made to reach all tumor cells with sufficient radiation dose by irradiating a target volume which is drawn around a known tumor volume with certain widths of margin. In BNCT, the role of finding all tumor cells is shifted to pharmaceutical agents. BNCT is a binary modality that brings together two components that when kept separate have only minor effects on cells. The first component is a stable isotope of boron,  $^{10}\text{B}$ , which is carried by a pharmaceutical

compound that concentrates selectively in the tumor cells when administered to the patient. The second is a beam of low-energy neutrons administered to the patient at a dose below the tolerance dose of the irradiated organs and tissues. The nuclei of  $^{10}\text{B}$  have a very large capture cross section for thermal neutrons, and break apart emitting very short-ranged high-LET  $\alpha$ -particles and  $^7\text{Li}$  nuclei. The ranges of these fission fragments ( $<10\ \mu\text{m}$ ) are shorter than the dimensions of a cell, and the fragments destroy cells in which capture took place while probably sparing neighboring cells. The success of this binary therapy depends on two factors, namely: the tumor selectivity of the  $^{10}\text{B}$  carrying drug and the availability of a neutron beam with a suitable energy spectrum and sufficient intensity.

A major advantage of a binary system is that each component can be manipulated independently of the other. With BNCT one can adjust the interval between administration of the capture agent and neutron irradiation to an optimum time when there is the highest differential in  $^{10}\text{B}$  concentrations between the tumor and normal tissues. Protection of normal tissues near and within the treatment volume is achieved by selective accumulation of  $^{10}\text{B}$  in the tumor. Furthermore, the neutron beam itself can be collimated so that the field of irradiation is circumscribed and normal tissues with high  $^{10}\text{B}$  concentration can be excluded from the treatment volume.

### **Early BNCT Clinical Trials**

In the 1950s BNCT was first used in a clinical trial to treat the most malignant and therapeutically resistant of all brain tumors, glioblastoma multiforme (GBM). GBM is a cancer of the glial supportive tissues of the central nervous system (CNS). Glial cells, which make up over 90% of the CNS, provide chemical

and physical support to neurons. Unlike neurons, glial cells are constantly undergoing mitosis, and this difference makes them susceptible to cancer. In 1951 Sweet and his colleagues, at Massachusetts General Hospital, started treating human GBM patients<sup>77</sup> using thermal neutron beams from the Brookhaven Graphite Research Reactor (BGRR) at Brookhaven National Laboratory (BNL). They continued treatment in 1959–1961 at the Brookhaven Medical Research Reactor (BMRR), which was specially built for this purpose. BNCT trials were also tried at the Massachusetts Institute of Technology research reactor (MITR-I) in 1959–1962. The capture agent used was sodium tetraborate, borax ( $\text{Na}_2\text{B}_4\text{O}_7 \cdot 10\text{H}_2\text{O}$ ). Unfortunately, boron concentrations were higher in the blood than in the tumors, and consequently severe radiation injury occurred to the vascular endothelium, resulting in radiation necrosis in the brain. Most of the patients in the trial showed a gradual deterioration, simulating GBM recurrences; however, autopsies revealed that the tumors were eradicated by the treatments. These failures were not due to flaws in the BNCT concept but from the biochemical and physical inadequacies encountered in the trials. There is now a consensus that these early trials failed because of the use of (a) inorganic boron compounds that lacked the necessary selectivity for malignant cells, and (b) thermal neutron beams that had a poor penetration in tissue (half-value layer,  $\text{HVL} \approx 1.8 \text{ cm}$ ) as thermal neutrons are rapidly attenuated in tissue due to absorption and scattering (Fig. 7.25).

Fig. 7.25

In spite of these poor clinical results, one of the researchers on Sweet's team, H. Hatanaka, returned to Japan to continue BNCT clinical trials in the early 1970s. Hatanaka reported encouraging clinical results in the treatment of malignant gliomas<sup>78</sup>, and Mishima reported similar results for melanoma<sup>79</sup>. These trials

used thermal neutrons and either sodium borocaptate (BSH) or boronophenylalanine (BPA) compounds. The Japanese teams reported the concentrations of  $^{10}\text{B}$  in tumor, the concentration ratios of tumor to normal tissue, and the concentration ratios of tumor to blood for BSH and BPA as listed in Table 7.3. BSH is excluded from healthy brain tissues, but concentrated similarly in tumor and in blood. BPA has a very low toxicity, a high affinity to tumor cells and a higher tumor-to-blood ratio. The Japanese treatments involved craniotomy to debulk the tumors about two weeks prior to the neutron irradiations. Because of the poor penetration of the thermal neutron beam, the scalp, skull and dura were reflected to expose the tumor bed directly to the incident neutrons. As with the early clinical trials in the U.S., these Japanese studies were also handicapped by inadequate neutron sources. Japanese researchers are currently exploring both epithermal and hyperthermal neutrons for treatment purposes.

Table 7.3

### **Renewed Interest in BNCT**

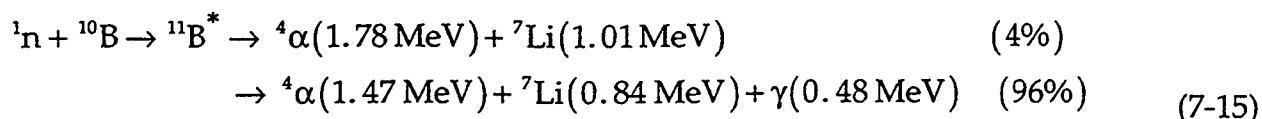
In the 1990s there has been renewed interest in BNCT in medical communities worldwide, and reaching its potential again appears promising. The recent development of improved epithermal neutron beams that can treat tumors in depth without surgery, and of improved drugs that give tumor-to-blood ratios approaching 3.5 or even higher, combine to give BNCT much more promise than it has shown in the past. Clinical trials for BNCT of high-grade GBM are in progress at BMRR since 1994<sup>80</sup>, and another trial has been started in 1997 at MITR-II.

The conventional treatment for GBM is external beam irradiation with 5-MeV x rays, given in total doses of ~60 Gy administered in fractions of 2.0 Gy daily, five days a week. Unfortunately, this method destroys much of the nearby healthy brain tissue in the beam path, and unless every cancer cell is killed, there is a possibility that the disease will recur. The median survival for conventionally treated GBM patients ranges ~8–14 months, while untreated patients have a median survival of ~3 months. Current BNCT trials suggest an increase of life expectancy and quality of life beyond that of conventional treatment, including the possibility of resuming employment. The ultimate objective of on-going research is, of course, a cure.

Although GBM is considered to be the top-priority target because its location and complicated geometry make it so resistant to complete removal through surgery, other cancers might well prove to be treatable with BNCT including anaplastic astrocytoma, squamous cell cancer of the head and neck, melanoma, and pancreatic cancer. For the latter two cases, local control may not improve overall survival if distant metastases are not treated.

### Rationale for BNCT

The  $^{10}\text{B}$  nucleus readily captures neutrons via the  $^{10}\text{B}(n,\alpha)^7\text{Li}$  reaction. Especially for very low-energy ( $<0.025$  eV, i.e., thermal) neutrons the capture cross-section reaches ~3840 barns ( $1 \text{ barn} = 10^{-24} \text{ cm}^2$ ), which is  $\sim 10^2$ – $10^7$  times greater than that of other nuclei in tissue components. The nuclear reactions of  $^{10}\text{B}$  capture of thermal neutrons produce  $^{11}\text{B}$  nuclei in the excited state, which very rapidly ( $\tau \approx 10^{-12}$  sec) decays in two fission reactions:



The outgoing  $\alpha$  particles and the recoil  ${}^7\text{Li}$  nuclei are slow, and therefore high-LET radiations. There is little cellular repair from radiation injury induced by these high-LET particles, the oxygen-effect is low, and the radiation effect is largely independent of the cell cycle. The  $\alpha$  particles and the  ${}^7\text{Li}$  nuclei travel very short distances,  $\sim 8\ \mu\text{m}$  and  $\sim 5\ \mu\text{m}$  respectively, probably damaging only the cells in which the boron neutron captures took place. A high concentration of  ${}^{10}\text{B}$  atoms in a tumor and a low concentration in surrounding normal tissues provides a significant therapeutic effect. This concentration difference is one of the keys to success with BNCT. Natural boron contains only  $\sim 20\%$   ${}^{10}\text{B}$ , with the remainder being  ${}^{11}\text{B}$  which does not exhibit high capture cross-section for thermal neutrons. Therefore, it is important to use enriched boron compounds ( $\sim 95\%$   ${}^{10}\text{B}$ ).

### Clinical Requirements

Among many stable nuclei that have high capture cross-sections for thermal neutrons (for example see Ref. 81),  ${}^{10}\text{B}$  is most intensely studied for NCT because of the many reasons listed below. It is not toxic and readily available, comprising  $\sim 20\%$  of naturally occurring boron. In addition, the particles emitted by the capture reaction ( $\alpha$  and  ${}^7\text{Li}$ ) are high-LET radiation, and their path lengths are approximately one cell diameter, thereby limiting the radiation effects to those tumor cells that have taken up a sufficient amount of  ${}^{10}\text{B}$  while sparing neighboring normal cells. Finally, and most importantly, the well-understood boron chemistry allows it to be readily incorporated into a multitude of different chemical structures.

### *Basic Requirements*

For BNCT to be clinically effective, how many  $^{10}\text{B}$  nuclei should be placed into each tumor cell? How large a thermal neutron fluence will be required? We will consider a set of very basic numbers with simple assumptions; however, these numbers will be useful as they can be scaled according to actual clinical conditions.

If a human glioma cell is assumed to be a sphere of a radius  $\approx 8 \mu\text{m}$ , its volume  $v$  is  $v \approx 2.15 \times 10^{-9} \text{ cm}^3$ , and its mass  $m$  is  $m \approx 2.15 \times 10^{-9} \text{ g}$ .

If we assume a  $^{10}\text{B}$  concentration of  $45.5 \mu\text{g}$  of  $^{10}\text{B}$  per gram of tissue (the value assumed at the current clinical trials at BMRR), then the number of  $^{10}\text{B}$  in each cell,  $n_{\text{B}}$  is:

$$n_{\text{B}} \approx 5.89 \times 10^9 \text{ }^{10}\text{B}/\text{cell}. \quad (7-16)$$

We will also assume a thermal neutron intensity at 2.5 cm depth to be  $\approx 1.9 \times 10^9$  neutrons/ $(\text{cm}^2 \cdot \text{s})$ , which is a typical number obtainable at existing nuclear reactors. In a 40-minute treatment time, the delivered thermal neutron fluence,  $\phi_{\text{th}}$ , becomes:

$$\phi_{\text{th}} \approx 4.56 \times 10^{12} \text{ neutrons}/\text{cm}^2. \quad (7-17)$$

Using the capture cross-section of  $\sigma = 3840$  barns, the number of boron neutron captures per cell,  $n_{\text{capt}}$ , may be calculated as:

$$\begin{aligned} n_{\text{capt}} &= \sigma \cdot \phi_{\text{th}} \cdot n_{\text{B}} & (7-18) \\ &\approx 3.84 \times 10^{-21} (\text{cm}^2) \cdot 4.56 \times 10^{12} (1/\text{cm}^2) \cdot 5.89 \times 10^9 (1/\text{cell}) \\ &\approx 103 \text{ captures / cell} \end{aligned}$$

As each boron neutron capture dissipates  $\Delta E=2.31$  MeV (fission fragment tracks are assumed to stay within a cell), the physical dose due to boron neutron captures becomes:

$$D_B = n_{\text{capt}} \cdot \Delta E / m \quad (7-19)$$

$$\approx 103 \cdot 2.31 \text{ MeV} / 2.15 \times 10^{-9} \text{ g} \approx 17.7 \text{ Gy} = 1770 \text{ rad.}$$

The dose  $D_B$  is often called the 'boron absorbed dose.' Remember that  $D_B$  is the *physical* dose due to the boron captures. The '*biological* boron dose,'  $\mathcal{D}_B$ , depends not only on the elevated value of RBE of the high-LET fission fragments, but also on compound specific properties expressed in a parameter called 'Compound Factor' (CF). Because of the extreme shortness of the fission fragment tracks emanating from the  $^{10}\text{B}$  neutron captures, the biologic effects critically depends on whether  $^{10}\text{B}$  nuclei are incorporated in the tumor DNA, in the cytoplasm and how far from DNAs, or on the surface of the cell. CF relates the impact of the cellular and subcellular localization of different boron compounds and their metabolites on the radiobiological effects of the high-LET boron capture dose. The biological boron dose,  $\mathcal{D}_B$ , is given by:

$$\mathcal{D}_B = \text{CF} \cdot D_B, \quad (7-20)$$

where the value of the tumor compound factor is  $\approx 3.8$  and the normal tissue compound factor is  $\approx 1.3^{80}$ . For the situation illustrated above, the value of biological boron dose becomes in gray-equivalent units:

$$\mathcal{D}_B = \text{CF} \cdot D_B \approx 3.8 \times 17.7 \text{ Gy} \approx 67.3 \text{ Gy-EQ.} \quad (7-21)$$

The importance of this biological dose is that it is the extra dose administered to those cells that contain  $^{10}\text{B}$  nuclei over and above the background dose due to the neutron beam. If the background dose is kept under the tolerance dose of the

irradiated organ (e.g., brain), and the sum of the background dose and the biological boron dose is greater than the tumoricidal dose of the tumor (e.g., GBM), then BNCT will be successful. For BNCT to be effective, one must strive to satisfy the following inequalities:

$$\mathcal{D}_B \geq (\text{Tumoricidal dose}) - (\text{Tolerance dose of irradiated organs}), \quad (7-22)$$

$$(\text{Background dose}) \leq (\text{Tolerance dose of irradiated organs}), \quad (7-23)$$

where all doses are biological doses in Gy-Eq units. These conditions may be achieved by providing a high boron concentration in tumor cells ( $n_B$ ) and/or a high thermal neutron fluence ( $\phi_{th}$ ) in the tumor cells. In practice, boron concentrations in normal tissue cells are not zero, and their effects should be added to the background dose.

### *Background Dose Calculation*

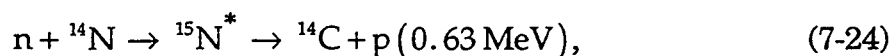
As in other radiotherapy modalities, the basic requirement for successful BNCT is to deliver a tumoricidal dose to the target volume without exceeding the tolerance dose limits of surrounding normal tissues and organs. In BNCT the tumor dose is boosted by a high  $^{10}\text{B}$  concentration in the tumor cells. Neutrons not captured by  $^{10}\text{B}$  nuclei produce unwanted background radiation through a number of reactions with normal nuclei in tissue, such as nitrogen, hydrogen, carbon, and chlorine. Additionally, there are contaminations in the neutron beam, such as the  $\gamma$  rays from the reactor core or fast neutron components not filtered out from the beam. These background radiations equally contribute to the dose in normal tissue and tumor volumes independent of  $^{10}\text{B}$  concentration.

The rationale of BNCT rests on the fact that the nuclear capture cross-sections of normal tissue elements for thermal neutrons are much smaller than that for  $^{10}\text{B}$ .

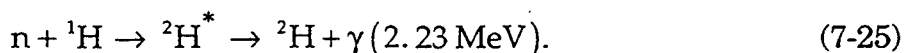
Even at a level of  $^{10}\text{B}$  concentration in tumor cells, ~45.5 ppm, there are, for example, ~15,000 times more oxygen atoms in the tissue, yet their thermal neutron captures contribute little to the radiation dose. Probabilities of thermal neutron captures by normal elements in tissue are shown in Table 7.4.

Table 7.4
-----------

From the numbers in Table 7.4, it is obvious that hydrogen and nitrogen contribute most to background radiation. The  $^{14}\text{N}(n,p)^{14}\text{C}$  neutron capture reaction produces very high-LET protons through the reaction:



and contributes to the so-called 'nitrogen dose' ( $D_N$ ). The main contributor to the 'gamma dose' ( $D_\gamma$ ) comes from the hydrogen capture reaction,  $^1\text{H}(n,\gamma)^2\text{H}$ , viz.:



In addition, neutrons lose their energy by scattering with hydrogen nuclei,  $^1\text{H}(n,n')^1\text{H}$ , which results in energetic recoil protons as secondary particles that deposit the 'recoil proton dose' ( $D_R$ ).  $D_R$  is obviously sensitive to the energy spectrum of the neutron beam, where higher energy (>20 keV) neutrons produce more recoil protons. Therefore, elimination of fast neutrons from clinical neutron beams becomes one of the most critical criteria of the neutron beam shaping requirement for BNCT. The unwanted radiations may be reduced by carefully tailoring the energy spectrum of the epithermal neutron beam, but can never be fully eliminated. The boron concentration in tumor of the order of 40–50  $\mu\text{g}$  of  $^{10}\text{B}$  per gram of tissue ( $6.0\text{--}7.5 \times 10^9$   $^{10}\text{B}$  nuclei/cell) will provide ~80% of total dose from  $^{10}\text{B}$  fission reactions. For successful BNCT, boron compounds that reach high concentrations in tumor tissue but not in blood and normal structures in the brain must be developed. The boron differential between tumor and

surrounding normal tissues irradiated by the neutron beam should be as high as possible so that normal tissue tolerance is not exceeded, while depositing enough dose to destroy tumor cells.

### *BNCT Dose Calculation*

Therapy planning of BNCT using epithermal neutron beams requires calculation of the biological dose distributions in tumor and normal tissues. In this calculation, one must take into consideration the fact that the different kinds of radiation contributing to the total dose have different values of RBE.

Furthermore, the biological boron dose due to neutron capture by the  $^{10}\text{B}$  nuclei depends on the Compound Factor (CF) as mentioned above. The compound factor and RBE make it possible to add the different dose components and calculate the total dose,  $\mathcal{D}_{\text{tot}}$ , in a photon-equivalent dose expressed in gray-equivalent (Gy-Eq) units:

$$\mathcal{D}_{\text{tot}} = \text{CF} \cdot D_{\text{B}} + \text{RBE}_{\text{N}} \cdot D_{\text{N}} + \text{RBE}_{\text{r}} \cdot D_{\text{r}} + \text{RBE}_{\gamma} \cdot D_{\gamma}. \quad (7-26)$$

To illustrate typical doses encountered in BNCT today, we will follow the dose calculation protocol developed for the BNCT clinical trial at BMRR<sup>82</sup>. This trial established boron concentrations and compound factors for the boron compound BPA. The values to be used are: normal tissue  $^{10}\text{B}$  concentration  $\approx 13$  ppm, normal tissue compound factor  $\approx 1.3$ , tumor  $^{10}\text{B}$  concentration  $\approx 45.5$  ppm, tumor compound factor  $\approx 3.8$ , fast neutron RBE,  $\text{RBE}_{\text{r}} \approx 3.2$ , nitrogen capture RBE,  $\text{RBE}_{\text{N}} \approx 3.2$ , and  $\gamma$ -ray RBE,  $\text{RBE}_{\gamma} \approx 1.0$ .

Once the spatial and energy distributions of a neutron beam, its  $\gamma$ -ray contamination, and the spatial distribution of  $^{10}\text{B}$  concentration are known inside the patient's body (or phantom), the biologically effective dose distribution can be calculated based on Eq. (7-26). As an illustration, shown in Fig. 7.26 are normal-

tissue depth-dose curves of boron dose ( $D_B$ ), gamma dose ( $D_\gamma$ ), proton-recoil dose ( $D_R$ ), nitrogen dose ( $D_N$ ), and the total dose as a function of the depth in a phantom. In this calculation, epithermal neutrons are produced by  ${}^7\text{Li}(p,n)$  reaction by 2.4 MeV protons and neutron energies are modified using an Al/AlF<sub>3</sub> moderator assembly<sup>83</sup>. In current treatments of GBM a patient is irradiated until the normal tissue dose limit is reached. Delivering a tumoricidal dose to the distal end of a deep seated tumor is, at present, not always possible. The BMRR protocol sets the maximum normal brain equivalent dose to 12.5 Gy-Eq. The maximum entrance surface dose should also be limited in order to limit radiation injury to the scalp. Doses to other organs and the whole body must be considered in the actual treatment planning process since they may impose limitations and may require special beam collimation and patient shielding in particular BNCT treatments.

Fig. 7.26

## Progress in Borated Compounds

### *Boron Compounds Used in BNCT Clinical Trials*

The two compounds that are being used in clinical trials in the U.S. and Japan are sodium undecahydro-mercapto-closo-dodecaborate ( $\text{Na}_2\text{B}_{12}\text{H}_{11}\text{SH}$ , also known as sodium borocaptate or BSH) and boronophenylalanine (BPA). These drugs are not new; both were synthesized and evaluated in the 1950s. BSH and BPA are tumor selective but not tumor specific compounds; nevertheless, clinical trials with BSH and BPA are in progress as they have more desirable biological properties than the compound used in the earlier clinical trials. The proposed clinical trials at reactors in Japan and at Petten, The Netherlands plan to use

BSH. BPA that is complexed to fructose (BPA-F) for enhanced solubility is used in clinical trials at BNL and MIT.

For example, Coderre and colleagues have demonstrated a therapeutic gain with BPA using the rat brain and rat 9L gliosarcoma models<sup>84</sup>. Tumors were cured with BNCT without detectable sequelae, while animals cured by photons showed severe evidence of histologic damage. BPA has been used to treat patients with GBM or ocular melanoma in Japan, Australia, and the U.S. The complexation of BPA with fructose increases its solubility in solution, and provides both tumor-to-blood concentration ratios of 3.6:1.

There is currently much effort to produce borated compounds that satisfy the crucial attributes of neutron capture agents for the successful working of BNCT. The desired clinical attributes are: ability to place more than 45.5  $\mu\text{g}$  of  $^{10}\text{B}$  per gram of tissue (a BMRR assumption, which translates to  $\sim 6 \times 10^9$   $^{10}\text{B}$  per tumor cell, see Eq. (7-16)) while depositing lower concentrations in normal dose limiting cells (i.e., vascular endothelium) in the path of the neutron beam; tumor selectivity resulting in  $^{10}\text{B}$  concentrations of high tumor/brain and tumor/blood ratios; and longer  $^{10}\text{B}$  retention times in the tumor and fast clearance from brain and blood. The ideal compounds should achieve high intracellular concentration in the tumor and preferably be bound to or incorporated into DNA, which is the ultimate target. Furthermore, such compounds should be able to cross the normal blood-brain barrier (BBB) and seek out those neoplastic cells that may be protected by this barrier. The BBB is formed by tight junctions of endothelial cells lining cerebral blood vessels and capillaries, and effectively limits the delivery of therapeutic agents to brain tumors and surrounding brain tissues. The BBB often becomes 'leaky' when tumors are present.

### *Development of New Boron Compounds for BNCT*

Discussions of the synthetic chemistry, pharmacology, pharmacokinetics (intercellular, in tissues, in organs), toxicology, and radiation biology of such drugs are outside of the scope of this article. For completeness, a brief description of boron compounds under development is presented. For an in-depth study of the subject, readers are referred to many available review articles<sup>85,86</sup>.

In a recent review paper, Soloway and his colleagues have listed the boron compounds used in BNCT<sup>87</sup>. Boron compounds for BNCT can be divided into two broad categories: (1) simple small molecular compounds; and (2) large complex molecular species. Synthetic boron analogues of cell building blocks are examples of the simple small molecular compounds. Brain tumor cells are either metabolically more active or have higher mitotic indices compared to normal brain cells, and therefore may take up such precursors, if the boron analogues simulate natural compounds. Examples in this group are boronated phospholipid ethers that may selectively accumulate in tumor plasma membranes, boron-containing amino acids that may be incorporated into tumor proteins, and boron-containing nucleosides that can be converted to nucleotides and subsequently incorporated into DNA and RNA. Porphyrins, DNA intercalators, radiation sensitizers, and polyamines also belong to this group. Macromolecular species of boron compounds include boronated liposomes, low-density lipoproteins, antisense oligonucleotides, antibodies and their fragments, bispecific antibodies, and tumor receptor binders. In all cases, it is essential that the agents be able to cross the BBB and accumulate in the tumor cells, whether or not the barrier is impaired. This requirement applies to both low and high molecular weight delivery agents. Large complex molecular species, due to their

size, may lack the ability to cross this barrier; and, for this reason, BBB disruption has been proposed as a means for achieving this objective.

Preliminary studies at the University of California, San Francisco with BOPP<sup>88</sup>, a boronated porphyrin, suggest that higher tumor concentrations can be achieved with BOPP than with BPA. BOPP is about 30% boron by weight (compared to less than 5% for BPA), is readily prepared in high yield from common starting materials, and is highly water-soluble (unlike BPA). Tumor boron levels in animal-model systems have consistently been measured in the 60-80 ppm range, which is ~2 times that necessary to carry out BNCT treatments of brain tumors and about twice that available from BPA. Biokinetics and toxicity studies with BOPP are in progress.

Malignant glioma may not be the only target for BNCT, as drugs will become available that concentrate in other tumors, such as anaplastic astrocytoma, squamous cell cancer of the head and neck, melanoma, pancreatic tumors, and sarcoma, potential gains in tumor control and long-term survival for these diseases may be achieved.

### *Possible NCT Isotopes Other Than $^{10}\text{B}$*

Nuclei other than  $^{10}\text{B}$  have been investigated for NCT.  $^{157}\text{Gd}(n,\gamma)$  capture reaction is also studied as an alternative to  $^{10}\text{B}$ . Gamma rays from  $^{157}\text{Gd}(n,\gamma)$  reactions are not localized within a cell dimension, but some of the associated internal conversion (IC) electrons and Auger (and Coster-Kronig) electrons are localized to enhance cell killing effect<sup>89</sup>. When  $^{151}\text{Eu}$  is irradiated with thermal neutrons, the  $^{151}\text{Eu}$  turns into  $^{152}\text{Eu}$  ( $\sigma \approx 5900$  barns) and photons of a total energy of 6.26 MeV are released. It may also be turned into metastable  $^{152}\text{Eu}$  ( $\sigma \approx 3300$  barns) emitting 6.3 MeV  $\gamma$  rays. Metastable  $^{152}\text{Eu}$  of half-life 9.32 hours decays to  $^{152}\text{Gd}$  via beta decay

(76%) and to  $^{152}\text{Sm}$  via electron capture (24%). The  $^{151}\text{Eu}$ -containing cells irradiated with thermal neutrons will emit two radiation components: spontaneously emitted photons and electrons emitted with half-life of 9.32 hours. Therefore, NCT with  $^{151}\text{Eu}$  as a capture agent will be a two step process: high dose rate brachytherapy followed by the low dose irradiation<sup>90</sup>. Also considered is the uranium isotope  $^{235}\text{U}$  which emits heavy fission fragments after capturing neutrons. The biological effectiveness of the fission fragments has been found to be very high, but no practical uranium compound with selective affinity to tumors has been identified<sup>91</sup>.

### **Nuclear Reactor Sources of Epithermal Neutrons for BNCT**

The only currently available neutron sources that can deliver a sufficient thermal neutron fluence,  $\phi_{\text{th}} \approx 4.56 \times 10^{12}$  neutrons/cm<sup>2</sup>, are nuclear reactors. However, the construction of new reactors for BNCT in a metropolitan area is not a realistic expectation, and therefore non-reactor neutron sources, such as accelerator-based sources, are seriously being considered for implementation of BNCT at medical centers.

#### ***Reactor-Based Epithermal Neutron Sources***

Early clinical trials in the U.S. and recent trials in Japan have relied on thermal neutron beams readily available from nuclear reactors. These beams lacked the ability to penetrate tissue and deliver suitable neutron fluxes to the tumors beyond 2-3 cm (see Fig. 7.25). It was necessary to reflect the scalp and bone flaps in the beam path to let the thermal neutrons enter the brain directly at the site of tumor resection. To avoid this difficulty Fairchild and colleagues at BNL produced epithermal neutron beams by optimizing the combination of  $\text{Al}/\text{D}_2\text{O}/\text{Al}_2\text{O}_3$  for moderator/filter assembly<sup>92</sup>. The epithermal neutrons lose their energy as they

penetrate tissue, and are consequently thermalized, producing maximum thermal neutron fluxes at depths that are several cm below the surface. Such epithermal neutron beams (Fig. 7.25) let thermal neutrons into shallow tumors without the need to reflect scalp and bone flaps. To prepare such a beam the energy spectrum of a neutron beam from the reactor core is shaped using moderator/filter assemblies, which shift the energies of the neutrons from the high energy range to the epithermal range (1 eV-10 keV), reduce the harmful fast neutrons (>25 keV), and suppress the contribution of low-LET  $\gamma$  rays from the reactor core. In practice, however, epithermal neutron beams prepared for BNCT at nuclear reactors are composed not only of those neutrons with the desired spectral characteristics, but are contaminated by those with higher and lower energies and by  $\gamma$  rays.

The use of a moderator/filter assembly to shape the energy spectrum of reactor neutrons into the one optimal for BNCT necessarily reduces the neutron fluence rate. All the reactors considered for BNCT are severely limited in available neutron fluence rate. Because the patient must be treated in a reasonable length of time, the designers of the beams are forced to make compromises in the process of beam optimization as the process usually reduces the available fluence rate. For future BNCT facilities, whether reactor-based or accelerator-based, it is desirable to limit the treatment time to less than one hour (the typical treatment time at BMRR is ~40 minutes) for the following reasons: (1) the boron compounds get washed out of the tumor cells over time— for example, the concentration of BPA in tumor is greatly reduced after several hours, (2) patient comfort can be a limitation, and (3) short treatment times are desirable at future hospital-based BNCT facilities for operational reasons.

The limited number of nuclear reactors possessing adequate fluxes has led to a consideration of the use of fission plate technology that could be applied to reactors that otherwise would not generate a sufficient epithermal flux. The use of fission plates increases the neutron flux and thereby would expand the number of existing reactors that could be adapted for BNCT.

### *Reactors for BNCT*

There are many nuclear reactors with a suitable neutron spectrum for BNCT; however, not all of them are usable for BNCT primarily because the attainable epithermal neutron fluence at the tumor position is too low. The patient must be positioned as close to the reactor as possible since the fluence rate decreases by  $1/r^2$ . In many situations it is not possible to place a clinical facility inside a reactor facility because most reactors are contained inside pressure vessels surrounded by shielding, and some are located in containment buildings or underwater in pools. In many other cases, it costs too much to convert existing research reactors to accommodate clinical facilities.

Epithermal neutron beams of suitable fluence rate can be obtained at several nuclear reactors. The early BNCT research in Japan was conducted at the Kyoto University Reactor (KUR), and at the reactors of the Japan Atomic Energy Research Institute (JAERI) in Tokai, and other reactor sites. In 1997 the only active BNCT clinical trial is being conducted at the remodeled Kyoto University Reactor (KUR), which is a 5 MW light-water moderated, tank-type research reactor with 93 % fuel enrichment. An energy-converter fission plate (90% enriched uranium, 1 kg, 25 cm in diameter) producing  $3 \times 10^{10}$  fission/sec, is available for fast neutron experiments. An irradiation room of 2.4 x 2.4 x 3.6 m is an integral part of the facility. Remodeling of the Heavy Water Thermal Neutron Irradiation Facility of the reactor in 1995–1996 and a new heavy-water shutter

system allow clinical irradiations during continuous operation of the KUR at full power. The updated facility can provide neutrons with energy spectra ranging from nearly pure thermal (pure Maxwellian distribution) neutrons to epithermal neutrons. The epithermal neutrons are shaped by an 80% Al/20% D<sub>2</sub>O moderator, a D<sub>2</sub>O spectrum shifter, and boral and cadmium thermal neutron filters.

In 1997 in the U.S. clinical BNCT trials are conducted at BMRR and MITR-II (Fig 27). Another reactor facility considered for BNCT, because of its outstanding neutron beam fluence rate and beam quality, is the Missouri University Research Reactor (MURR). The conversion of Washington State University reactor may provide a new animal irradiation facility. Outside the U.S., the High Flux Reactor (HFR) at Petten in the Netherlands<sup>93</sup>, and a TRIGA-II reactor (FiR-I) at Epsoo, Finland<sup>94</sup> are prepared for clinical trials.

Fig. 7.27

Table 7.5 summarizes the physical characteristics of reactors available for BNCT<sup>95</sup>. The parameter 'current/fluence rate' ( $J/\phi$ ) is used to indicate the forward directionality of the neutrons, which would range from 0.5 for a completely isotropic beam to 1.0 for a purely parallel beam toward the patient.

Table 7.5

### Alternative neutron sources for BNCT

One of alternative sources for the epithermal neutrons for BNCT is the isotope Californium-252. <sup>252</sup>Cf has a half-life of 2.645 years, and one gram of <sup>252</sup>Cf has a prompt neutron emission rate of  $2.31 \times 10^{12}$  neutrons/sec. The entire supply of <sup>252</sup>Cf for the western world comes from the High Flux Isotope Reactor (HFIR) at the Oak Ridge National Laboratory, which produces <1 g/year. Over a gram of <sup>252</sup>Cf is

needed to produce an epithermal neutron beam of sufficient strength, thus this option is economically unfeasible.

### *Accelerator-Based BNCT*

The construction of new reactors for BNCT in a metropolitan area is not a realistic expectation because of the rejection of the technology by the public as well as high operating and eventual decommissioning costs. Thus, non-reactor neutron sources, such as accelerator-based sources, are seriously considered for implementation of BNCT at medical centers. Accelerator-based sources would also provide epithermal neutron beams with more desirable neutron energy spectra than those obtainable from nuclear reactors. Furthermore, the accelerated proton energy, moderator/filter assembly configuration, and neutron beam collimator can relatively easily be changed to optimize the neutron beam for each patient configuration. The future of BNCT is clearly accelerator-based.

Accelerator-based neutron sources consist of an accelerator, a neutron production target and a moderator/filter assembly for shaping the epithermal neutron beam. A higher neutron yield at the production target may not necessarily result in a higher thermal neutron fluence in the treatment volume if there are high energy components that must be severely moderated or filtered out. The entire process of modeling the neutron beams from the production target, through a moderator/filter assembly, and into a phantom is necessary for evaluating different neutron sources for BNCT.

A variety of accelerator-based neutron sources for BNCT has been proposed and investigated<sup>10</sup>. The most promising options are those relying on accelerated protons or deuterons to produce neutrons in Li or Be targets. Other interesting options are neutron production near the threshold of the  ${}^7\text{Li}(p,n){}^7\text{Be}$  reaction<sup>96</sup>

and photo-neutron sources<sup>97</sup>. Recently Bleuel et al. reviewed the epithermal neutron production through  ${}^9\text{Be}(p,n)$ ,  ${}^9\text{Be}(d,n)$ , and  ${}^7\text{Li}(p,n)$  reactions<sup>83</sup>. The neutron yields of these reactions vary by two orders of magnitude. The  ${}^9\text{Be}(p,n)$  reaction at a proton energy  $E_p = 19$  MeV produces the highest total neutron yield of  $\sim 6 \times 10^{13}$  neutrons (for neutrons energies  $E_n \geq 0.7$  MeV) per millicoulomb of incident protons (n/mC). But the neutron energy spectrum extends to  $E_n \approx 15$  MeV necessitating a thick moderator, and therefore loss of the neutron fluence rate. At  $E_p = 4$  MeV the upper neutron energy limit drops to  $E_n \approx 2$  MeV but the neutron yield is much reduced. The neutron spectrum of the  ${}^9\text{Be}(d,n)$  reaction at a deuteron energy  $E_d = 2.6$  MeV exhibits its highest yield at neutron energies  $E_n \leq 2$  MeV, but also features high energy components up to  $E_n \approx 6$  MeV. The upper neutron energy for the  ${}^7\text{Li}(p,n){}^7\text{Be}$  reaction at  $E_p = 2.4$  MeV is 700 keV and the total yield is  $\sim 7.69 \times 10^{11}$  n/mC. As can be seen in Table 7.6 the beam current requirement is dramatically lowered when bombarding a Be target with 19 MeV protons. Compact cyclotrons are an attractive option for providing beam currents of a few mA at energies between 10 and 20 MeV. Although such neutron sources may be suitable for BNCT, because the neutron energies are so high that they can not match the quality of the epithermal neutron beams that can be produced at lower proton beam energies.

Table 7.6

### *Comparison Between Epithermal Neutron Beams from Reactors and Accelerators*

To arrive at accelerator specifications for an accelerator-based BNCT facility, Bleuel et al. performed a detailed calculation of neutron yields for  ${}^7\text{Li}(p,n){}^7\text{Be}$ ,  ${}^9\text{Be}(p,n)$ , and  ${}^9\text{Be}(d,n)$  reactions<sup>83</sup>. Significantly lower thermal fluences, particularly at more than 3 cm depth, were found for the sources for which the

primary neutron energy spectrum extends to higher energies,  $^9\text{Be}(p,n)$  at 19 MeV,  $^9\text{Be}(d,n)$ , and the fission reactor. This is due to the increased moderator thickness needed for the suppression of the recoil proton dose. This discussion was based on single beam treatments of brain tumors although in practice two or more fields, e.g., parallel opposed ports, are often used. At proton beam energies of 4 MeV the thermal fluence distribution for the  $^9\text{Be}(p,n)$  source is closer to that of the  $^7\text{Li}(p,n)$  source. Table 7.6 lists for each source the equivalent tumor doses at the point of maximum thermal fluence, at 5 cm depth, and at 8 cm depth. It also gives the beam currents required to match the BMRR treatment time of 40 min. The range given for the neutron sources using a beryllium target reflects the uncertainties in the neutron yield estimates.

Studies have identified a  $^7\text{Li}$  target as an excellent choice for producing neutrons for BNCT via the  $^7\text{Li}(p,n)^7\text{Be}$  reaction. This reaction has a 1.88 MeV proton energy threshold, and a prominent resonance at 2.3 MeV which drops sharply at 2.5 MeV. Therefore, use of 2.5 MeV protons is generally thought to produce the highest neutron yield for BNCT. Bleuel et al. have studied the dose rate and quality of the epithermal neutron beam as a function of moderator thickness and incident proton energy for three moderator materials, namely, BeO, D<sub>2</sub>O, and Al/AlF<sub>3</sub><sup>98</sup>. The useful (1 eV to 10 keV) neutron flux peaks at an incident proton energy around 2.3 MeV, where the epithermal neutron flux is roughly 35% higher than that at a proton energy of 2.5 MeV. The neutron energy spectrum can be varied by changing the proton beam energy and moderator thickness with the potential of optimization for different tumor depths. Therefore, the accelerated proton energy should be tunable from 2.0 to 2.5 MeV. Bleuel et al. have also shown that 2.3–2.5 MeV protons at a current of 20 mA impinging onto a Li target produce enough neutrons to achieve the same dose rate available at the BMRR

operating at 3 MW, and with appropriate moderation and filtering, provide a clinically superior neutron energy spectrum. Therefore, the accelerated proton current should exceed 20 mA d.c.

In Fig. 7.28, the epithermal neutron spectrum obtained at the BMRR is compared with that calculated for neutrons obtainable from  ${}^7\text{Li}(p,n)$  reaction for an incident energy of proton at 2.4 MeV. Accelerator-produced epithermal neutrons exhibit higher penetration than reactor-produced neutrons; the maximum dose occurs deeper for the accelerator-produced neutrons than for the reactor-produced neutrons.

Fig. 7.28

### *Accelerator Options for BNCT*

#### *ESQ-based BNCT system developed at LBNL in Berkeley, California*

At LBNL, Kwan et al. have been developing high-current D.C. accelerators using electrostatic quadrupole (ESQ) columns for neutral particle beam injectors for tokamak fusion reactors, and injectors for heavy ion induction linear accelerators (for inertial fusion reactors)<sup>99</sup>. An ESQ accelerating a 200 keV of  $\text{He}^+$  beam to 100 mA and another 2.0 MeV ESQ injector delivering 800 mA of  $\text{K}^+$  beam of 1- $\mu\text{s}$  long pulses have been successfully tested. This technology is ripe, and will be able to produce an accelerator which is well suited for BNCT applications<sup>100</sup>.

Accelerators using electrostatic quadrupole (ESQ) columns can be operated with a high beam current, variable beam energies, and a high reliability. The key advantage of an ESQ accelerator is that the transverse focusing can be very strong without incurring a longitudinal field exceeding the breakdown limit. In addition, the secondary electrons generated within the accelerator column are quickly removed by the strong transverse electric field instead of being allowed to

multiply and then develop into a column arc-down. The LBNL BNCT accelerator has been designed for 100 mA proton beam current. A new power supply, an air-core multistage transformer-rectifier stack will allow operation at a proton current exceeding 50 mA<sup>101</sup>. The size of such an accelerator, ~5 m in length and ~2 m in diameter including the power supply, is suitable for placing in the hospital environment (Fig. 7.29). Located at the front end is a multicusp ion source that can deliver positive hydrogen ion beams with monoatomic ion fraction higher than 90%<sup>102</sup>. Accelerating molecular hydrogen will contribute excess heat load in the neutron production target without producing neutrons, and therefore a high purity proton source is desired. An extractable hydrogen ion current density of 100 mA/cm<sup>2</sup> has been achieved demonstrating that this ion source can meet the requirement for BNCT. Computer simulation showed that the ESQ column can accelerate up to an 125-mA beam<sup>100</sup>.

Fig. 7.29

A crucial component of an accelerator-based neutron source is the neutron production target. Because metallic lithium has a low melting point of 179°C, very effective target cooling is mandatory. In the LBNL design, a 50 μm thick Li layer is deposited on an aluminum backing. Applying the microchannel absorber concept<sup>103</sup> many channels are cut into the substrate for convective water cooling. The result of a finite element analysis and a recent heat-load test of a prototype aluminum panel, performed at the Plasma Materials Test Facility at Sandia National Laboratory indicate that for a heat-load of ~600 W/cm<sup>2</sup> the surface temperature can be kept below 150°C. Further analyses showed that by optimizing the beam profile and increasing the target area up to 15 cm x 15 cm beam currents of up to 50 mA can be handled.

The ESQ technology opens up the possibility of building a high-current, D.C. electrostatic accelerator that can meet the requirements of BNCT. Simulation calculations indicate that an accelerator-based neutron source for BNCT is practical and superior to reactor-produced neutron sources.

### ***Other Types of Accelerators for BNCT***

A recent symposium proceedings show many other developments in accelerators for BNCT<sup>10</sup>. At MIT's Laboratory Accelerator Beam Applications (LABA), a tandem accelerator is studied to produce proton or deuteron beams with energies up to 4.1 MeV and total power levels of up to 10 kW<sup>104</sup>. Beam currents of up to 4 mA are possible using a multicusp, high current negative ion source in combination with magnetic suppression of secondary particles along the accelerating tube. At Birmingham, UK, Beynon and colleagues are preparing an accelerator-based BNCT facility<sup>105</sup>. The existing Dynamitron accelerator is upgraded to produce ~5 mA of 3 MeV H<sup>+</sup> D.C. current, and a stable Li target is designed to be used with <sup>7</sup>Li(p,n) reaction.

### **Other Applications of BNCT**

#### ***BNCT Enhanced Fast-Neutron Therapy***

A hybrid method that combines the features of fast-neutron therapy and BNCT is also currently a subject of increasing research interest. In BNCT enhanced fast-neutron therapy, a neutron capture agent is introduced preferentially into the malignant tissue prior to the administration of fast-neutron therapy. Because a small fraction of the neutrons from the high-energy treatment beam are thermalized in the irradiation volume, it is possible to obtain a selective incremental absorbed dose within the target volume from the neutron capture

interactions that result<sup>106</sup>. In some cases this incremental dose, or 'augmentation' may be sufficient to produce a dramatic improvement in tumor control probability. This idea is currently under investigation at the University of Washington and elsewhere<sup>107</sup>.

### *Boron Neutron Capture Synovectomy*

Boron neutron capture synovectomy is an approach to treat rheumatoid arthritis relying on the use of  $^{10}\text{B}(n,\alpha)$  reaction for the destruction of inflamed synovium<sup>108</sup>.

### **Future Development of BNCT**

In the treatment of tumors close to the midline of brain, 5-8 cm deep, epithermal beams with higher energy than what is currently available at reactors may be required. As discussed above, an ESQ-based BNCT facility can produce such epithermal neutrons with a sufficient flux for BNCT. It will not be possible to achieve it at reactors without a great sacrifice in delivered neutron flux because the fission neutrons start out at energies too high. The window for therapeutic success in which a tumoricidal dose is delivered while staying under the tolerance doses of surrounding healthy tissues is narrow for BNCT, probably narrower than those for other hadron therapy modalities. Widening the window should be tried both in developing more effective boron compounds and more effective epithermal neutron beams. Accelerator-based epithermal neutron sources should be built, and the clinical efficacy derived from reactor-produced neutrons and that from accelerator-produced neutrons should be compared.

More effective boron compounds must be developed that are capable of crossing the blood brain barrier, or to do so through BBB disruption, and of reaching the tumor cells, even those dispersed in healthy brain at various distances from the

primary tumor. The compounds must possess pharmacokinetics characteristics (e.g., boron retaining time in tumor, clearing time from blood, etc.) suitable for BNCT.

BNCT has been used clinically in Japan since 1968, and in the U.S. since 1995 and may be initiated in Europe within the next few years. When these studies have been completed, it finally should be possible to conclude whether or not BNCT has a place in treating presently incurable tumors of the CNS.

Because successful BNCT may require that a significant fraction, if not all subpopulations, of tumor cells have adequate concentrations of boron compound, it seems highly unlikely that a single administration of a particular compound will achieve the desired goal. This may be especially true for heterogeneous populations of tumor cells at various phases in the cell cycle. Multiple administrations may be employed not only of a single boron compound, but ultimately of a combination of various compounds with differing mechanisms for achieving the targeting of tumor cells. As chemotherapy requires multiple drugs with varying time patterns for dosing, so too BNCT may ultimately require a similar method for ensuring adequate uptake of boron compounds by tumor cells<sup>87</sup>.

## **G. OTHER HADRON BEAMS FOR RADIATION THERAPY**

### **Negative Pions for Radiation Treatment**

The existence of pions ( $\pi^\pm$ ) as the carrier of the strong force was predicted by Hideki Yukawa in 1935 and the pion was experimentally found in 1947. Shortly

after the discovery in cosmic rays,  $\pi^+$  and  $\pi^-$  as well as  $\pi^0$  were produced at the 184-Inch Synchrocyclotron at Berkeley. When  $\pi^-$  come to rest in a nuclear emulsion, they are captured by heavier nuclei and cause these nuclei to explode leaving a characteristic 'nuclear star' in the emulsion (Fig. 7.30). Tobias and Richman discussed the possibility of using  $\pi^-$  for cancer therapy as early as 1951<sup>109</sup>, and their clinical use was advocated by Fowler and Perkins in 1961<sup>110</sup>. Because the pion intensities at accelerators were so low that it was said that all the negative pions produced in physics laboratories worldwide could not eradicate one tumor. The  $\pi^-$  production cross-section was measured and it was shown that existing accelerators were inadequate for cancer therapy<sup>111</sup>. However, the future of negative pion therapy looked brighter as 'meson factories' were constructed at the Los Alamos Meson Physics Facility (LAMPF) at the Los Alamos National Laboratory in New Mexico, the Tri-University Meson Facility (TRIUMF) at Vancouver, Canada, and the Paul Scherrer Institute (PSI) at Villigen, Switzerland. They were called 'meson factories' because they were designed to produce high-energy proton beams of high intensity that were capable of producing large numbers of pions after collisions in target material.

Fig. 7.30

### *Physical Characteristics of $\pi^-$*

Negative pions ( $m_\pi \approx 267 m_e$ ) are the lightest particles in hadron radiation. The  $\pi^-$  lifetime is only 26 nsec, and it decays into a muon, which in turn decays into an electron:

$$\pi^- \rightarrow \mu^- + \bar{\nu}_\mu \quad (\text{mean life } \tau = 2.603 \times 10^{-8} \text{ sec}) \quad (7-27)$$

$$\mu^- \rightarrow e^- + \bar{\nu}_e + \nu_\mu \quad (\text{mean life } \tau = 2.197 \times 10^{-6} \text{ sec}) \quad (7-28)$$

But 26 nsec is a long enough time to produce  $\pi^-$  at an accelerator, transport them into a target volume, where they are captured by atomic nuclei, which in turn disintegrate emitting several particles in nuclear-star formations to destroy cancer cells. Because in the nuclear reactions that produce  $\pi^-$  great numbers of  $\gamma$  rays and neutrons are produced, and because they must be shielded from reaching the patient, the distance from the production to treatment volume cannot be arbitrarily shortened. To obtain the practical range of  $\pi^-$  for treating deep-seated tumors requires an energy ~50–100 MeV, and for these energies, ~50% of  $\pi^-$  survive a 5-meter path length, and ~30% survive in 10 meters.

There are several components in the  $\pi^-$  dose. The first is the ionization process throughout the range of  $\pi^-$ , producing a Bragg peak as the  $\pi^-$  come to rest provided they did not decay. As the  $\pi^-$  comes to rest, being negatively charged, it is attracted to the nucleus of a nearby oxygen, nitrogen, or carbon atom of the tissue and forms a  $\pi^-$  mesic atom (an atom in which an orbital electron is replaced with a  $\pi^-$ ). The  $\pi^-$  cascades down the atomic levels emitting low- and intermediate-energy x-rays (called mesic x-rays) in the process. Because of its large mass, the orbit radius ( $\sim h/m_\pi/(Ze)^2$ ) is small, and eventually the  $\pi^-$  intersects the nucleus. When it reaches the nucleus, it is captured, its entire mass energy (~140 MeV) is converted into energy, and the capturing nucleus explodes throwing out nuclear fragments in all directions ('nuclear-star' formation). Out of the 140 MeV, ~40 MeV is used to overcome the nuclear binding energy; ~60 MeV as is carried off as kinetic energy of neutrons; a small amount is released as energetic nuclear  $\gamma$ -rays; and the rest (~30 MeV) becomes kinetic energy of protons,  $\alpha$ -particles, and heavier nuclear fragments (e.g., lithium and carbon nuclei). Table 7.7 shows the multiplicity and energy partition among nuclear-star fragments from a  $\pi^-$  capture in  $^{16}\text{O}$  nuclei<sup>112</sup>. Mesic x-rays, nuclear

$\gamma$  rays, and neutrons escape from the patient body without doing much damage either to the tumor or the surrounding normal tissue. Because of their charge and relatively large mass, the protons,  $\alpha$ -particles, and heavier nuclei have a very short range in tissue and, for the most part, are densely ionizing. If a  $\pi^-$  decays into a  $\mu^-$ , in flight or at rest, which in turn decays into an  $e^-$ , it gives rise to a dose beyond the Bragg peak.

Table 7.7
-----------

### *Negative Pion Biology*

Pion beams exhibit several physical and biological advantages for cancer therapy. The dose distribution has a narrow Bragg peak, and the nuclear-star fragments have intermediate to high LET (30–40 keV/ $\mu\text{m}$  on average). In soft tissue, ~73% of the  $\pi^-$  are captured by oxygen, ~20% in carbon, and ~3% in nitrogen. A typical oxygen disintegration results in three  $\alpha$  particles (average energy  $\approx 7.5$  MeV), one proton (average energy  $\approx 8$  MeV), and three neutrons. Thus the particles of the nuclear star are primarily high-LET radiation. The particles from the nuclear star formations in  $\pi^-$  capture have an RBE of ~3 for an acute exposure, and greater for a fractionated treatment schedule. However, for large treatment volumes where there is an overlap between the slowing down and stopping regions, and the average RBE is lower. Furthermore, the  $\mu^-$  and  $e^-$  contaminations reduce the RBE values of the high-LET 'stars' at the Bragg peak and reduce the advantages of confining the high-RBE radiation to the tumor volume.

For treatment volumes that require a spread out Bragg peak, and fractionated treatment, it has been found that the value of RBE is high,  $\text{RBE} \approx 1.5$ , and the value of OER low,  $\text{OER} \approx 2.2^{113}$ . In animal models a therapeutic gain has been demonstrated for slower growing tumors with a high proportion of hypoxic cells.

The pion beam dose boundaries are not as distinct as proton or light ion beams as the pions have smaller mass and suffer greater scattering and straggling effects in penetrating the patient's body. Also, the star formation is accompanied by emission of neutrons, and  $\pi$ - $\mu$ - $e$  decay processes smear the dose further. In contrast to protons and heavier ions which are primary particles,  $\pi^-$  are secondary particles produced by the interactions of the primary beams, usually proton beams, with target materials. Because of the lighter mass of pions, therapeutically useful pion beams, with a maximum range of approximately 30 cm in soft tissue, they possess relatively low magnetic rigidities.

### *Negative Pion Clinical Trials*

Clinical advantages of negative pions have been studied at LAMPF<sup>114</sup>, at TRIUMF<sup>115</sup>, and at PSI<sup>116</sup>. Even though they were called 'meson factories,' all three did not have enough  $\pi^-$  intensity to deliver treatments in a few minutes. To counter this limitation, these three sites and the Stanford Linear Accelerator Center (SLAC) developed very effective beam delivery methods. LAMPF developed a vertical beam to treat patients lying on a treatment table, and a dynamic line scanning technique shortly before closing their  $\pi^-$  therapy program. At TRIUMF, although only the horizontal  $\pi^-$  beam was available, a spot scanning technique was used for the treatments<sup>117</sup>. The 3-cm diameter spot was delivered on a hexagonal grid of 2-cm spacing by moving the patient in two dimensions by means of couch motion. The beam was scanned in depth by means of a rotating variable thickness propeller. To collect most of the secondary pions produced in large solid angles and focus them onto the target volumes, a rather specialized multichannel pion applicator, named the 'Piotron,' was fashioned at PSI<sup>114</sup> after a Stanford system<sup>118</sup>. The  $\pi^-$  beam produced in the forward direction was divided into 60 separate azimuthal bins, and magnetically steered so that they converge

into the target volume like spokes of a wheel. By placing the patient in a cylindrical water-equivalent bolus, a spot of uniform biological effect was produced and was scanned throughout the target volume by means of couch motion.

Although there have been noteworthy clinical results at each site, they have not been encouraging enough to continue the programs or to construct new  $\pi^-$  facilities.

### **Antiproton Beams for Cancer Therapy**

The energy loss by antiprotons stopping in water shows that the radiation transferred is localized within 1 mm of the stopping point. This 'focusing' of the radiation is mainly due to heavily ionizing particles emitted from the nuclei on which the annihilation takes place. At present antiproton beams for medical purposes may not be cost effective compared to other heavy charged-particle beams, but the sharpness of their radiation transfer combined with antiproton radiography are highly attractive and unique features that may invite special applications<sup>119</sup>. Experiments have been performed at BNL to see the usefulness of antiproton beams; no clinical use of these beams has been tried until now.

## **H. FUTURE OF HADRON THERAPY**

Several general remarks on the future physics development of hadron radiation therapy are presented .

- Very exciting and strong proton and light-ion beam clinical trials to treat human cancer are in progress all over the world. Hospital-based proton and

heavier-ion accelerator facilities are continuously being built. Although medical accelerators, often cyclotrons or synchrotrons, are based on well-established technologies, much inventiveness is required to satisfy the clinical requirements including reliability, serviceability, compactness, and operation economy.

- To compare the clinical efficacy of heavy charged-particle beam therapy to modern photon therapy, it is imperative to develop three-dimensional conformal therapy delivery using beam scanning technology. Accuracy of heavy charged-particle therapy delivery should be improved by integrating the isocentric delivery of scanned particle beams and anatomical information of patients derived from particle-beam CT.
- To compare the clinical results of fast neutron therapy to those from modern photon therapy, future fast neutron clinical trials should be conducted at facilities that provide neutrons with adequate penetrating power, and with a capability of isocentric beam delivery of conformal therapy aided by multileaf collimators.
- Accelerator-based epithermal neutron sources should be built, and the clinical efficacy derived from reactor-produced neutrons and that from accelerator-produced neutrons should be compared.

## ACKNOWLEDGMENTS

For supplying information used in this chapter, the author wishes to thank George Coutrakon of the Loma Linda University Medical Center, Inder Daftari of UC San Francisco, Dan Jones of NAC, Faure, South Africa, Gerhard Kraft of GSI, Darmstadt, Germany, Richard Maughan of the Gershenson Radiation Oncology Center at the Harper Hospital, Detroit, Eros Pedroni of PSI in Villigen, Switzerland, Mark Phillips of the University of Washington Medical Center, Seattle, and Al Smith of NPTC, Boston. This work is supported by the Director, Office of Energy Research, Energy Research Laboratory Technology Transfer Program, of the U.S. Department of Energy under Contract No. DE-AC03-76SF00098.

**REFERENCES**

1. R. R. Raju, J. T. Lyman, T. Brustad, and C. A. Tobias, in *Radiation Dosimetry*, F. H. Attix and E. Tochilin, Eds. (Academic Press, 1969), Vol. III, p. 178.
2. *Biological and Medical Research with Accelerated Heavy Ions at the Bevalac, 1977-1980*, Lawrence Berkeley Laboratory, M. C. Pirruccello and C. A. Tobias, Eds., Lawrence Berkeley Laboratory Report LBL-11220, 423 pages (1980).
3. M. R. Raju. *Heavy Particle Radiotherapy*. (Academic Press, New York, 1980).
4. J. F. Fowler. *Nuclear Particles in Cancer Treatment*, Medical Physics Handbook (Adam Higler Press, Bristol, UK, 1981).
5. C. A. Tobias. *Heavy Ion Radiobiology Related to Oncology*. Lawrence Berkeley Laboratory, Pub-5144 (1985.).
6. *Protocols for Heavy Charged Particle Beam Dosimetry*, A Report of Task Group 20, Radiation Therapy Committee, American Association of Physicists in Medicine, AAPM Report No. 16, (American Institute of Physics, New York, 1986).
7. *Ion Beams in Tumor Therapy*, U. Linz, Ed., (Chapman & Hall, London, 1995), 387 pages.
8. *Hadrontherapy in Oncology*, U. Amaldi, and B. Larsson, Eds., (Elsevier, Amsterdam, 1994) 755 pages.

9. T. W. Griffin, *Critical Rev. in Oncology/Hematology* **13**, 17-31 (1992).
10. *Proc. of the First International Workshop on Accelerator-Based Neutron Sources for Boron Neutron Capture Therapy, September 1994, Jackson, Wyoming*, D. E. Nigg, Ed., (National Center for BNCT Measurement and Development, Idaho National Engineering Laboratory, CONF-940976, 1994), Vols. I-II, 526 pages.
11. *Boron Neutron Capture Therapy of Brain Tumors— Current Status and Future Prospects*, Special Issue, A. H. Soloway and R. F. Barth, Eds., *J. of Neuro-Oncology*, Vol. 33, Nos. 1 and 2, (Kluwer Academic Publisher, Dordrecht, The Netherlands, 1997) 188 pages.
12. W. H. Bragg and R. Kleeman, *Phil. Mag.* **8**, 726-738 (1904).
13. M. J. Berger and S. M. Seltzer, *Multiple scattering corrections for proton range measurements*, (NAS-NRC Report 1133, 1964).
14. G. Litton, J. T. Lyman, and C. A. Tobias, *Penetration of high-energy heavy ions with the inclusion of Coulomb, nuclear and other stochastic processes*, (Lawrence Berkeley Laboratory, UCRL-17392 rev., UC-34 Physics, TID-4500 (2nd ed.), 1968).
15. R. R. Wilson, *Radiology* **47**, 487-491 (1946).
16. C. A. Tobias, H. O. Anger and J. H. Lawrence, *Am. J. Roentgenol.* **67**, 1-27 (1952).
17. C. A. Tobias, J. H. Lawrence, J. L. Born, R. K. McComb, J. E. Roberts, H. O. Anger, B. V. A. Low-Beer, and C. B. Huggins, *Cancer Res.* **18**, 121-134, 1958.

18. H. D. Suit, M. Goitein, J. Tepper, A. M. Koehler, R. A. Schmidt, and R. Schneider, *Cancer* **35**, 646-1657 (1975).
19. S. Graffman and B. Jung, *Acta Radiol. Therapy Phys. Biol.* **9**, 1-23, 1970.
20. L. L. Gol'din, V. P. Dzhelepov, M. F. Lomanov, O. V. Savchenko, and V. S. Khoroshkov, *Soviet Phys. Usp.* **16**, 02-413 (1973).
21. W. T. Chu, *Nucl. Instrum. & Methods in Phys. Res.* **B99**, 835-838 (1995).
22. I. Daftari and J. R. Castro, J. R., in *Proc. of the XVI International Cancer Congress, Delhi, India, Oct. 30–Nov. 5, 1994*, Abstract # OPGU2-04, p. 35.
23. J. M. Schippers, "A 200 MeV proton therapy facility at the AGO cyclotron in the Netherlands," in the 18th PTCOG meeting in Nice, France, April 1993 (1993).
24. P. Bryant, H. D. Kogelnik, M. Pavlovic, R. Pötter, M. Regler, and H. Schönauer, *Hadrontherapy in Oncology*, U. Amaldi, and B. Larsson, Eds., (Elsevier, Amsterdam, 1994), pp. 390-399.
25. W. T. Chu, J. W. Staples, B. A. Ludewigt, T. R. Renner, R. P. Singh, M. A. Nyman, J. M. Collier, I. K. Daftari, H. Kubo, P. L. Petti, L. J. Verhey, J. R. Castro, and J. R. Alonso. *Performance Specifications for Proton Medical Facility*. Lawrence Berkeley Laboratory Report, LBL-33749, 1993.
26. K. P. Gall, L. Verhey, J. Alonso, J. Castro, J. M. Collier, W. Chu, I. Daftari, M. Goitein, H. Kubo, B. Ludewigt, J. Munzenrider, P. Petti, T. Renner, S. Rosenthal, A. Smith, J. Staples, H. Suit, and A. Thornton, *Nucl. Instrum. Methods in Phys. Res.* **B79**, 881-884 (1993).

27. *Request for Proposals to Design and Construct the Proton Therapy Equipment for the Northeast Proton Therapy Center at the Massachusetts General Hospital*, Administrative Director, NPTC, Massachusetts General Hospital, Boston, MA, NPTC-10,12/18/92 (1992).
28. W. T. Chu, B. A. Ludewigt, and T. R. Renner, *Rev. of Sci. Instrum.* **64**, 2055-2122 (1993).
29. B. Gottschalk and M. S. Wagner, *Contoured scatterer for proton dose flattening*. (Harvard Cyclotron Laboratory, a preliminary report 3/29/89).
30. T. R. Renner and W. T. Chu, *Med. Phys.* **14**, 825-834 (1987).
31. B. A. Ludewigt, W. T. Chu, M. H. Phillips and T. R. Renner, *Med. Phys.* **18**, 36-42 (1991).
32. R. L. Martin, *Nucl. Instrum. Methods Phys.* **25**, 1087-1091 (1987).
33. P. Mandrillon, in *Hadrontherapy in Oncology*, U. Amaldi and B. Larsson, Eds., (Elsevier, Amsterdam, 1994), pp. 256-265.
34. T. Renner, M. Nyman, and R. P. Singh, in *Ion Beam in Tumor Therapy*, U. Linz, Ed., (Chapman & Hall, London, 1995) pp. 256-265.
35. G. Coutrakon, J. Hubbard, J. Johanning, G. Maudsley, T. Slaton, and P. Morton, *Med. Phys.* **21**, 1691-1701 (1994).
36. T. Ogino, S. Murayama, N. Moriyama, H. Ikeda, S. Yoshida, and S. Ebihara, "Proton Treatment Facility at NCC, Kashiwa, Japan: A Progress Report," in the 26th PTCOG meeting, April 1997, Boston, MA, 1997.

37. J. Flanz, S. Durlacher, M. Goitein, A. Levine, P. Reardon, and A. Smith, *Nucl. Instrum. and Methods in Phys. Res.* **B99**, 830-834 (1995).
38. P. Mandrillon, F. Farley, N. Fiétier, J. Y. Tang, F. Anton, and R. Savoy, Proc. of the Eur. Particle Accelerator Conf., June 27-July 1, 1994 (1994).
39. U. Amaldi, G. Arduini, R. Cambria, D. Campi, C. Canzi, F. Gerardi, F. Gramatica, R. Leone, G. Manfredi, M. Nonis, G. Petrucci, S. Rossi, L. Sangaletti, M. Silari, G. Tosi, L. Vecchi, and M. Weiss, in *Hadrontherapy in Oncology*, U. Amaldi and B. Larsson, Eds., (Elsevier, Amsterdam, 1994), pp. 329-339.
40. *The TERA Project and the Centre for Oncological Hadrontherapy*. U. Amaldi and M. Silari, Eds., (Progetto ADROTERAPIA, Istituto Nazionale di Fisica Nucleare, 1994).
41. I. I. Averbukh, A. D. Cherniakin, L. L. Danilov, V. N. Karusyuk, M. M. Karliner, V. N. Marusov, G. I. Silvestrov, V. G. Volokhov, T. A. Vsevolozhskaya, and G. S. Willewald, "Project of small-dimensional 200 MeV Proton Synchrotron," (INS Report, 1991, unpublished).
42. Q. Yu, H. Zhang, and S. Liu. *Conceptual Design of Beijing Proton Therapy Synchrotron*. (Institute of High Energy Physics, Chinese Academy of Sciences, 1996).
43. C. A. Tobias and P. W. Todd, in *Heavy charged particle in cancer therapy. Radiobiology and Radiotherapy*. (National Cancer Inst. Monogr. 24, 1967), pp. 1-21.

44. E. A. Blakely, F. Q. H. Ngo, S. B. Curtis, and C. A. Tobias, *Adv. Radiat. Biol.* **11**, 295-389 (1984).
45. J. F. Fowler, *Int. J. Radiat. Biol.* **47**, 115-117 (1985).
46. J. R. Castro, *Radiat. Environ. Biophys.* **34**, 45-48 (1995).
47. J. R. Castro, in *Progress in Radio-Oncology V. Monduzzi Editore, Bologna, Italy*, D. Kogelnik, Ed., (1995), 643-648.
48. P. K. Lillis-Hearne and J. R. Castro, in *Ion Beam in Tumor Therapy*, U. Linz, Ed., (Chapman & Hall, London, 1995), 133-141.
49. S. Yamada, Commissioning of the Medical Synchrotron HIMAC, in the Thirteenth Int. Conf. on the Application of Accelerator in Research & Industry, Denton, Texas, Nov. 7-10, 1994, Abs. (1994).
50. "EULIMA Feasibility Study Report," Commission of the European Communities, unpublished report, February 1991 (1991).
51. J. R. Castro, D. E. Linstadt, J. P. Bahary, P. L. Petti, I. Daftari, J. M. Collier, P. H. Gutin, G. E. Gauger, and T. L. Phillips, *Int. J. Radiat Onc Biol. Phys.* **29**, 647-655 (1994).
52. L. T. Yonemoto, J. D. Slater, C. L. Rossi, J. E. Antoine, L. Loreda, J. O. Archambeau, R. W. M. Schulte, D. W. Miller, S. L. Teichman, and J. M. Slater, *Int. J. Radiat. Oncol. Biol. Phys.* **37**, 21-29 (1997).
53. R. P. Levy, K. A. Frankel, and G. K. Steinberg, in *Ion Beams in Tumor Therapy*, U. Linz, Eds., (Chapman and Hall, London, 1995) pp. 142-153.

54. R. P. Levy, K. A. Frankel, R. A. Ricciardi, A. E. Rhoades, and L. L. Xu, in *Radiosurgery 1995*, D. Kondziolka, Ed., (Karger, London, 1996) pp. 66-74.
55. M. Goitein and G. T. Y. Chen, *Med. Phys.* **10**, 831-840 (1983).
56. T. R. Renner, W. T. Chu, and B. A. Ludewigt, in *Hadrontherapy in Oncology*, Amaldi, U. and Larsson, B. (eds.), Elsevier, Amsterdam, 1994; pp 453-461.
57. H. Eickhoff, B. Franczak, U. Krause, C. Reidel, and R. Steiner. *Accelerator development and tests for the GSI Therapy-Project*, GSI Report (1997).
58. G. Coutrakon, A. Ghebremedhin, J. Johanning, P. Koss, and G. Jenkins, in *Application of Accelerators in Research and Industry*, Proc. of the Fourteenth Int. Conf. November 1996, Denton, Texas, J. L. Duggan and I. A. Morgan, Eds., (AIP Conference Proceedings 392, American Institute of Physics, Woodbury, NY), **Part Two**: 1265-1268, 1997.
59. E. Pedroni, R. Bacher, H. Blattmann, T. Böhringer, A. Coray, A. Lomax, S. Lin, G. Munkel, S. Scheib, U. Schneider, and A. Tourovsky, *Med. Phys.* **22**, 37-53, 1995.
60. A. Brahme, P. Källman, and B. K. Lind, *Radiotherapy and Oncology* **15**, 189-197, 1989.
61. R. S. Stone and J. C. Larkin, *Radiology* **39**, 608, 1942.
62. R. S. Stone, *Am. J. Roentgenol.* **59**, 771, 1948.
63. G. E. Sheline, T. L. Phillips, S. B. Field, J. T. Brennan, and A. Raventos, *J. Roentgenol.* **111** (1971).

64. M. Catterall, D. K. Bewley, and I. Sutherland, *Brit. Med. J.* **1**, 1642 (1977).
65. A. Wambersie, *Strahlenther. Onkol.* **166**, 52-60 (1990).
66. H. Tsunemoto, T. Arai, S. Morita, T. Ishikawa, Y. Aoki, N. Takada, and S. Kamata, *Int. J. Radiat. Oncol. Biol. Phys.* **8**, 2169-2172 (1982).
67. T. Griffin, T. Pajak, G. Laramore, and L. Davis, *Bull. Cancer (Paris)* **73**, 586 (1986).
68. J. J. Batterman, K. Breur, G. A. M. Hart, and H. A. van Peperzeel, *Eur. J. Cancer* **17**, 539-548 (1981).
69. P. Wooton, *Rad. Prot. Dosimetry* **32**, 349 (1988).
70. H. G. Blosser, J. Dekamp, J. Griffin, D. Johnson, F. Marti, B. Milton, J. Vincent, G. Blosser, E. Jemison, R. Maughan, W. Powers, and W. Young, *IEEE Trans. Nucl. Sci.* **NS-32**, 3287-3291 (1985).
71. R. L. Maughan, W. E. Powers, and H. G. Blosser, *Med. Phys.* **21**, 779-785 (1994).
72. C. Stannard, F. Vernimmen, D. Jones, J. Wilson, L. van Wijik, S. Brennan, N. Schreuder, J. Symons, V. Levin, E. Mills, A. Alberts, D. Werner, B. Smit, and G. Schmitt, *Radiat. Oncol. Investigations* **2**, 245-255 (1995).
73. R. D. Errington, *Bull. Cancer (Paris)* **73**, 569-576 (1986).
74. L. Cohen, F. R. Hendrickson, P. D. Kurup, J. A. Mansell, M. Awschalom, I. Rosenberg, and R. K. Ten Harken, *Cancer* **55**, 10 (1985).
75. G. L. Locher, *Am. J. Roentgenol. Radium Ther.* **36** (1936).

76. P. G. Kruger, *Proc. Nat. Acad. Sci.* **26**, 181 (1940).
77. W. H. Sweet, *Int. Symp. on Neutron Capture Therapy*, (Brookhaven National Laboratory, 1983), 376-378.
78. H. Hatanaka, and Y. Nakagawa, *Int. J. Radiat. Oncol., Biol., Phys.* **28**, 1061-66 (1994).
79. Y. Mishima, M. Ichihashi, M. Tsui, S. Hatta, M. Ueda, C. Honda, and T. Susuki, *Lancet* **2**, 388-389 (1989).
80. J. A. Coderre, R. Bergland, J. Capala, M. Chadha, A. J. Chanana, E. Elowitz, D. D. Joel, H. B. Liu, and D. Slatkin, *J. of Neuro-Oncology* **33**, 93-104 (1997).
81. G. Friendlander, J. W. Kennedy, E. S. Macias, and J. M. Miller, in *Nuclear and Radiochemistry*, (John Wiley & Sons, New York, 1981), 610-650.
82. "Boron Neutron-Capture Therapy of Glioblastoma Multiforme at the Brookhaven medical research reactor, A Phase I/II Study" (FDA IND # 43,317), Protocol #4, A. D. Chanana, Med. Dept., Brookhaven National Laboratory, Upton, NY 11973-5000, January, 1996.
83. D. L. Bleuel, R. J. Donahue, B. A. Ludewigt, and J. Vujic, J., "Designing accelerator-based epithermal neutron beams for BNCT," submitted for publication in *Med. Phys.*, 1997.
84. J. Coderre, P. Rubin, A. Freedman, J. Hansen, T. S. Wooding, Jr., D. Joel, and D. Gash, *Int. J. Radiat. Oncol., Biol., Phys.* **28**, 1067-1077 (1994).
85. M. H. Hawthorne, *Angew. Chem. Int. Ed. Engl.* **32**, 950-984 (1993).

86. R. F. Barth, A. H. Soloway, and R. M. Brugger, *Cancer Invest.* **6**, 534-560 (1996).
87. A. H. Soloway, R. F. Barth, R. A. Gahbauer, T. E. Blue, and J. H. Goodman, *J. Neuro-Oncology* **33**, 9-18 (1997).
88. S. B. Kahl and M. S. Koo, *J. Chem. Soc., Chem. Commun.* 1769-1771 (1990).
89. C.-K. C. Wang, M. Sutton, and T. M. Evans, "Dosimetric aspects of IC and Auger emissions from  $^{157}\text{Gd}(n,\gamma)$  reactions for neutron capture therapy," *Advances in Neutron Capture Therapy- Vol. 1, Medicine and Physics*, B. Larsson, J. Crawford and R. Weinreich, Eds., (Elsevier Science, Amsterdam, 1997), to be published.
90. J. G. Wierzbicki, W. Roberts, M. J. Rivard, and D. S. Waid, " $^{151}\text{Eu}$  isotope for neutron capture therapy?" *ibid.*
91. C. A. Tobias, P. P. Weymouth, and L. R. Wasserman, *Science* **107** (1948).
92. R. G. Fairchild, S. K. Saraf, J. Kalef-Ezra, and B. H. Laster, *Med. Phys.* **17**, 1045-1052 (1990).
93. R. L. Moss et al., in *Neutron Capture Therapy of Cancer*, Allen, B. J. (ed.), Plenum Press, New York, 1992.
94. I. Auterinen and P. Hiismäki, *Proc. of the 6th Int. Symp. on Neutron Capture Therapy*, Kobe, Japan, 1995.
95. R. L. Moss, O. Aizawa, D. Beynon, R. Brugger, G. Constantine, O. Harling, H. B. Liu, and P. Watkins, *J. Neuro-Oncology* **33**, 27-40 (1997).

96. J. F. Harmon, R. J. Kudchadker, J. F. Kunze, S. W. Serrano, X. L. Zhou, Y. D. Hacker, and R. W. Hamm, *Application of Accelerators in Research and Industry*, Proc. of the Fourteenth Int. Conf. November 1996, Denton, Texas, J. L. Duggan and I. A. Morgan, Eds., (AIP Conference Proceedings 392, American Institute of Physics, Woodbury, NY), **Part Two**, 1285-1288 (1997).
97. D. Nigg et al., *Computational and Experimental Studies of an Electron Accelerator Base Epithermal Photoneutron Source Facility for BNCT*, (Idaho National Engineering Laboratory, INEL-96-0139, 1996).
98. D. L. Bleuel, R. J. Donahue, and B. A. Ludewigt, *Application of Accelerators in Research and Industry*, Proc. of the Fourteenth Int. Conf. November 1996, Denton, Texas, J. L. Duggan and I. A. Morgan, Eds., (AIP Conference Proceedings 392, American Institute of Physics, Woodbury, NY), **Part Two**, 1297-1300 (1997).
99. J. W. Kwan, G. D. Ackerman, O. A. Anderson, C. F. Chan, W. S. Cooper, G. J. deVries, W. B. Kunkel, L. Soloka, W. F. Steele, and R. P. Wells, in *Accelerator and Technology*, (Conference Record of the 1991 IEEE Particle Accelerator Conference, May 1991, San Francisco, CA, 1991), 1955-1957.
100. J. W. Kwan, E. Henestroza, C. Peters, L. L. Reginato and S. S. Yu, in *Application of Accelerators in Research and Industry*, Proc. of the Fourteenth Int. Conf. November 1996, Denton, Texas, J. L. Duggan and I. A. Morgan, Eds., (AIP Conference Proceedings 392, American Institute of Physics, Woodbury, NY, 1997), **Part Two**, 1313-1315.
101. L. L. Reginato J. Ayers, R. Johnson, C. Peters, and R. Stevenson, *ibid.*, 1305-1308 (1997).

102. K.-N. Leung, *ibid.*, 1203-1205 (1997).
103. *Heat Transfer Microstructures for Integrated Circuits*, NTIS #5285, (NTIS, Port Royal Road, Springfield, VA, 1984).
104. J. C. Yanch, R. E. Shefer, R. E. Klinkowstein, W. B. Howard, H. Song, B. Blackburn, and E. Binello, in *Application of Accelerators in Research and Industry*, Proc. of the Fourteenth Int. Conf. November 1996, Denton, Texas, J. L. Duggan and I. A. Morgan, Eds., (AIP Conference Proceedings 392, American Institute of Physics, Woodbury, NY), **Part Two**, 1281-1284, 1997.
105. T. D. Beynon, D. A. Allen, A. Beddoe, G. Constantine, L. G. Earwaker, N. James, S. Green, W. Morgan, and D. R. Weaver, in *Advances in Neutron Capture Therapy- Vol. 1, Medicine and Physics*, B. Larsson, J. Crawford and R. Weinreich, Eds., (Elsevier Science, Amsterdam, 1997), to be published.
106. T. A. Buchholz, G. E. Laramore, K. J. Stelzer, R. Risler, P. Wooton, and T. W. Griffin, *J. Neuro-Oncology* **33**, 171-178 (1997).
107. K. J. Stelzer, G. E. Laramore, R. Risler, L. Wiens, and T. W. Griffin, in *Application of Accelerators in Research and Industry*, Proc. of the Fourteenth Int. Conf. November 1996, Denton, Texas, J. L. Duggan and I. A. Morgan, Eds., (AIP Conference Proceedings 392, American Institute of Physics, Woodbury, NY, 1997), **Part Two**, 1277-1279.
108. E. Binello, R. E. Shefer, and J. C. Yanch, in *Advances in Neutron Capture Therapy- Vol. 1, Medicine and Physics*, B. Larsson, J. Crawford and R. Weinreich, Eds., (Elsevier Science, Amsterdam, 1997), to be published.

109. C. A. Tobias, *Radiology* **108**, 145-158 (1973).
110. P. H. Fowler and D. H. Perkins, *Nature* **189**, 524 (1961).
111. D. Berley, L. N. Blumberg, D. C. Bonar, R. Fairchild, J. D. Fox, W.-C. Lam, D. M. Lazarus, Y. Y. Lee, C. L. Wang, A. S. Kanofsky, W. T. Chu, and M. Blecher, *IEEE Trans. Nucl. Sci.* **NS-20**, 997-1001 (1973).
112. C. Richman, *Med. Phys.* **8**, 273-291 (1981).
113. L. D. Skarsgard, B. Palcic, B. G. Douglas, and G. K. Y. Lam, *Int. J. Radiat. Oncol. Biol. Phys.* **8**, 2127-2132 (1982).
114. C. F. von Essen, M. A. Bagshaw, S. E. Bush, A. R. Smith, and M. M. Kligerman, *Int. J. Radiat. Oncol. Biol. Phys.* **13**, 1389-1398 (1987).
115. T. Pickles, J. Bowen, P. Dixon, C. Gaffney, M. Pomeroy, D. Rheaume, F. Vernimmen, and G. B. Goodman, *Int. J. Radiat. Oncol. Biol. Phys.* **21**, 1005-1011 (1991).
116. G. Schmitt, C. von Essen, R. Greiner, and H. Blattmann, *Radiat. Res. Suppl.* **S272** (1985).
117. G. K. Y. Lam, *Rev. Sci. Instrum.* **53**, 1067-1071 (1982).
118. D. A. Pistenmaa, P. Fessenden, D. P. Boyd, G. Luxton, R. Taber, and M. A. Bagshaw, *Radiology* **122**, 527-529, (1977).
119. L. Gray and T. E. Kalogeropoulos, *Radiat. Res.* **97**, 246-252 (1984).

### List of Figure Captions

- Fig. 7.1. A Bragg curve is schematically superimposed on a patient indicating the ability of placing the Bragg peak in the target volume by adjusting the beam range. The entrance dose is low compared with the peak dose, and the dose abruptly falls off beyond the distal edge.
- Fig. 7.2. Physical dose distributions as a function of penetrating depth of (a) a pristine beam (Bragg curve) and (b) a beam whose range is modulated to widen the stopping region (spread-out Bragg peak, SOBP). The names given to several regions of the curves are labeled in the figure.
- Fig. 7.3. (A) The variance of straggling,  $\sigma_z$ , and (B) the variance of multiple scattering,  $\sigma_y$ , as a function of depth for various heavy charged particles.
- Fig. 7.4. Relative increase in the penumbra due to multiple scattering in water and copper for proton, helium-ion, and neon-ion beams. The variance ( $\sigma$ ) of the lateral dose falloff is expressed in terms of the variance ( $\sigma_0$ ) at the entrance of the absorber.
- Fig. 7.5. (a) Tumor control probability (TCP) vs. dose, (b) normal tissue complication probability (NTCP) for photon treatment, and (c) NTCP for proton treatment which is shifted to a higher dose because of the better dose localization characteristics of proton beams. Tumor control probabilities without normal tissue complication for proton treatments is higher than that for photon treatments.

Fig. 7.6. Results of six-field conformal therapy planning on the central axial CT slice for a patient with prostate carcinoma using (a) 18 MV x rays and (b) 230 MeV proton beams.

Fig. 7.7. Dose-volume histograms for the six-field conformal therapy planning for a patient with prostate carcinoma using high-energy x rays and proton beams as described in Fig. 7.6.

Fig. 7.8. A range modulating wheel. When rotated, it inserts various thicknesses of absorber material in the beam path, thereby modulating the beam range producing desired SOBP widths. The multi-track design and the capability of turning the proton beam on and off at pre-programmed angular orientations of the wheel produce many different SOBP widths.

Fig. 7.9. A cross-section of a bi-material contoured scatterer for producing a large uniform field.

Fig. 7.10. Schematic plan view of the proton facility at the Loma Linda University Medical Center. The synchrotron is a small part of the entire facility.

Fig. 7.11. Schematic plan view of the proton facility constructed at the Northeast Proton Therapy Center of the Massachusetts General Hospital in Boston.

Fig. 7.12. Bragg peaks of 670-MeV Ne-ion and Si-ion beam. Dashed curves represent the dose contributions due to nuclear fragments (the numerals indicate the atomic number,  $Z$ , of the fragments) created in

the water by the projectile particles. The number of cm Pb indicates the thickness of lead in the beam path to spread the beam spot for the measurements. Most of the fragmentation occur in the water.

Fig 13. A plot of RBE vs. LET for various cell lines. A simple relationship does not exist between the two. The shaded curve illustrates the general trend of the data.

Fig. 7.14. The Bragg peak is widened by using ridge-shaped filters, and then the range of the mini-spread beam is modulated to spread out the stopping region to cover an extended target by Bragg-peak doses. A relatively large dose is from the longest range beam in order to preserve the sharpness of the distal falloff edge.

Fig. 7.15. (a) The RBE values measured at various depth in water of a range-modulated beam, and (b) the associated physical dose as a function of penetration depth. By combining the two curves, i.e., multiplying the physical dose at each depth by the corresponding RBE value, a biological dose curve may be obtained. The slope in the physical dose curve in the SOBP region is shaped in such a way that the biological dose is uniform throughout the SOBP region.

Fig. 7.16. One of the three treatment rooms at LBNL for heavy charged-particle therapy trial. Many instruments used in heavy charged-particle therapy were developed in this kind of experimental setups.

Fig. 7.17. Heavy Ion Medical Accelerator in Chiba (HIMAC).

FIG 18. A fixed-modulation method produces a cylindrical treatment volume whose length is equal to the thickest part of the target volume. A compensator adjust the penetrating depth laterally across the target in such a way that the dose falloff region at the distal peak conform with the distal surface of the target. Much normal tissues upstream of the target are irradiated in this method. The fixed-modulation method is now employed at practically all heavy charged-particle facilities.

Fig. 7.19. (a) The dose distribution obtained by a variable-modulation method, and (b) a schematic illustration of a three-dimensional dynamic conformal therapy delivery using a variable-speed scanner and a multileaf collimator assembly.

Fig. 7.20. Schematic diagram showing the concept of the pixel scanning system at PSI.

Fig. 7.21. (a) Dose profile of a wide treatment area created by a uniform scan, (b) 'optimized' dose profile obtained by scanning according to the occupation function obtained in Eq. (7-9), and (c) comparison of the lateral dose falloffs produced by the two methods with the Gaussian beam spot profile used in scanning. (From Pedroni et al., 1995.)

Fig. 7. 22. A comparison of depth-dose curves for a variety of neutron beams and for  $^{60}\text{Co}$   $\gamma$  rays. (Data from BJR Supplement No. 17, 1983.)

Fig. 7.23. The superconducting cyclotron facility for fast neutron therapy at the Harper Hospital, Detroit.

Fig. 7.24. National Accelerator Centre in Faure, South Africa. The accelerator facility has a fast neutron treatment room (N) with an isocentric gantry and a proton beam treatment room (P1).

Fig. 7.25. Thermal neutron flux density in head phantom for thermal and epithermal neutron beams. (From R. G. Fairchild and V. P. Bond, *Int. J. Radiat. Oncol. Biol. Phys.* **11**, 831-840, 1985.)

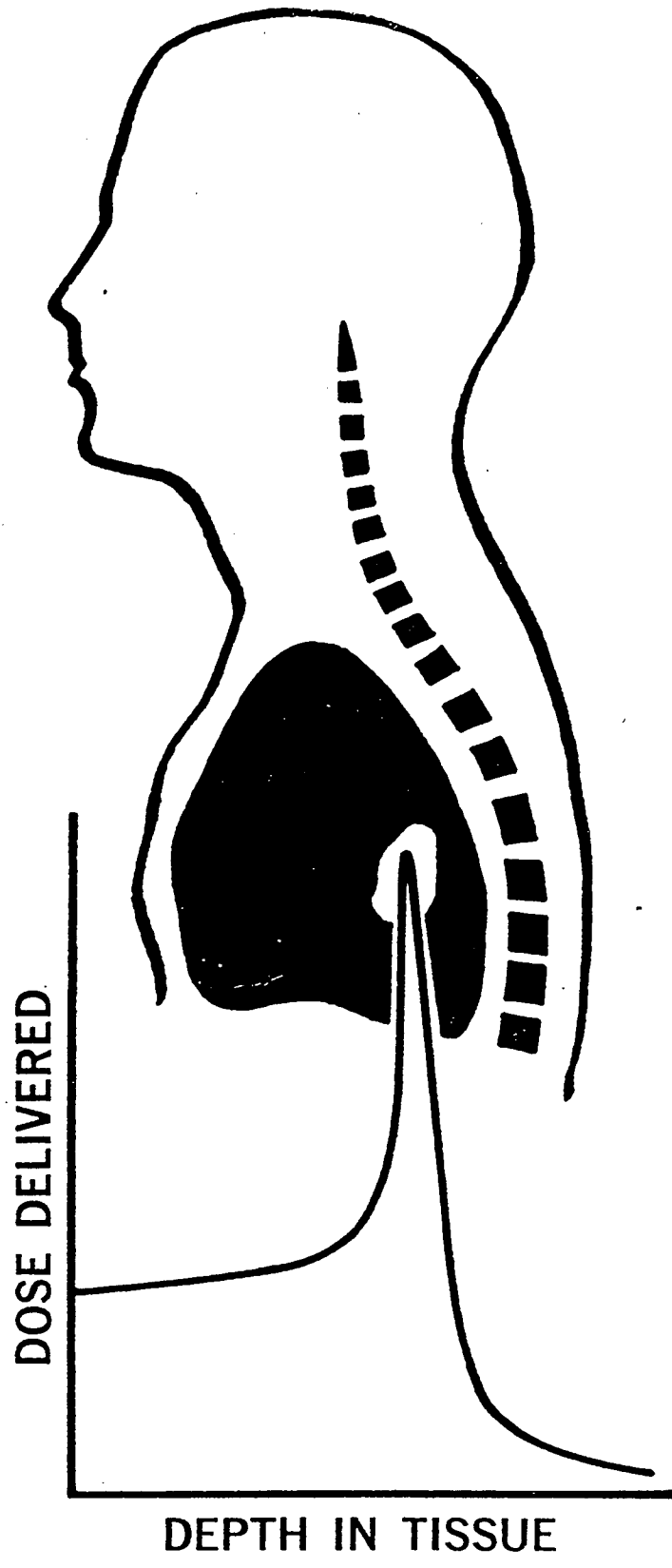
Fig. 7.26. Normal-tissue depth-dose curves in a phantom for epithermal neutrons produced by  ${}^7\text{Li}$  (p,n) reaction of 2.4 MeV protons and using an Al/AlF<sub>3</sub> moderator assembly. Boron dose, gamma dose, proton-recoil dose, nitrogen dose, and the total dose are shown as a function of the depth in phantom.

Fig. 7.27. Proposed configuration of two reactor-based BNCT facilities, MITR-II and BMRR, using fission plate and new moderator/filter assemblies. (Based on Ref. 95.)

Fig. 7. 28. Depth distribution of a) total equivalent tumor doses, and b) total thermal fluence for an accelerator-based epithermal neutrons moderated with D<sub>2</sub>O,  ${}^7\text{LiF}$ , and Al/AlF<sub>3</sub>. For comparison, the same quantities for a reactor-produced epithermal neutron beam (from BMRR) are shown.

Fig. 7.29. Schematic diagram of the 2.5 MeV ESQ accelerator. (Based on Ref. 100.)

Fig. 7.30. An example of a nuclear star in emulsion. (Based on Ref. 110.)



XBL 737-969

Fig. 7.1

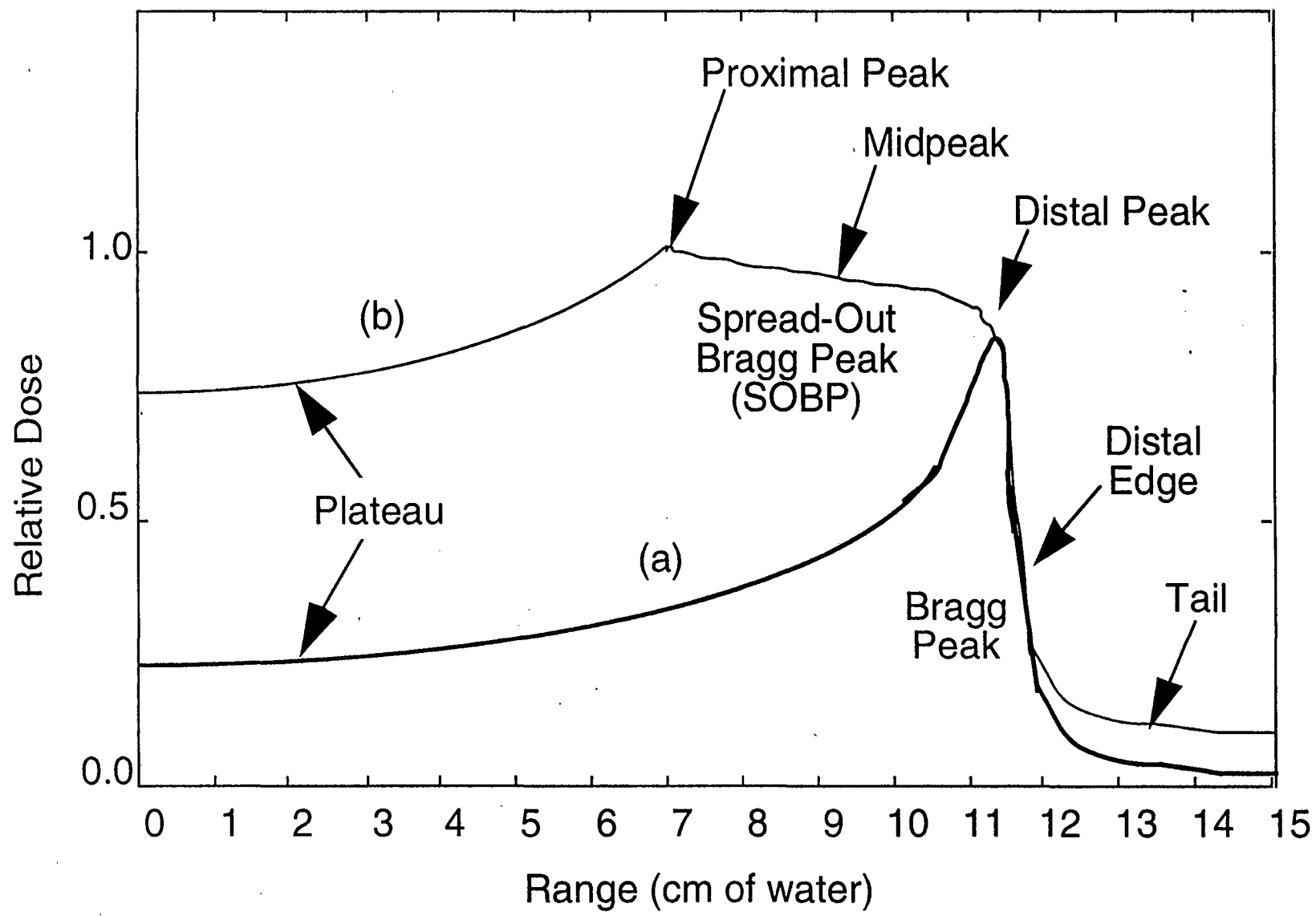


FIG. 7.2

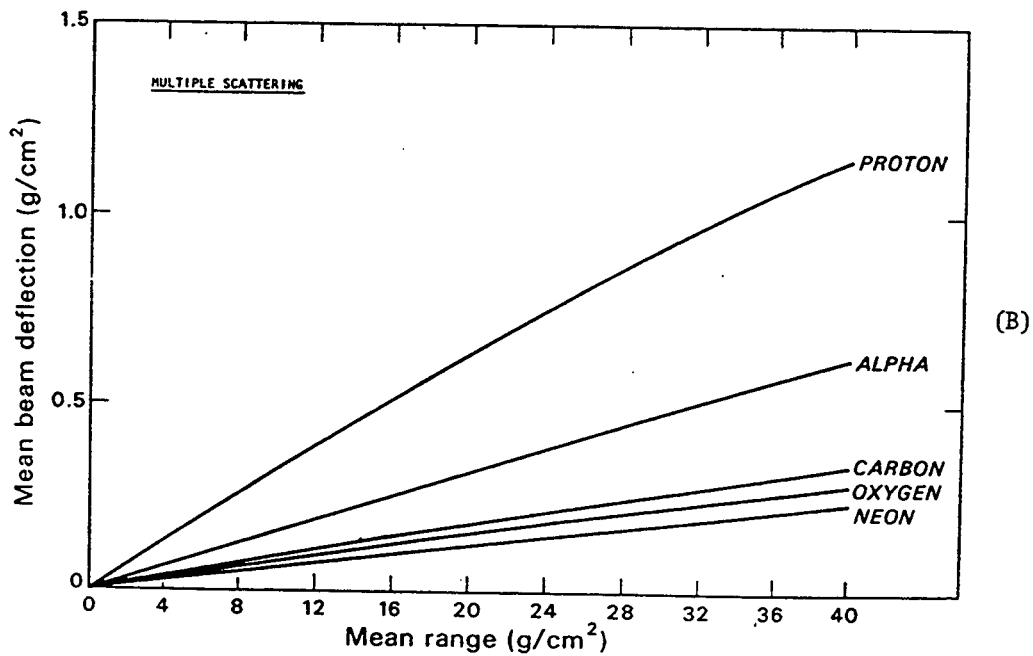
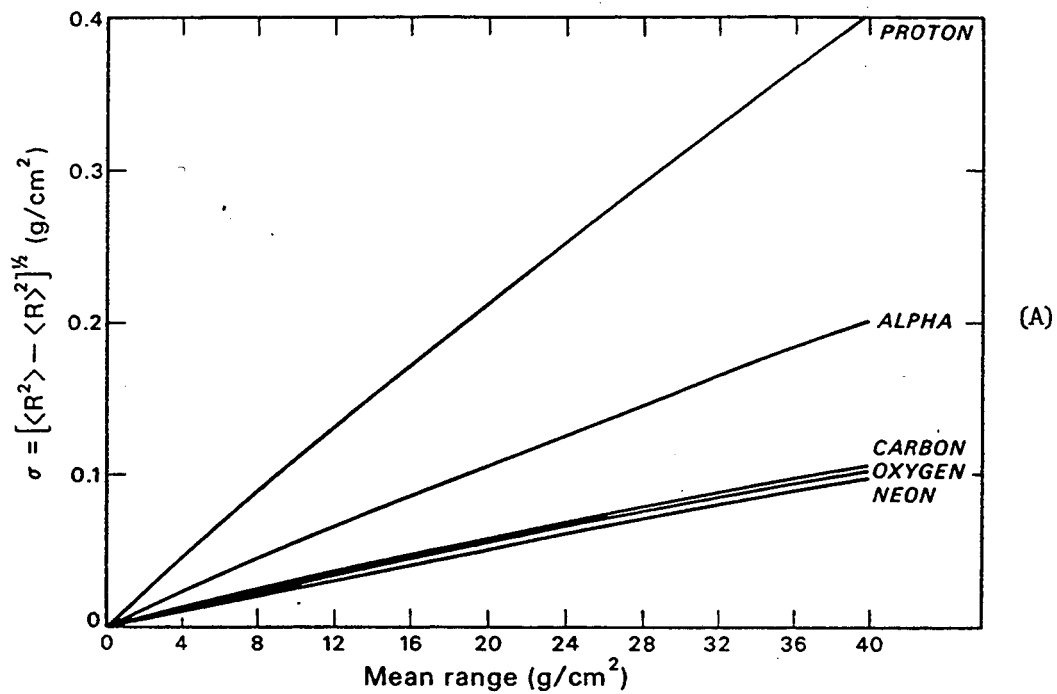


Fig 3

FIG. 7.3

Fig. 4  
Fig. 7-4

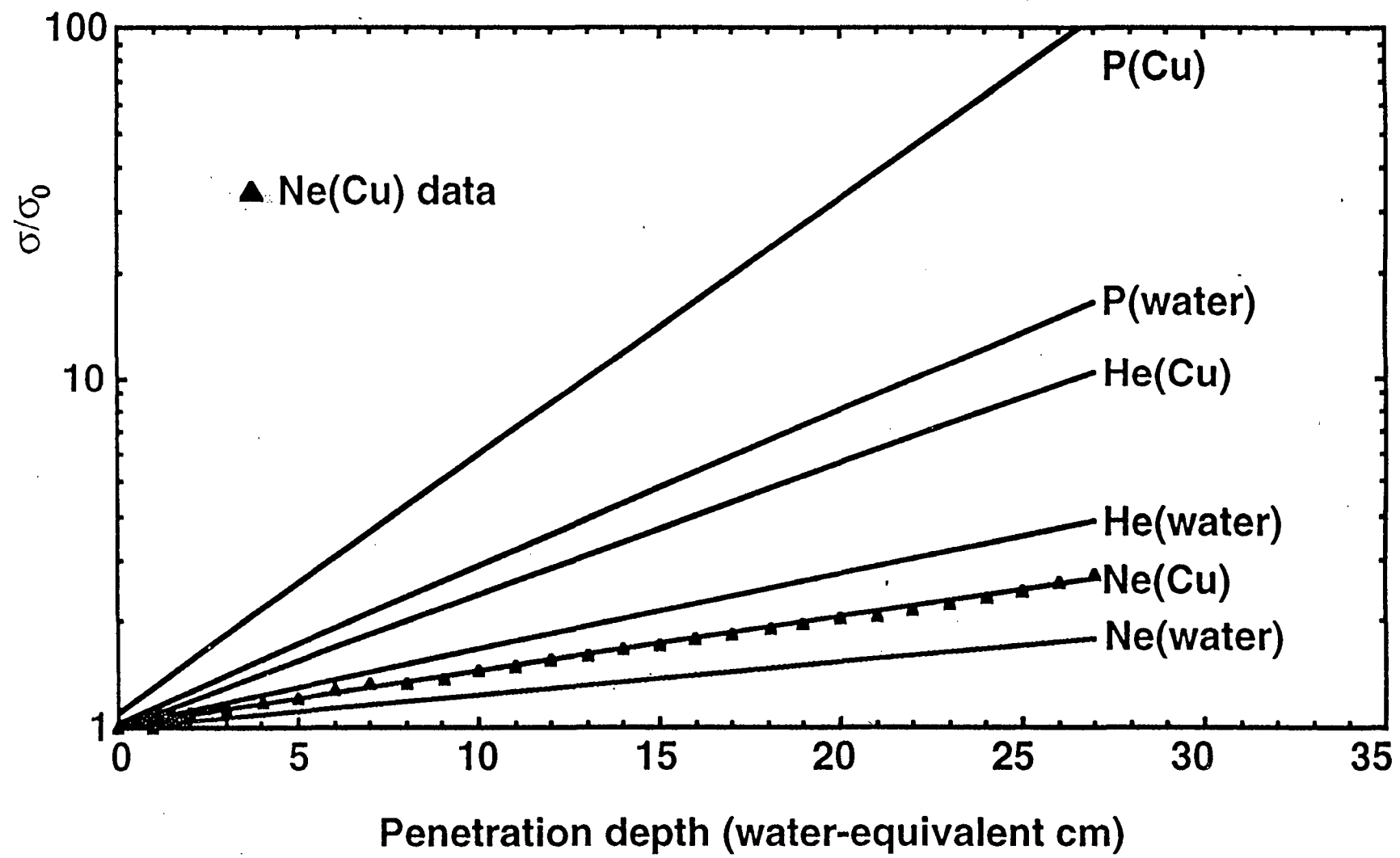


FIG. 7.4

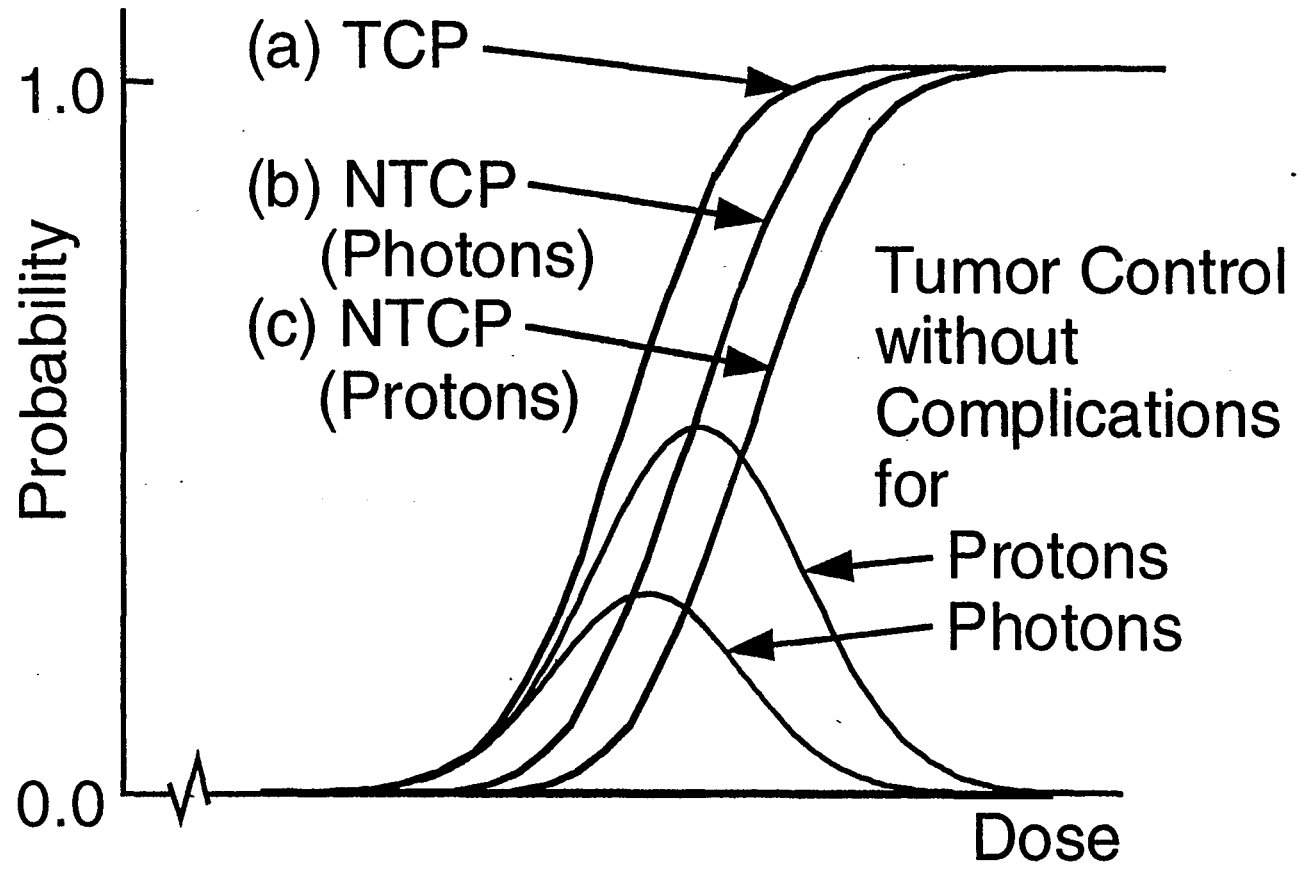
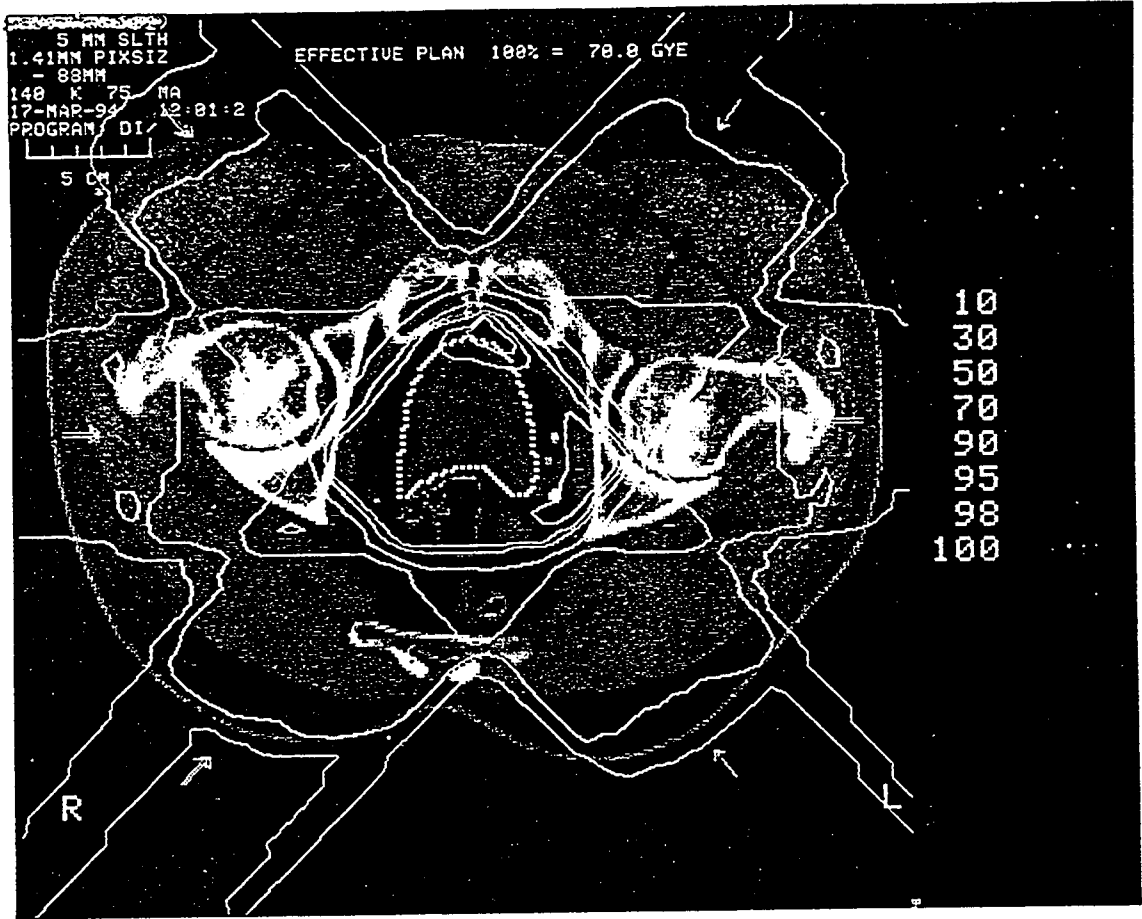


FIG. 7.5

5  
5  
5

(a)



(b)

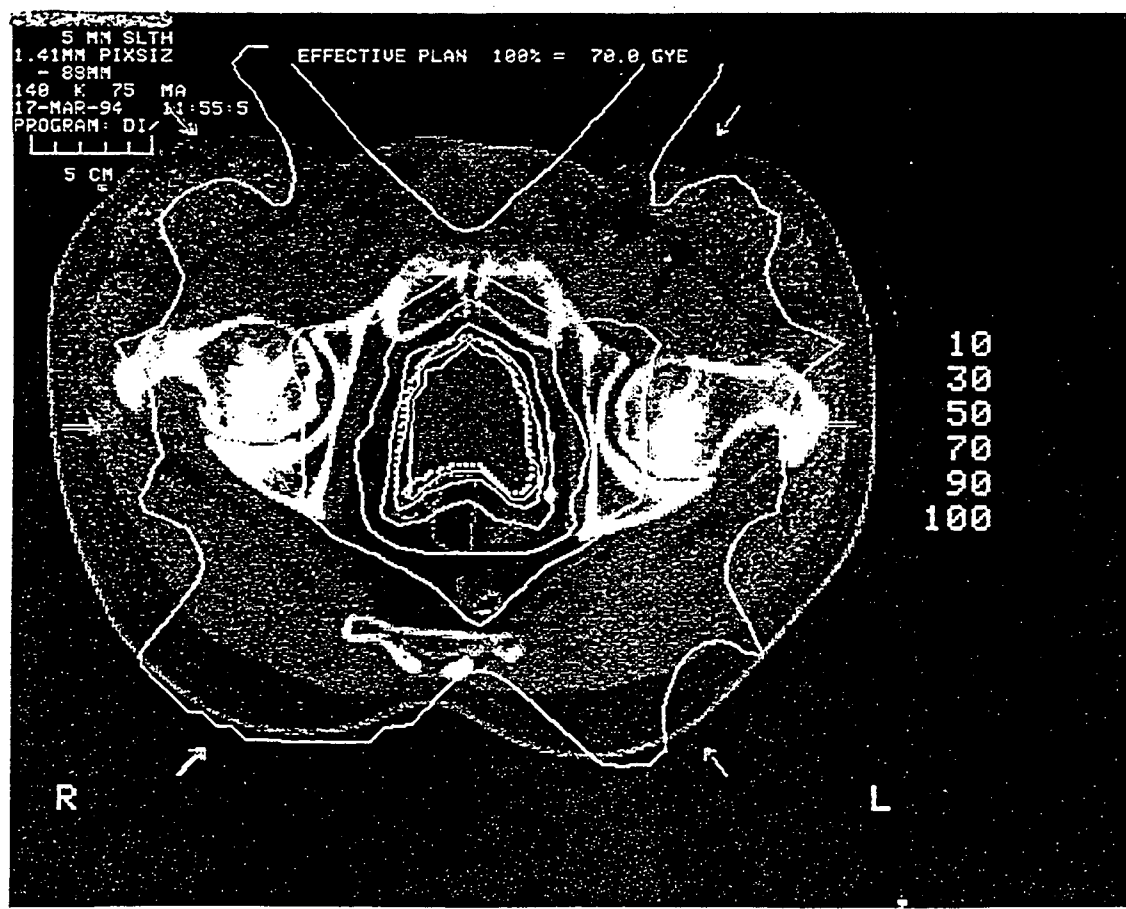


FIG. 7.6

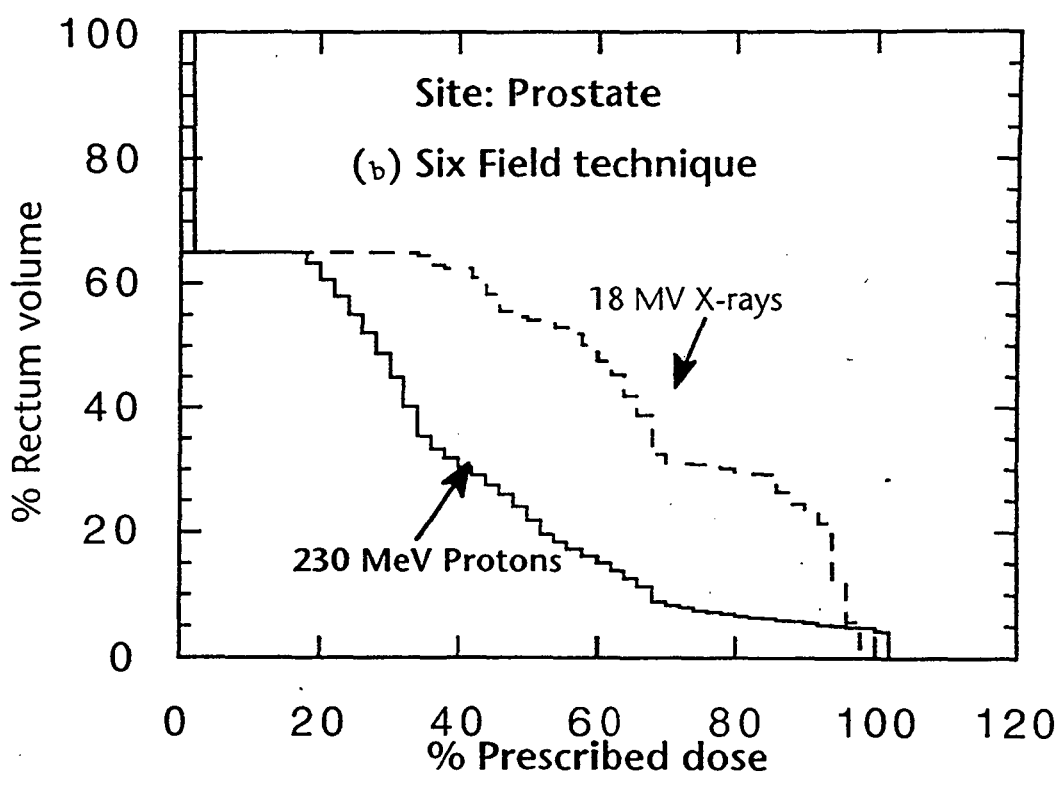


FIG. 7.7

Fig. 7.8



C - C VIEW

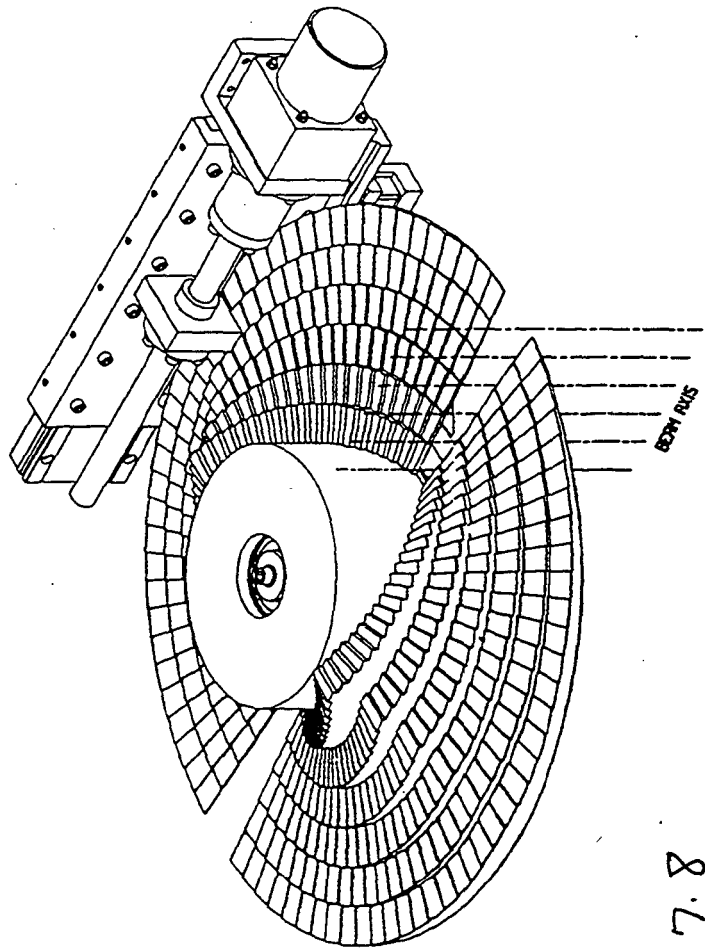
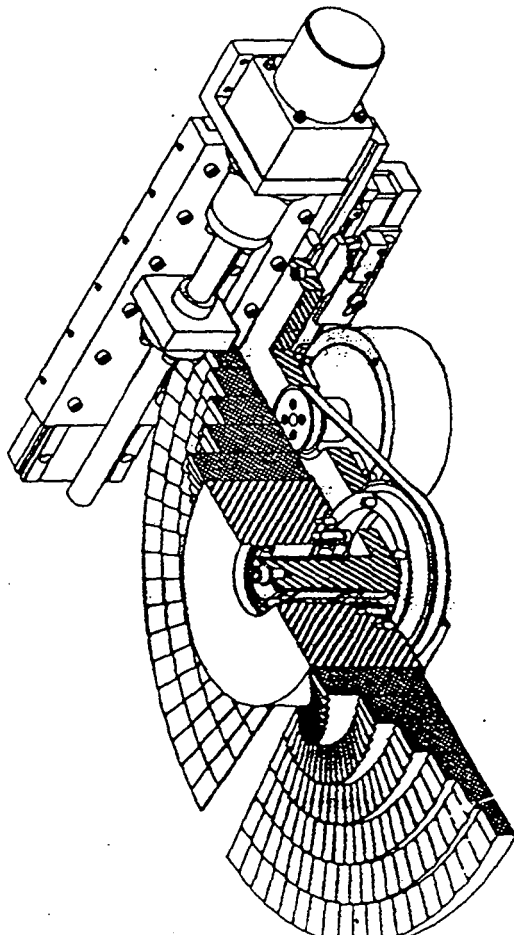
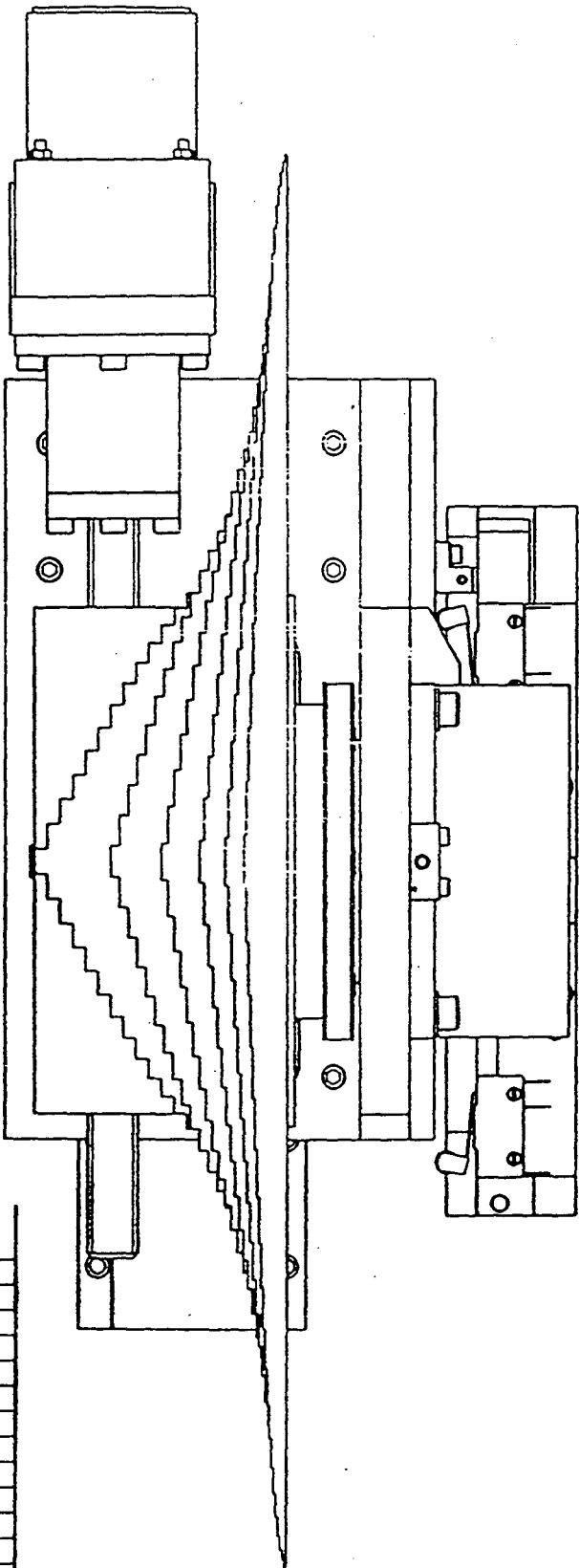


Fig. 7.8

Fig. 7-9

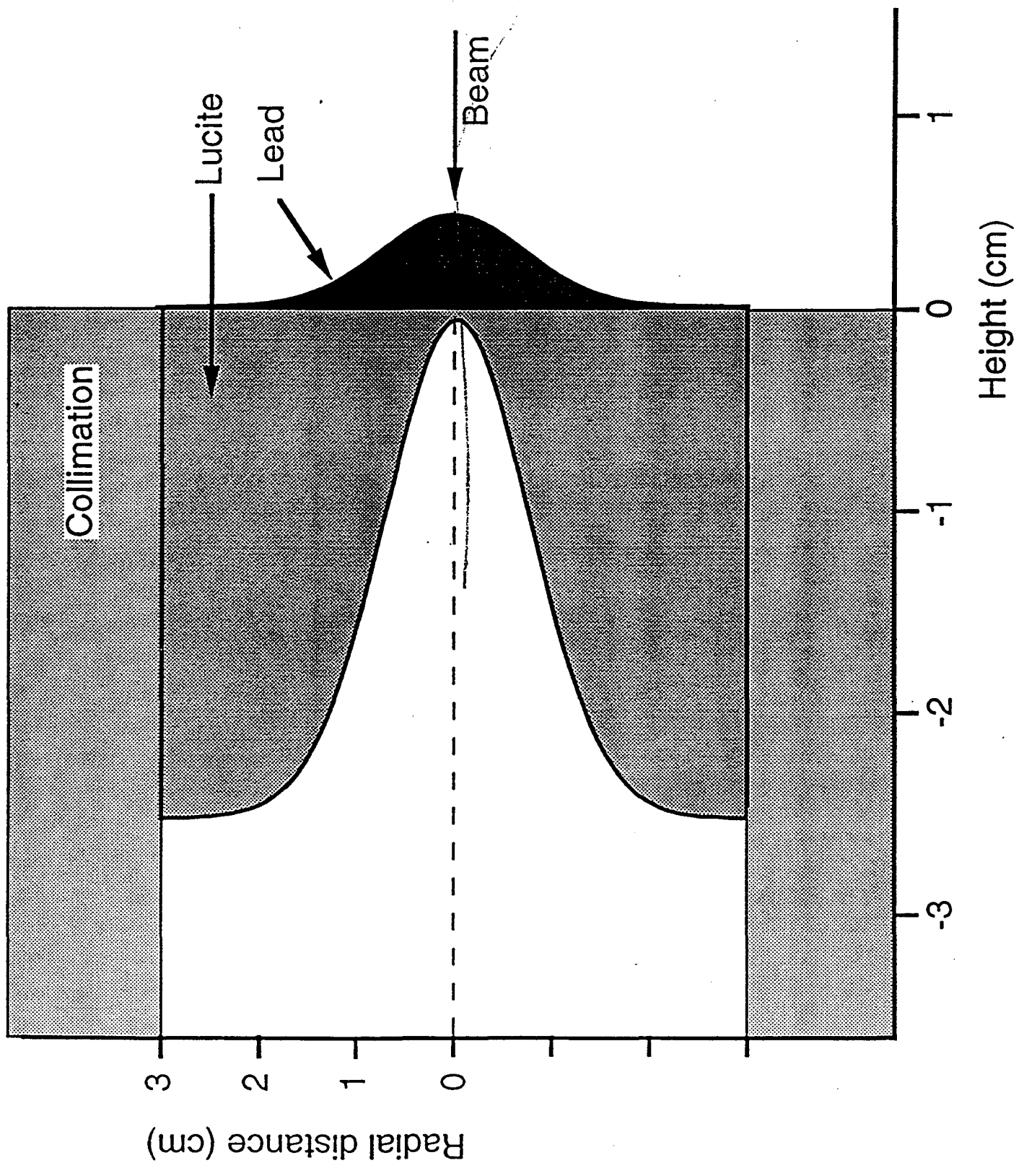


FIG. 7.9

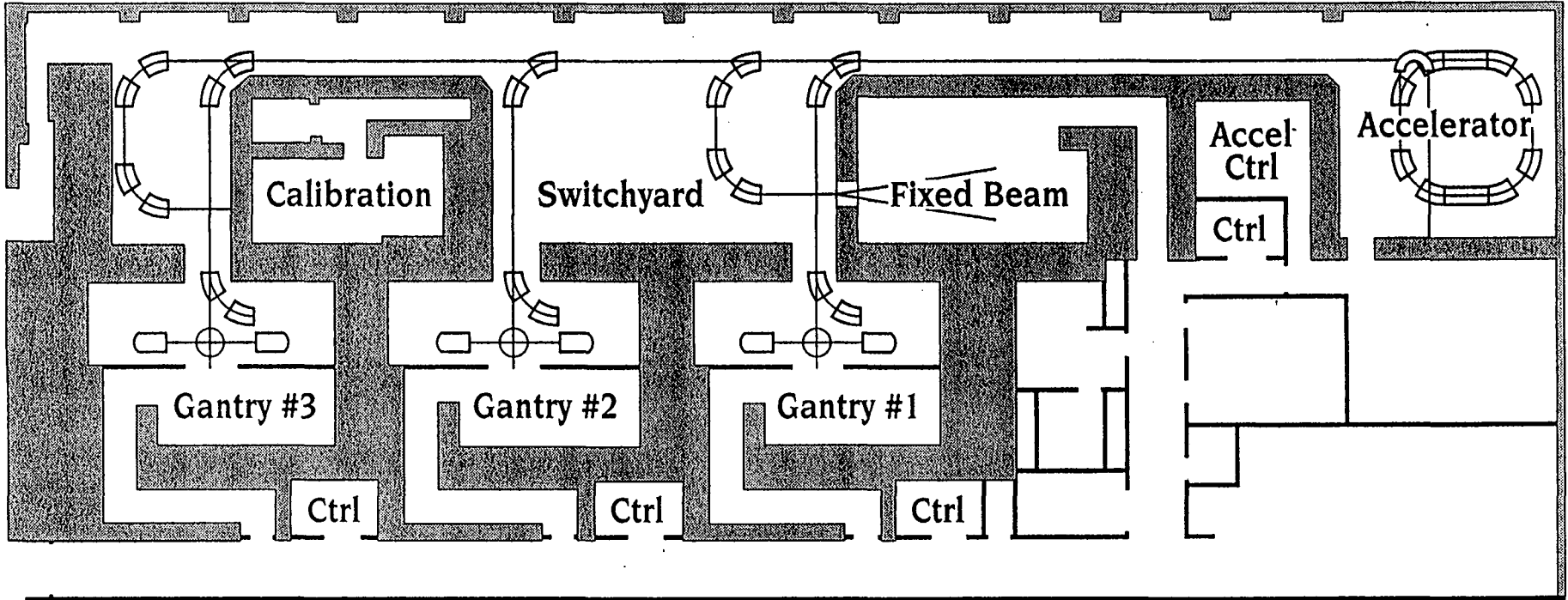
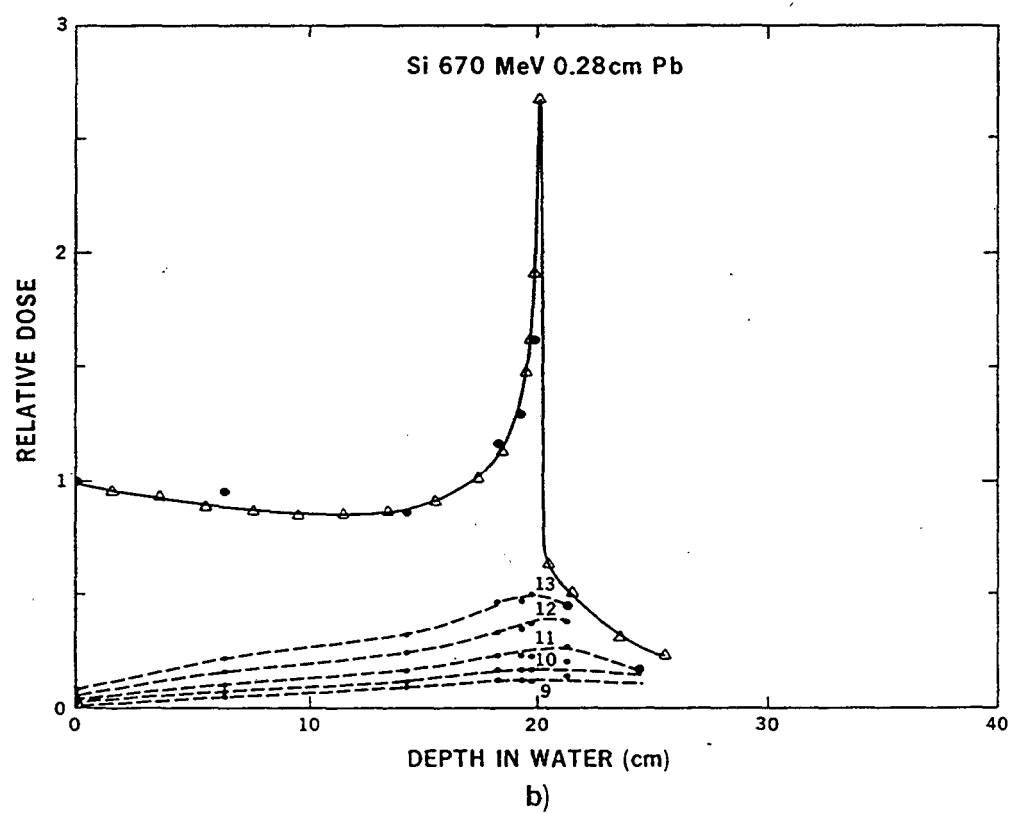
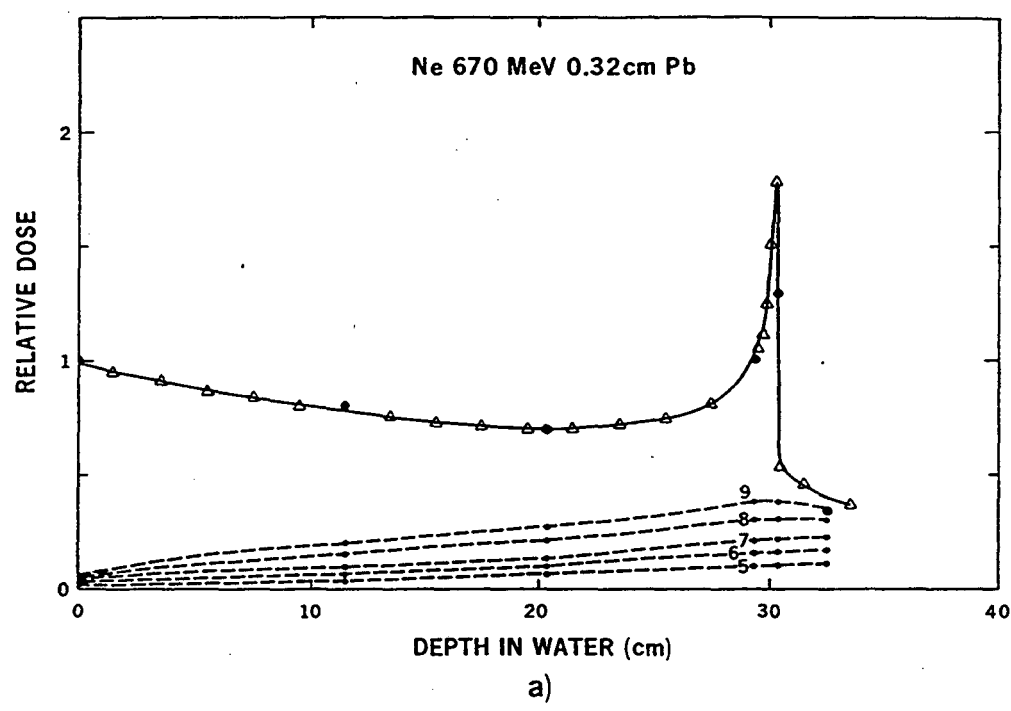


FIG. 7.10



Fig. 12  
Fig. 7-1



XBL 837-10785

FIG. 7.12

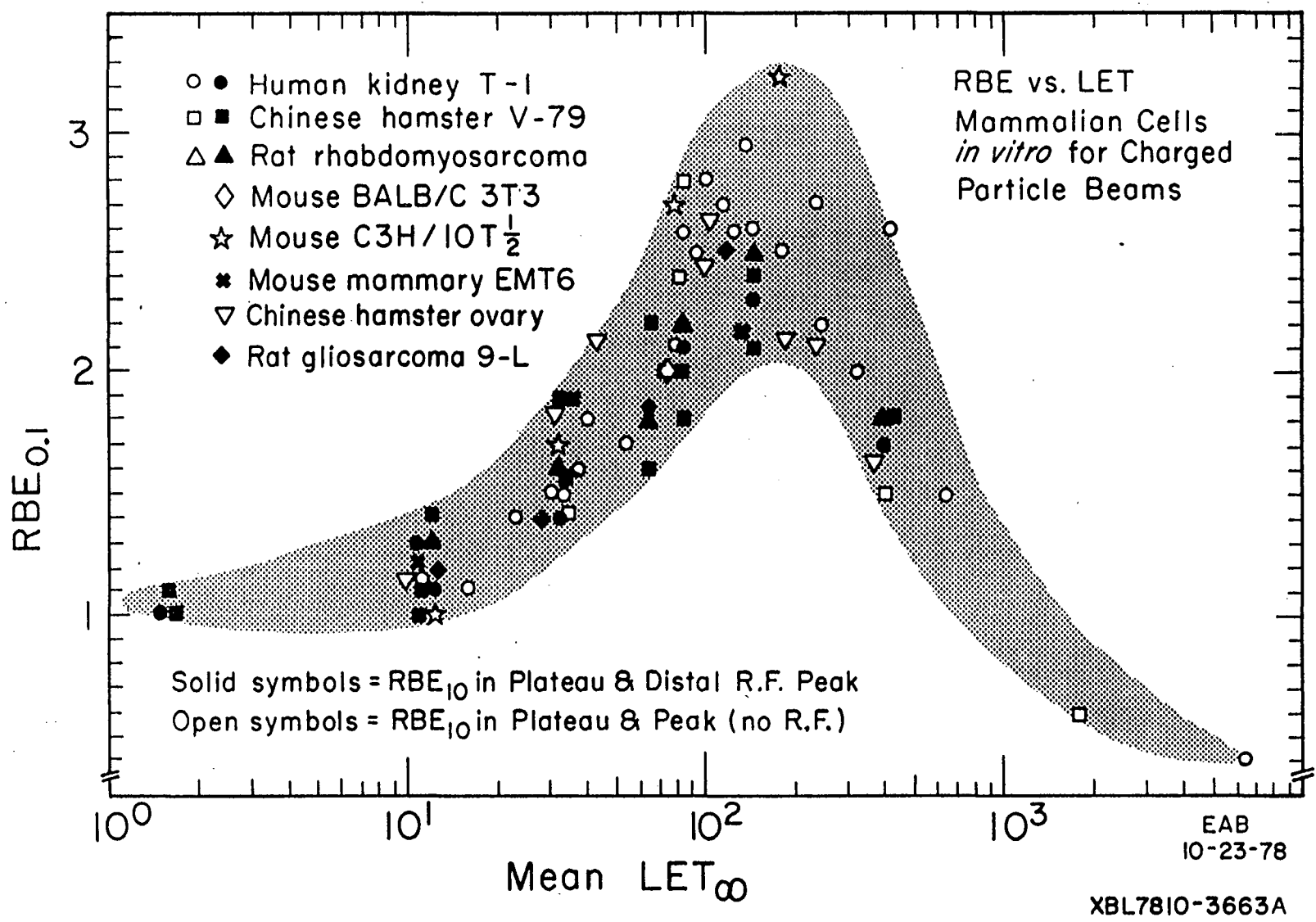


FIG. 7.13

Fig. 14  
Fig. 7-14

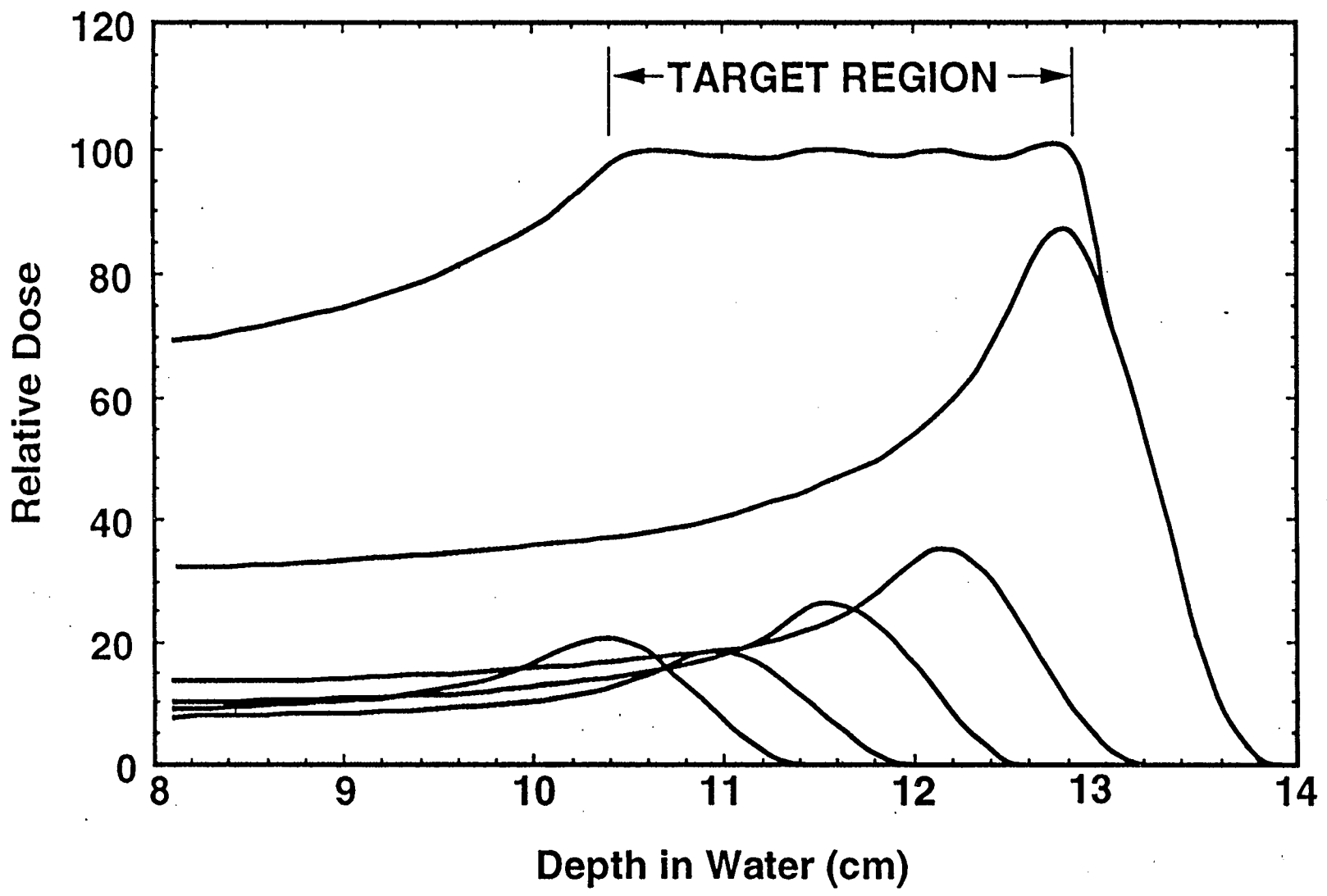


FIG. 7.14

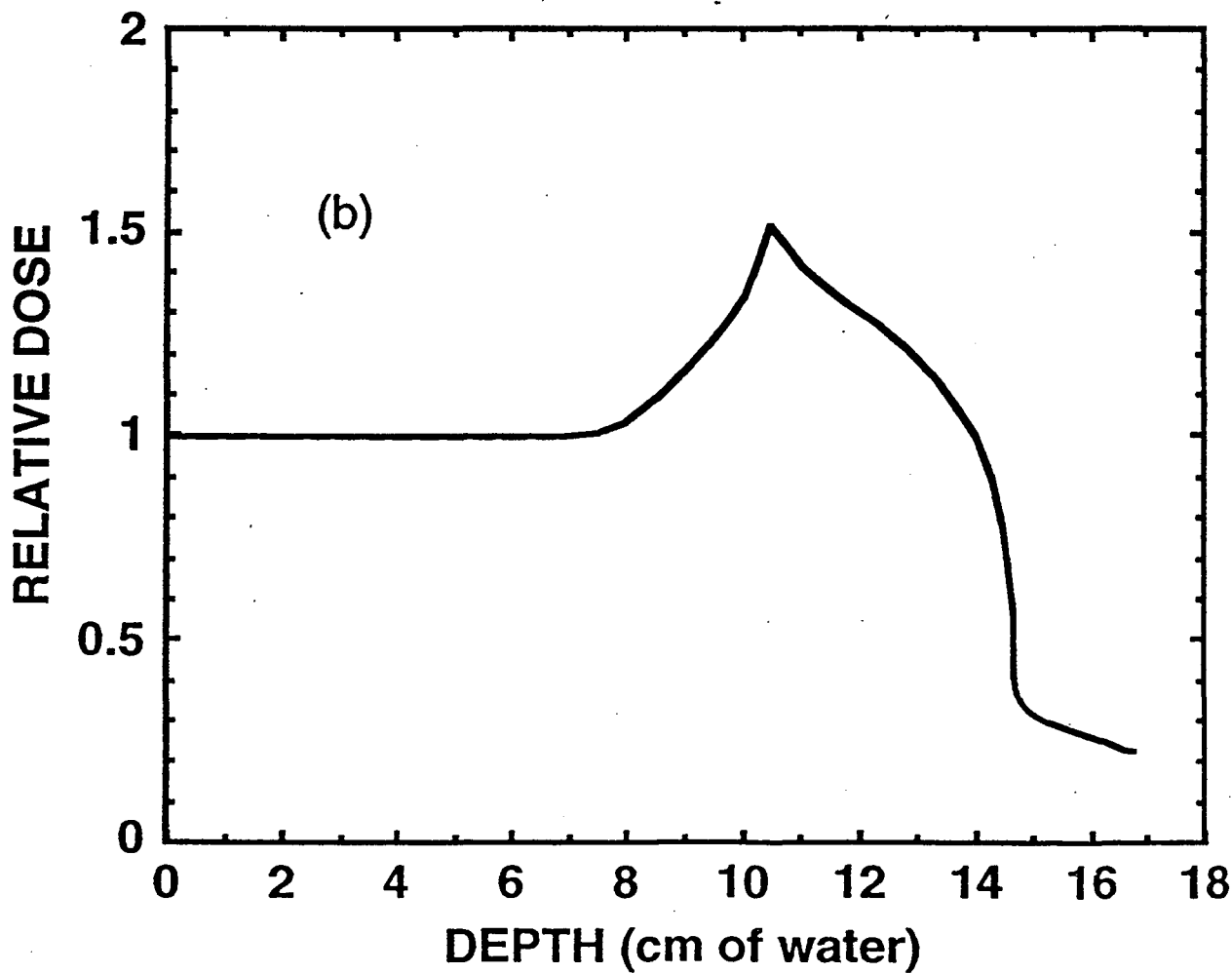
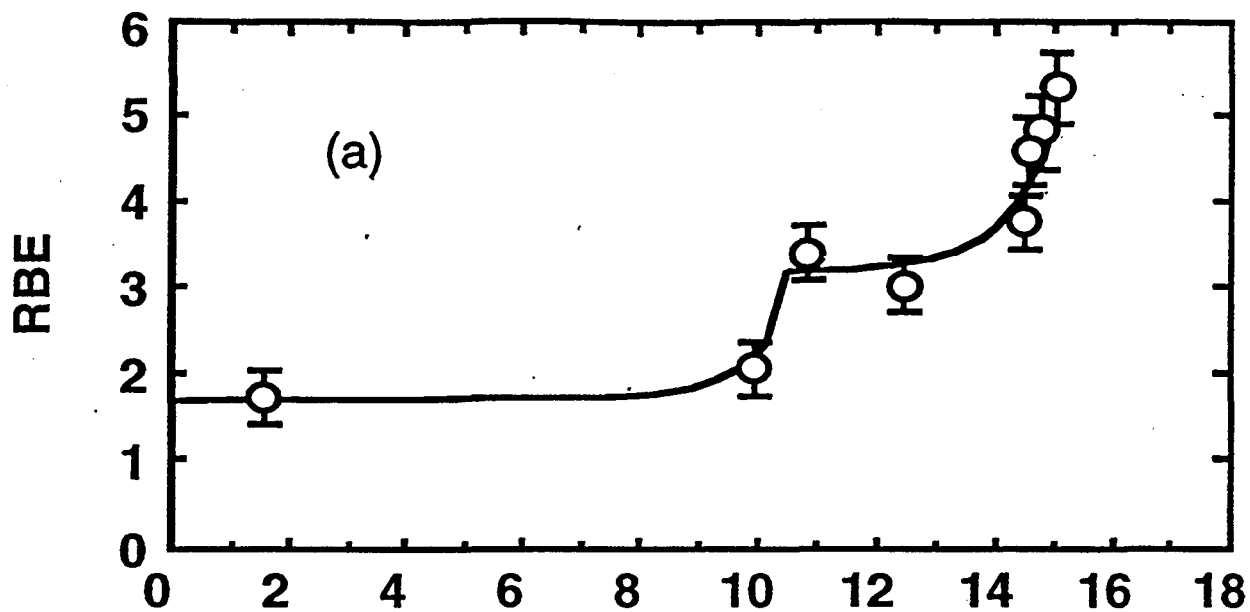
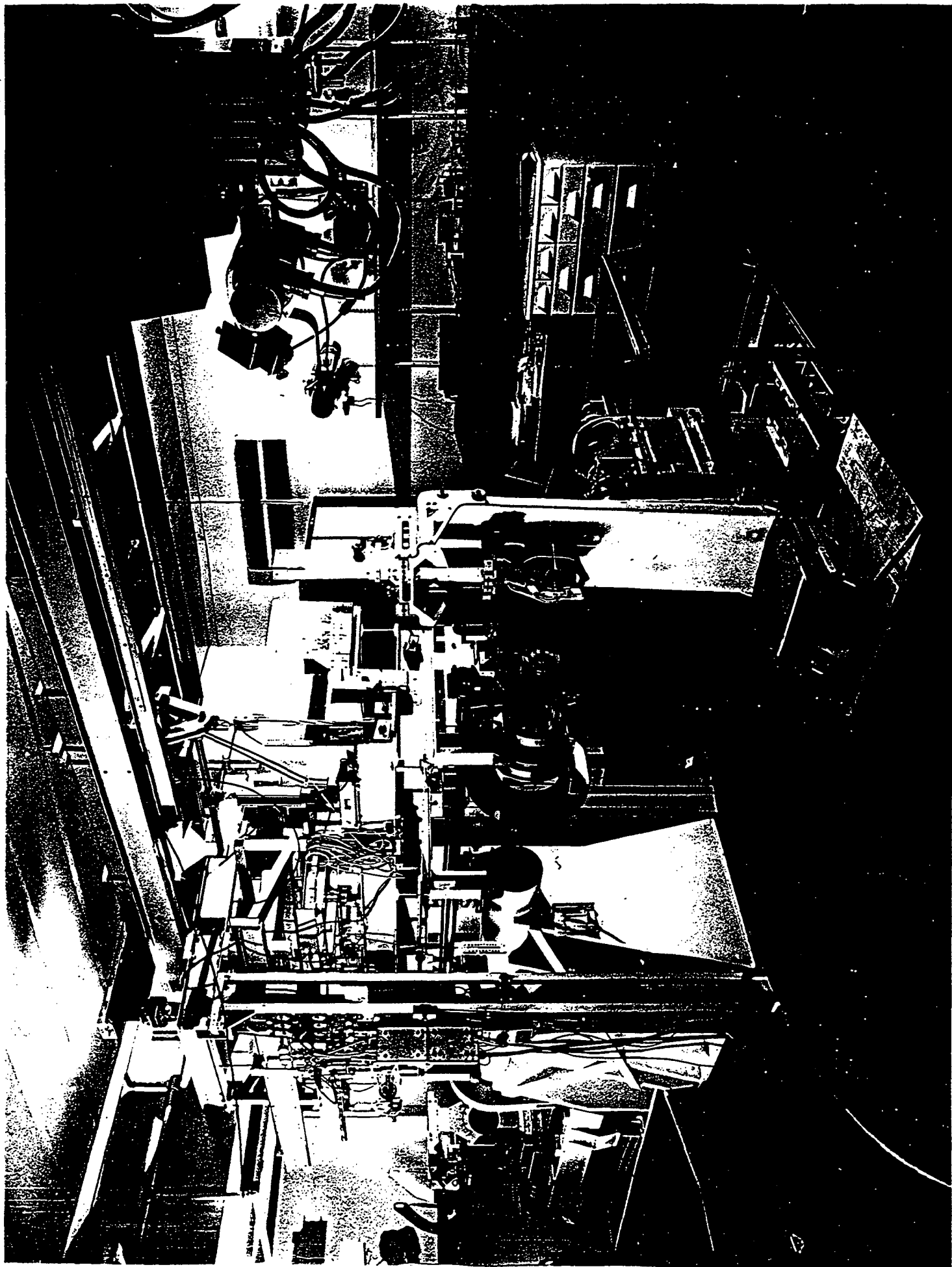


FIG. 7.15

Fig. 1-16



5.6.15

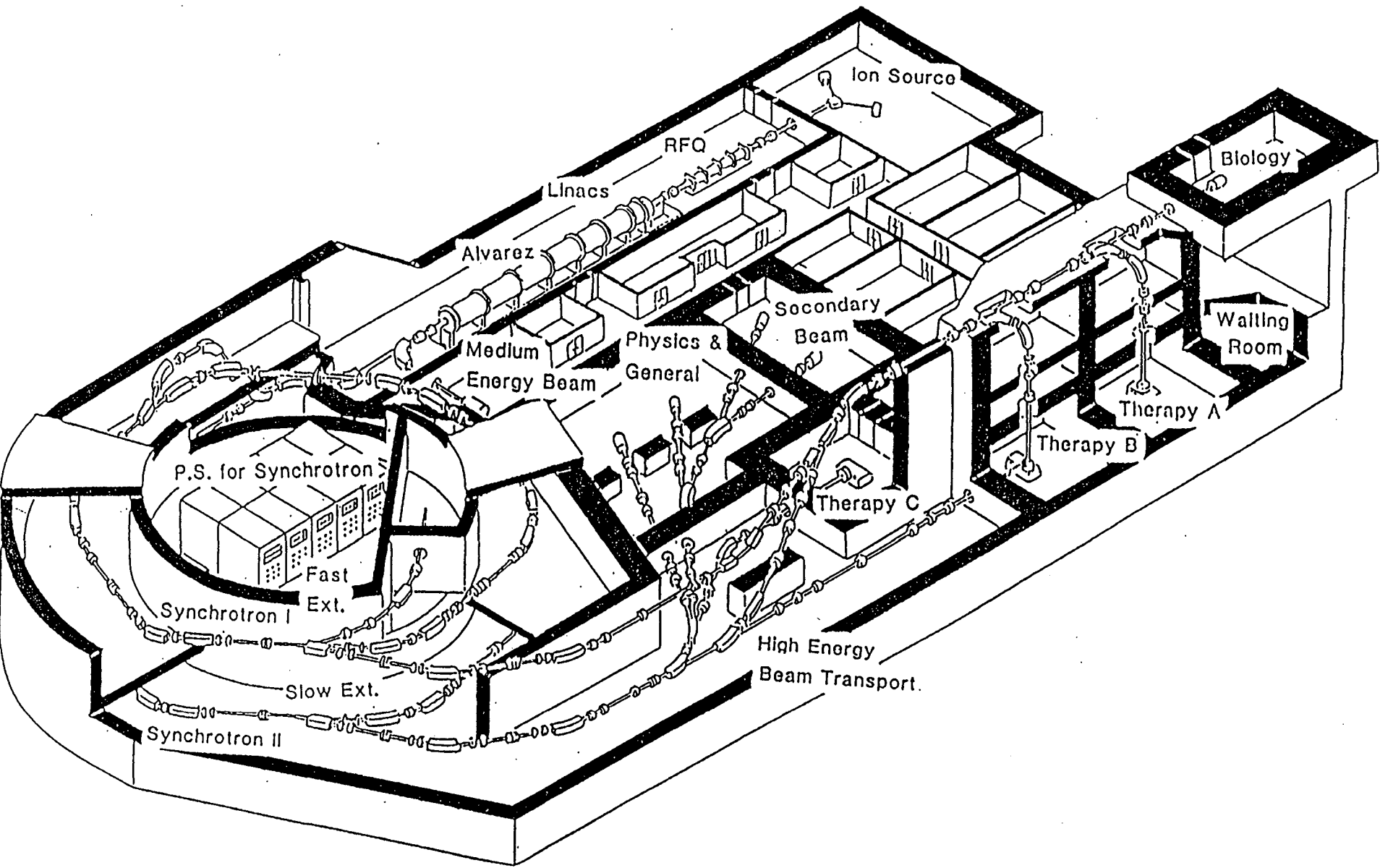


FIG. 7-17

Fig. 18  
Fig. 7-18

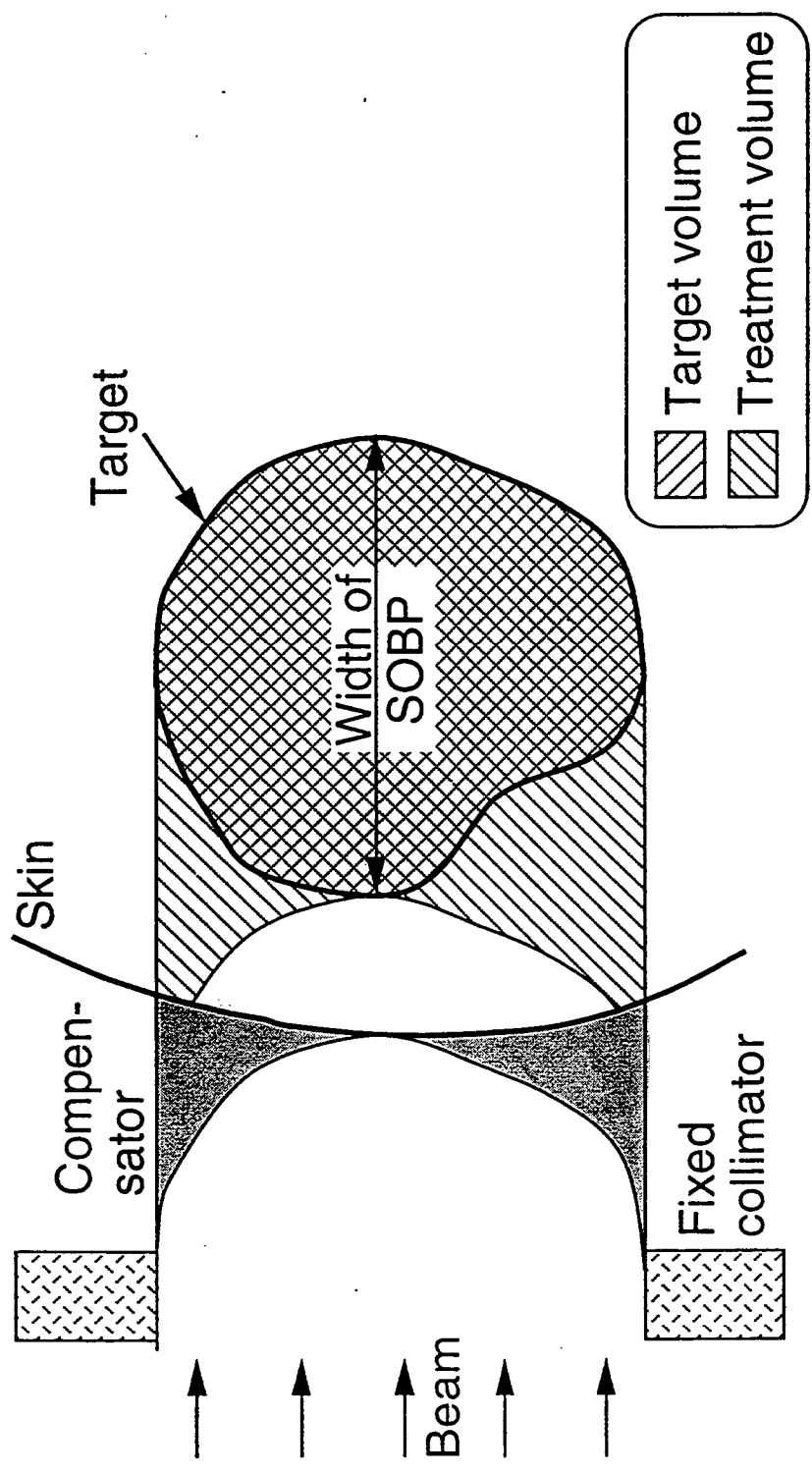


FIG. 7.18

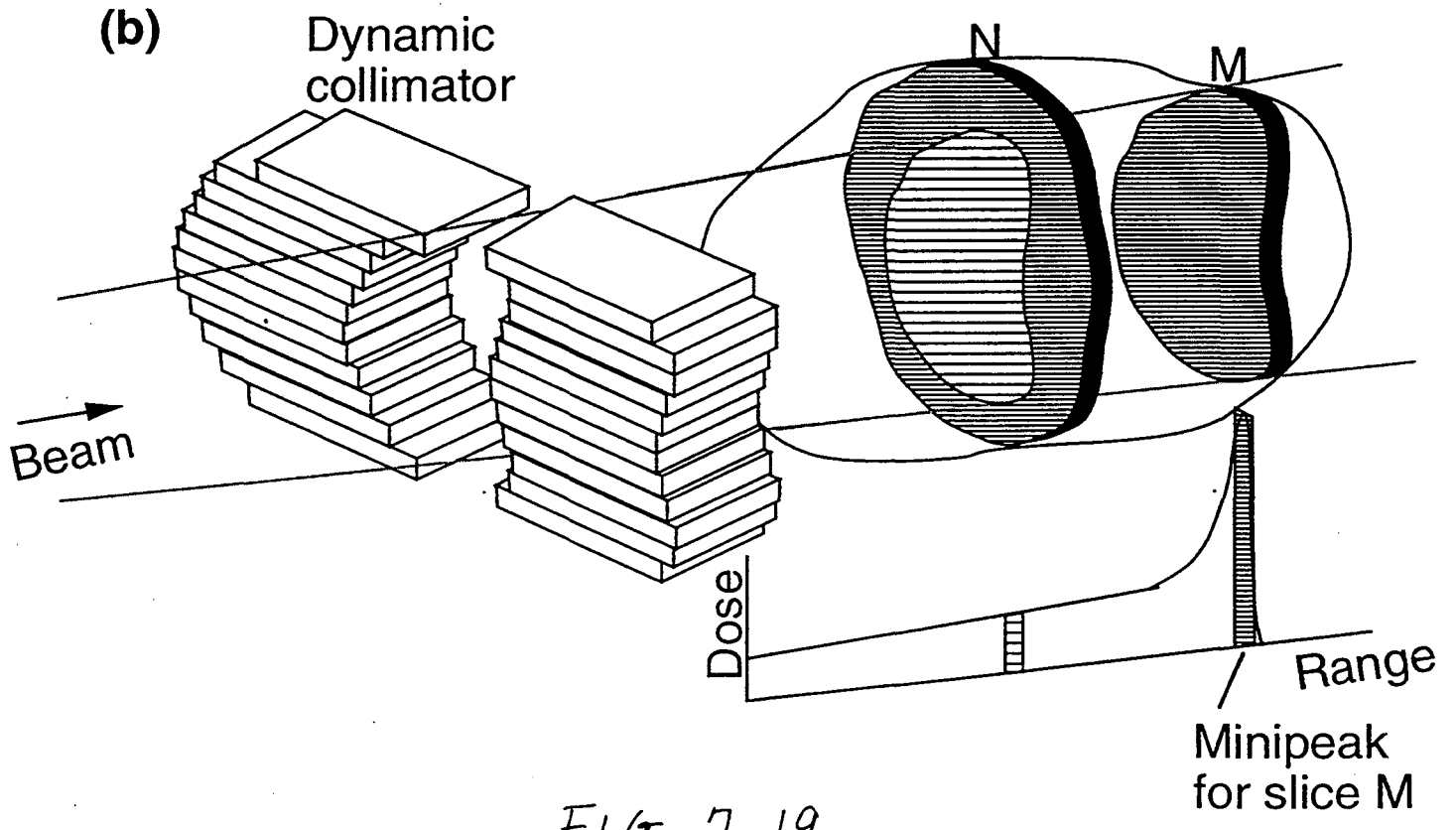
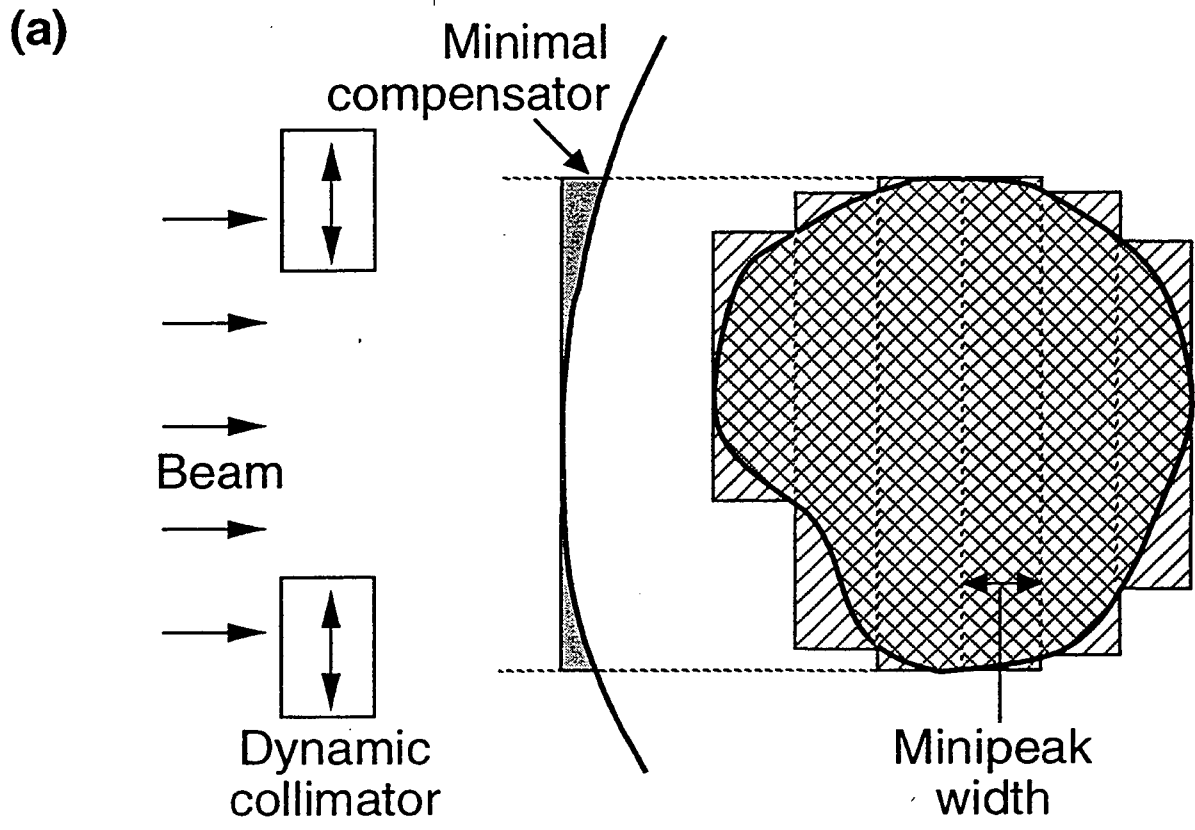


FIG. 7.19

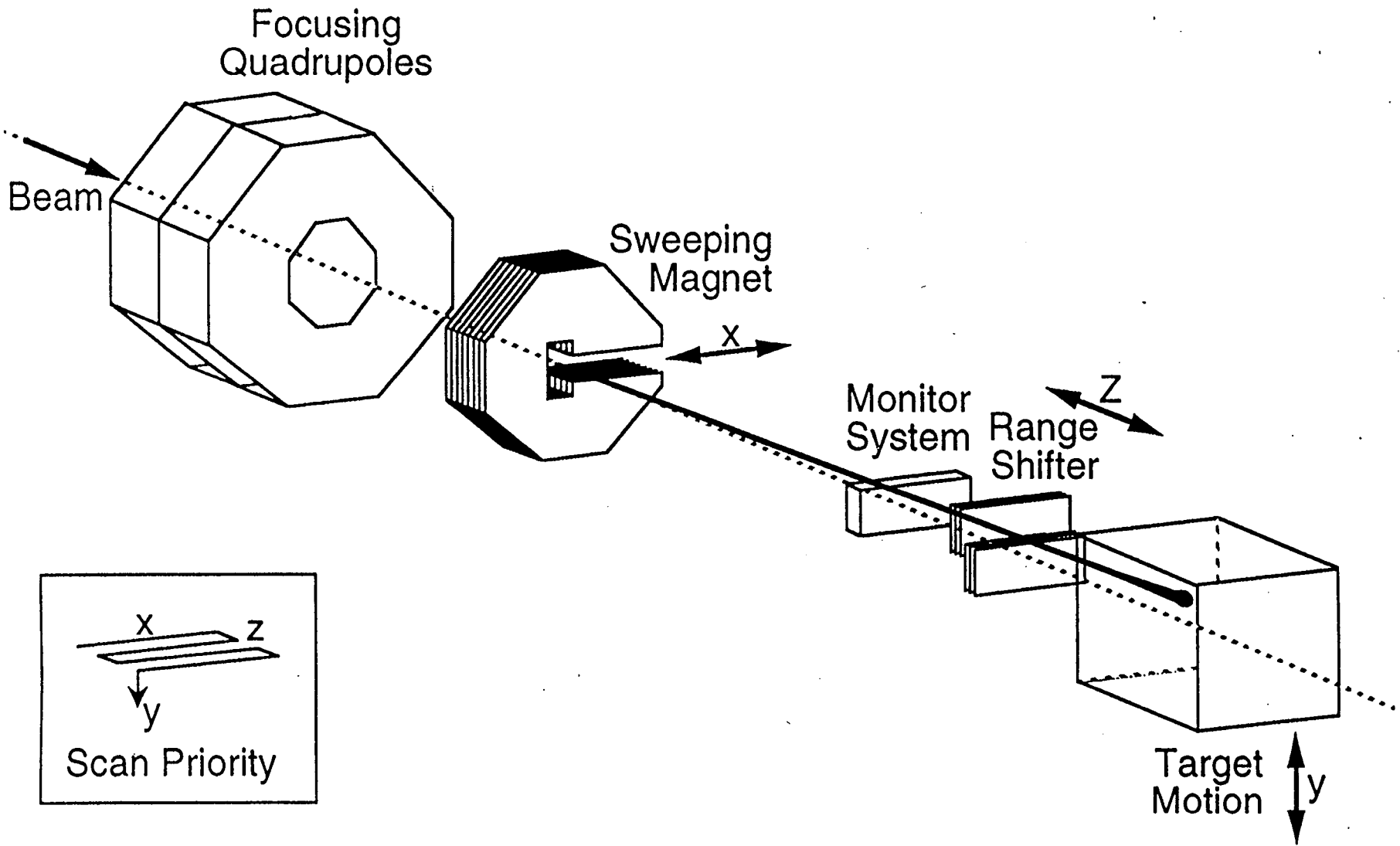


FIG. 7. 20

~~Fig. 7-21~~  
Fig. 7-21

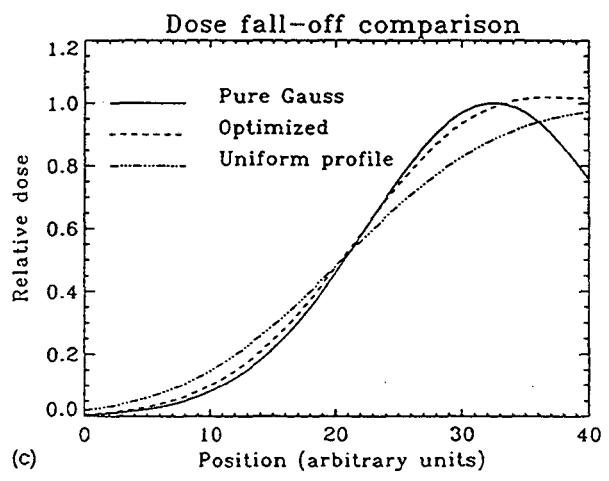
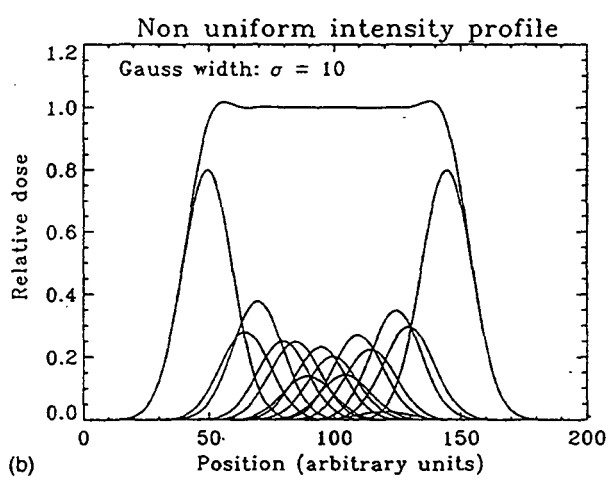
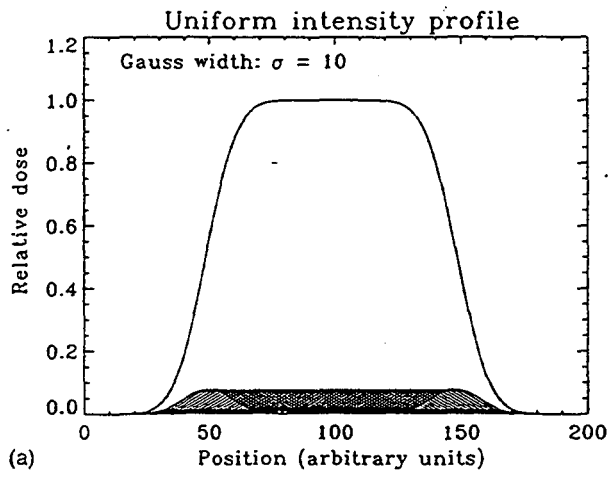


FIG. 7.21

Fig. 7.22  
Fig. 7-22

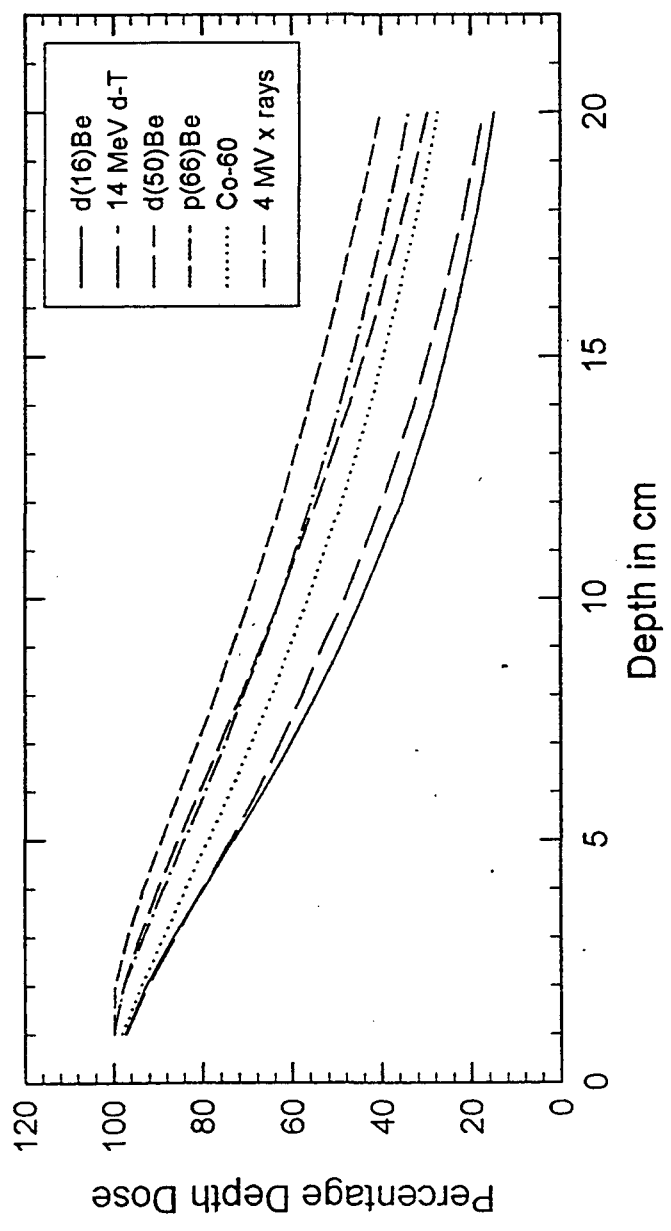


FIG. 7.22

Fig. 7-23

FIG. 23

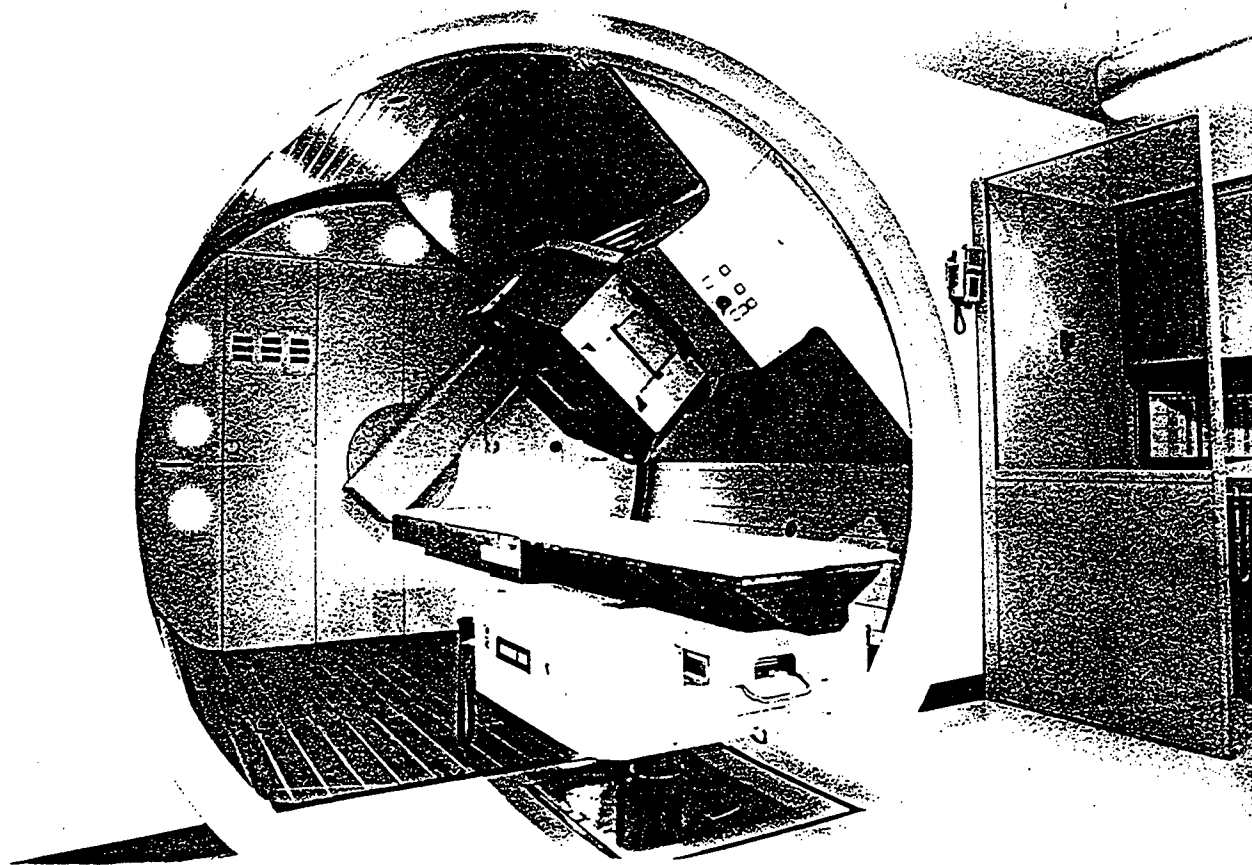


FIG. 7.23

Fig. 24  
Fig. 7-24

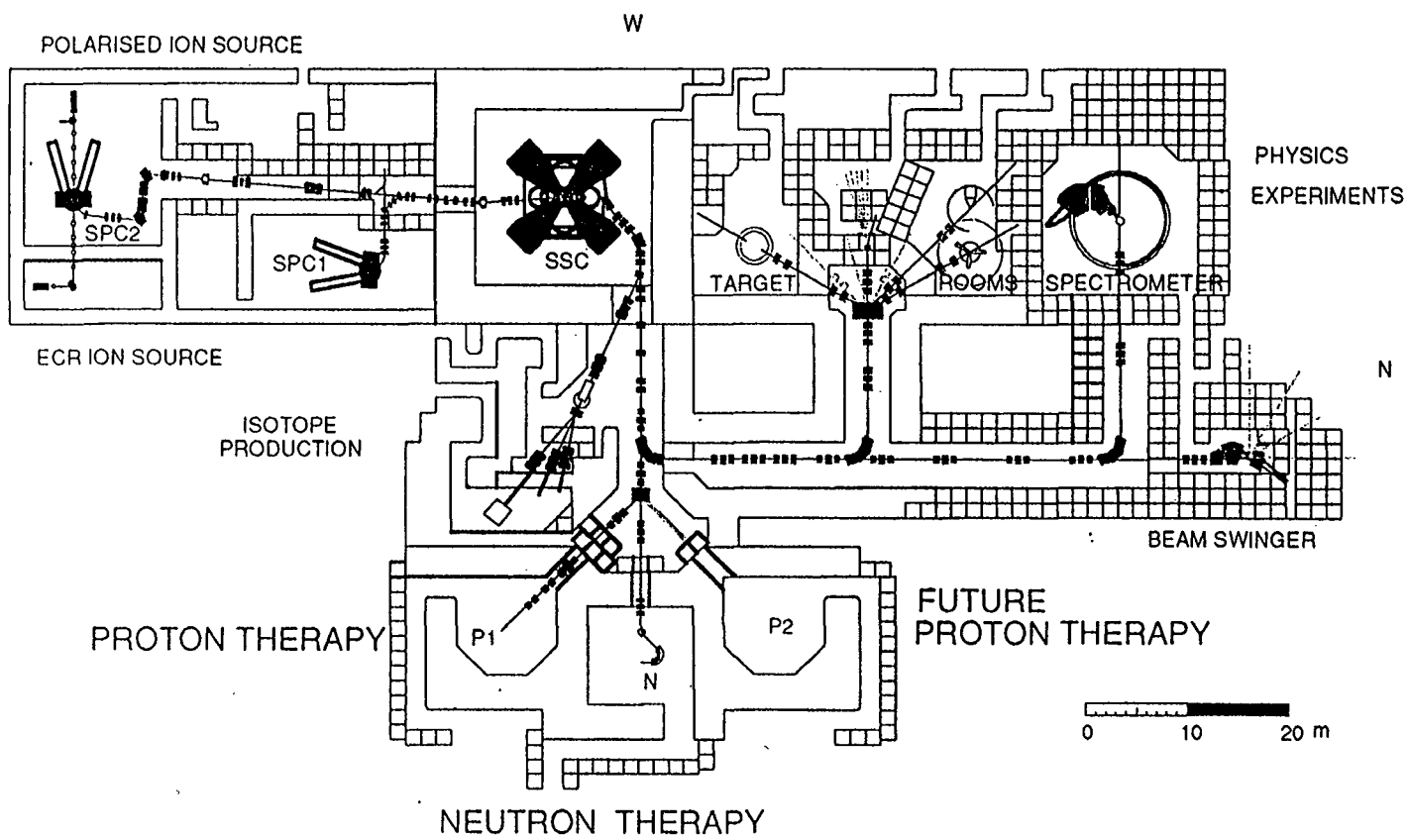


FIG. 7.24

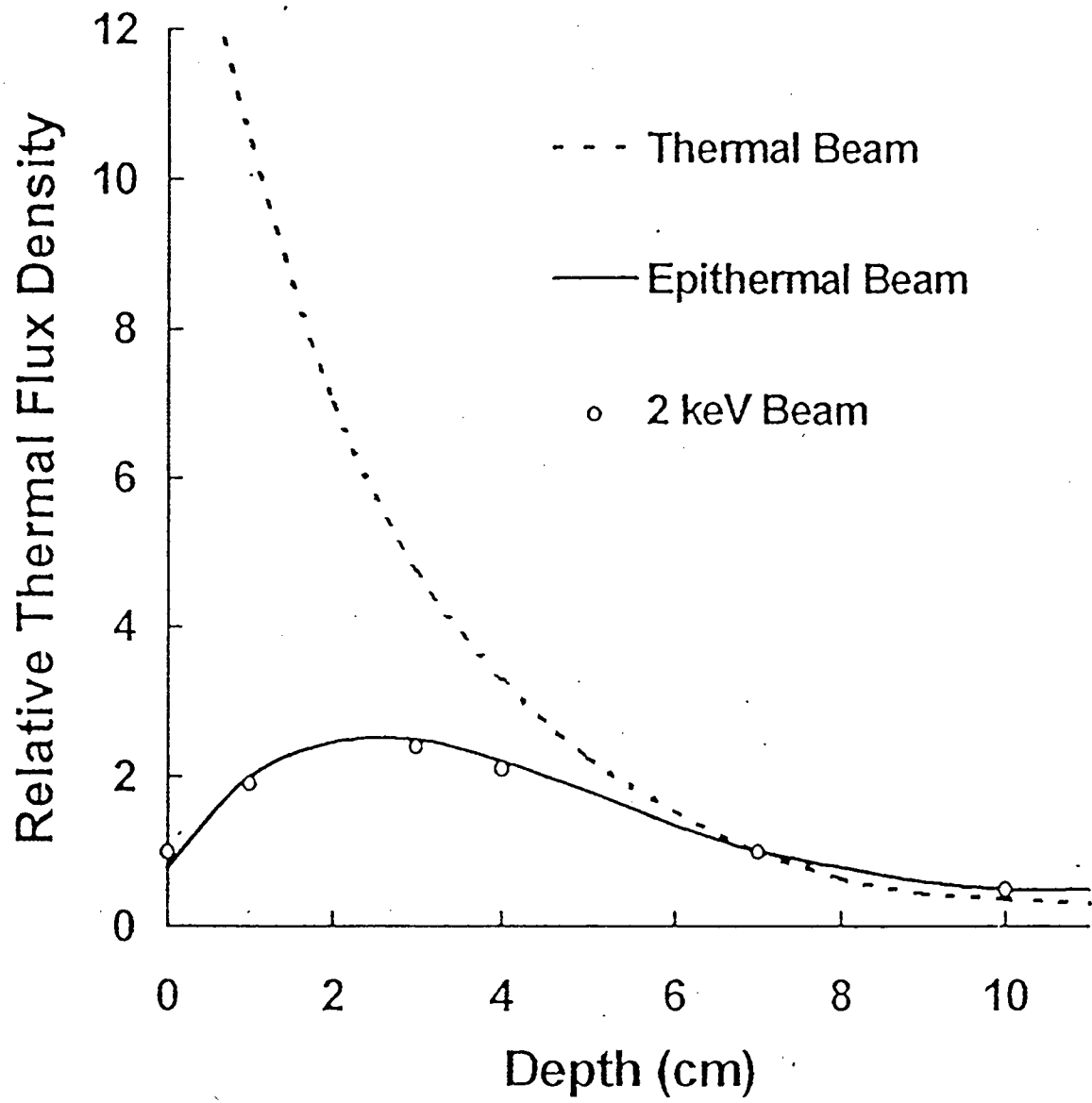


Fig. 7.25

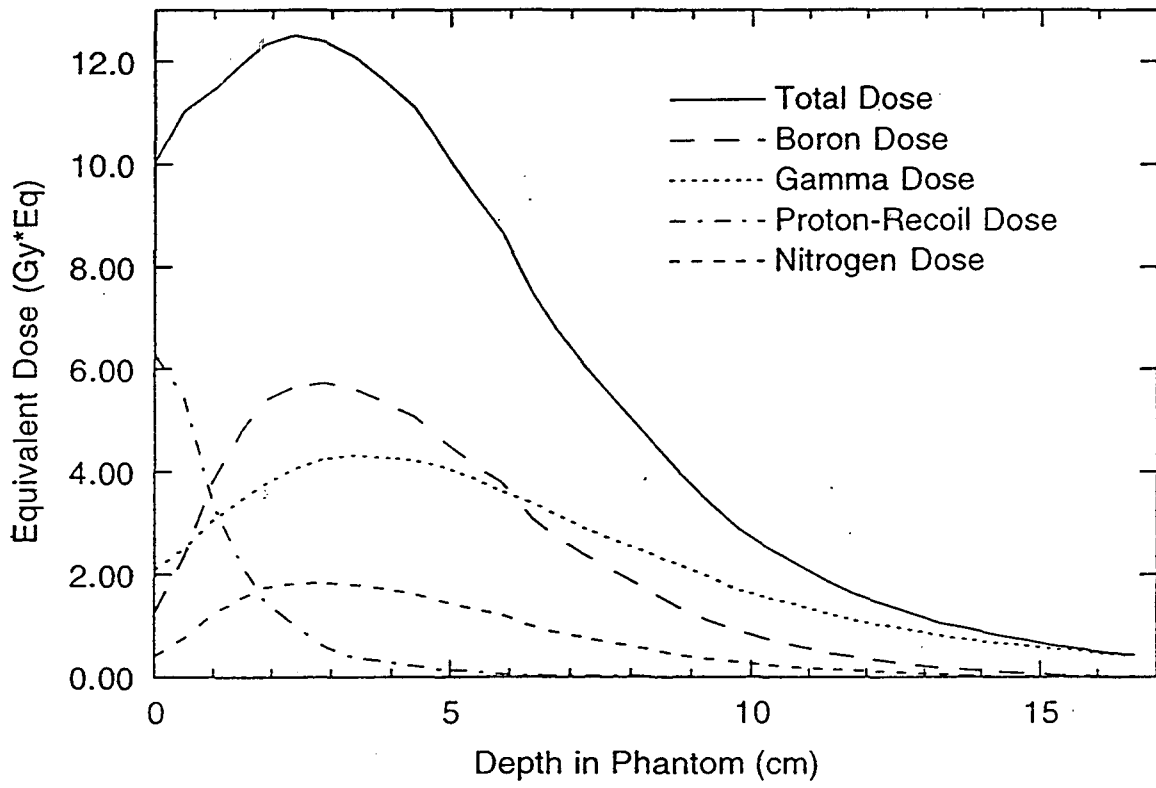


FIG. 7.26



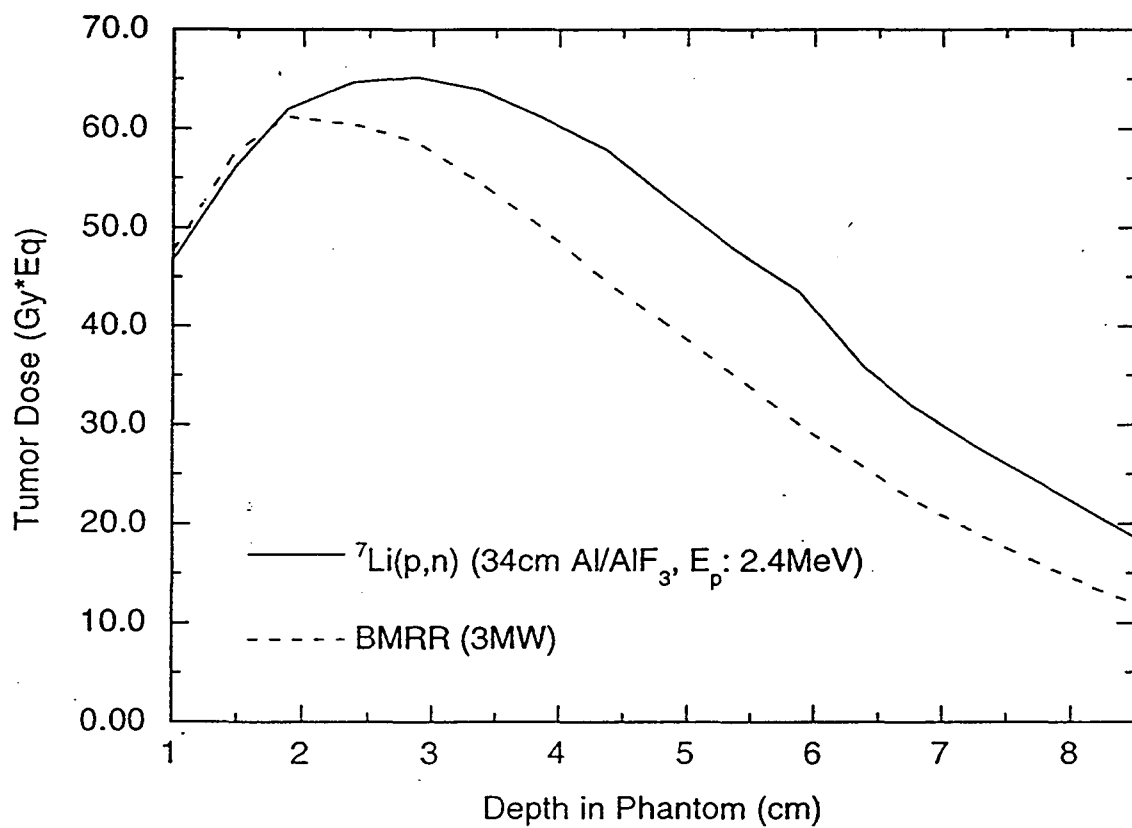


FIG. 7.28

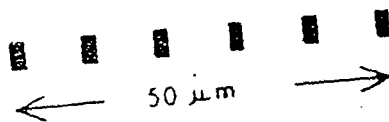


FIG. 7.30

Fig. 7-  
F

Fig. 20  
Fig. 7-29

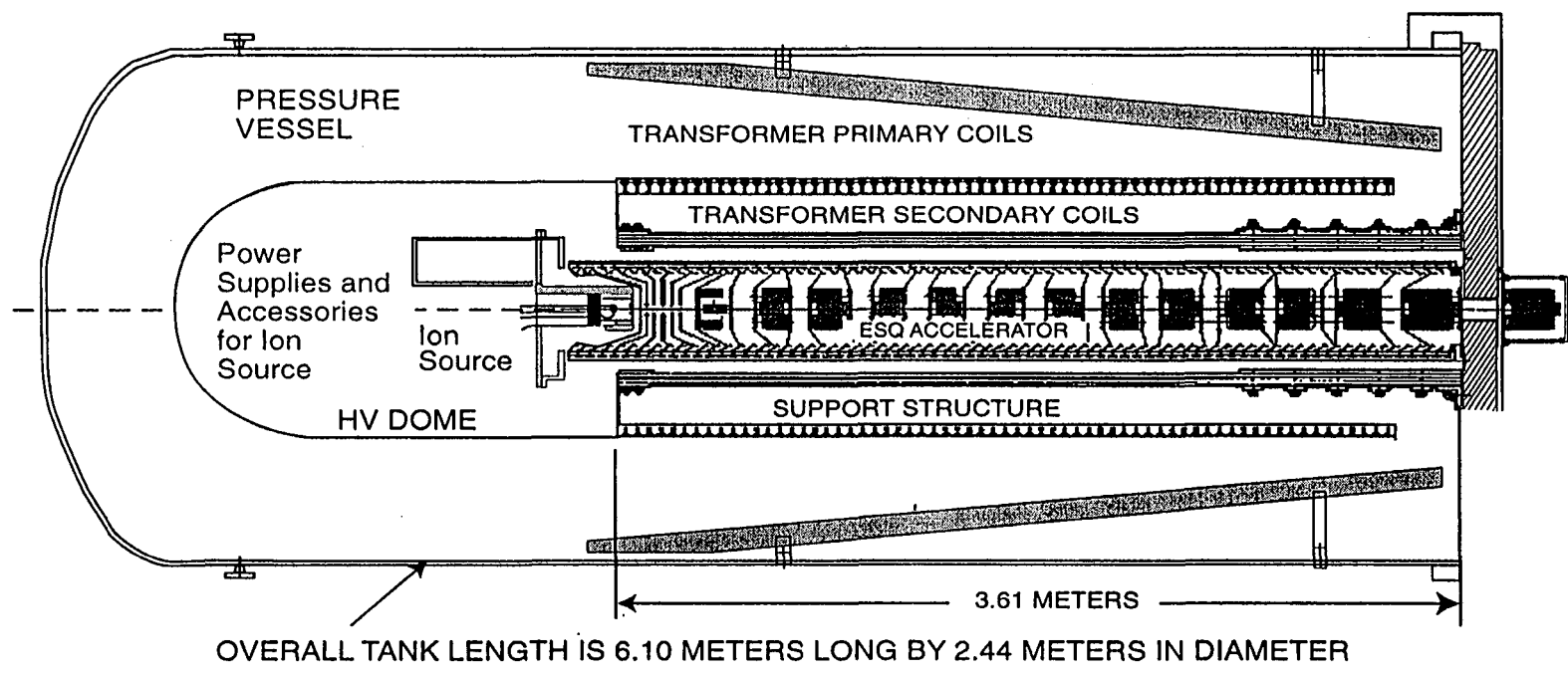


FIG. 7.29

## LIST OF CAPTIONS FOR TABLES

**Table 7.1** Clinical trials using proton beams at accelerators originally built for physics research (1997)

(Based on data supplied by Janet Sisterson, Harvard Cyclotron Laboratory, Cambridge, MA 02138 (sisterson@huhepl.harvard.edu).)

**Table 7.2** Fast Neutron Radiotherapy Centers (1997)

For brevity, the production of fast neutrons by 50 MeV protons on a Be target, for example, is abbreviated as p(50)Be. The year of the first patient treated is also shown for each location.

**Table 7.3** Concentration of  $^{10}\text{B}$  in tumor, tumor/normal tissue ratio, and tumor/blood ratio for BSH and BPA compounds

**Table 7.4** Relative abundance of normal elements in tissue and their neutron capture cross sections

The numbers of nuclear captures of thermal neutrons per cell are calculated assuming a thermal neutron fluence of  $\phi_{\text{th}} \approx 4.56 \times 10^{12}$  neutrons/cm<sup>2</sup> and a human glioma cell with a mass,  $m \approx 2.15 \times 10^{-9}$  g. The  $^{10}\text{B}$  data, for a concentration of 45.5  $\mu\text{g/g}$ , are shown in the last row for comparison.

**Table 7.5** Beam characteristics of reactor neutron sources for BNCT (1997)

(Based on Ref. 93.)

**Table 7.6** Comparison of accelerator-produced epithermal neutron beams and a reactor-produced epithermal neutron beam

Equivalent tumor doses and thermal fluences are given at the depth of maximum thermal fluence, 5 cm and 8 cm. The data for BMRR are used for the reactor-produced neutrons. The treatment time for all sources is 40 min.

**Table 7.7** Calculated multiplicity and energy partition from  $\pi^-$  capture in  $^{16}\text{O}$   
(Based on data in Ref. 112.)

Table 7.1

Facility, Location	Proton beam energy (otherwise specified)	Years of treatments	Number of patients treated (Report date)
Lawrence Berkeley National Laboratory, Berkeley, California, U.S.A.	184-inch synchrocyclotron	1954-1957	30
Lawrence Berkeley National Laboratory, Berkeley, California, U.S.A.	184-inch synchrocyclotron 934-MeV He ion	1957-1992	2054
Gustaf Werner Institute, Uppsala, Sweden	230-cm synchrocyclotron	1957-1976	73
Harvard Cyclotron Laboratory (HCL), Cambridge, Massachusetts, U.S.A.	160-MeV cyclotron	1961-	7181 (6/97)
Joint Institute of Nuclear Research (JINR), Dubna, Russia	680-MeV cyclotron	1967-1974 1987-	84 40 (11/96)
Institute of Theoretical and Experimental Physics (ITEP), Moscow, Russia	70 - 200 MeV synchrotron	1969-	2838 (5/96)
B. P. Konstantinov Inst. of Nuclear Physics in Gatchina, near St. Petersburg, Russia	1000-MeV synchrocyclotron	1975-	969 (12/95)
National Institute of Radiological Sciences (NIRS), Chiba, Japan	70-90 MeV cyclotron	1979 and 1991-	96 (10/96)
Proton Medical Research Center (PARC), University of Tsukuba, Japan	250-MeV from the booster synchrotron at KEK	1983-1993	525
Paul Scherrer Institute (PSI), Villigen, Switzerland	72 MeV 200 MeV cyclotron	1984- 1996-	2324 (6/97) 1 (12/96)
Theodore Svedberg Laboratory, Uppsala, Sweden	200-MeV three-sector, variable-energy cyclotron	1989-	112 (4/97)
Medical Research Council Cyclotron Unit, Clatterbridge Hospital, Merseyside, UK	62.5-MeV fixed energy AVF cyclotron	1989-	764 (6/97)
University of Louvain, Louvain-la-Neuve, Belgium	85-MeV cyclotron	1991-	21 (11/93)
Centre Antoine-Lacassagne, Nice, France	63-MeV Medicyc cyclotron	1991-	636 (11/95)
Centre de Protonthérapie d'Orsay (CPO), France	200-MeV cyclotron	1991-	956 (5/97)
National Accelerator Centre, Faure, South Africa	200-MeV variable-energy sector cyclotron	1993-	191 (3/97)
Indiana University Cyclotron Facility (IUCF), Bloomington, Indiana, U.S.A.	185 - 200 MeV cyclotron	1993-	1 (12/94)
Crocker Nuclear Laboratory, University of California, Davis, California, U.S.A.	67 MeV cyclotron	1994-	127 (8/97)
TRIUMF, Vancouver, Canada	500 MeV H <sup>-</sup> cyclotron	1995-	23 (12/96)
Total number of patients treated at physics accelerators			~17,000

Table 7.2

Location	Neutron production reaction	Year started
Fermi National Accelerator Laboratory, Batavia, IL	p(66)Be	1981
Centre Hospitalier Regional, Orleans, France	p(34)Be	1981
University of Washington Medical Center, Seattle, WA	p(50)Be	1984
Korea Cancer Center Hospital, Seoul, Korea	p(50)Be	1986
National Accelerator Centre, Faure, South Africa	p(66)Be	1988
Harper-Grace Hospital, Detroit, MI	d(48)Be	1991
Centre Antoine Lacassagne, Nice, France	p(65)Be	1993
Institute for High Energy Physics, Beijing, China	p(35)Be	
National Institute of Radiological Sciences, Chiba, Japan	d(30)Be	
Virchow-Klinikum, Berlin, Germany	d(13.5)Be	

Table 7.3

	Concentrations of $^{10}\text{B}$ in tumor (ppm)	Tumor/normal tissue ratio	Tumor/blood ratio
BSH	3-20	>10	~1
BPA	15-45 and higher	2-4	3-5

Table 7.4

Nuclide	Fraction in tissue by weight	Thermal neutron capture cross section	Mean free path $\lambda$ (cm)	Number of captures per cell
H	0.1	0.332	47.2	227.9
C	0.18	0.0034	$3.8 \cdot 10^4$	0.35
N	0.03	1.82	721.6	26.77
O	0.65	$1.8 \times 10^{-4}$	$1.8 \cdot 10^5$	0.050
Na	0.0011	0.43	$5.1 \cdot 10^4$	0.14
Mg	0.0004	0.053		5.99
P	0.0116	0.18	$6.9 \cdot 10^4$	0.46
S	0.002	0.53		0.23
Cl	0.0016	32.68	$8.3 \cdot 10^3$	10.11
K	0.002	2.1		0.74
Ca	0.02	0.4		1.37
Fe	0.0001	2.57		0.032
$^{10}\text{B}$	0.0000455	3840	19.7	119.9

Table 7.5

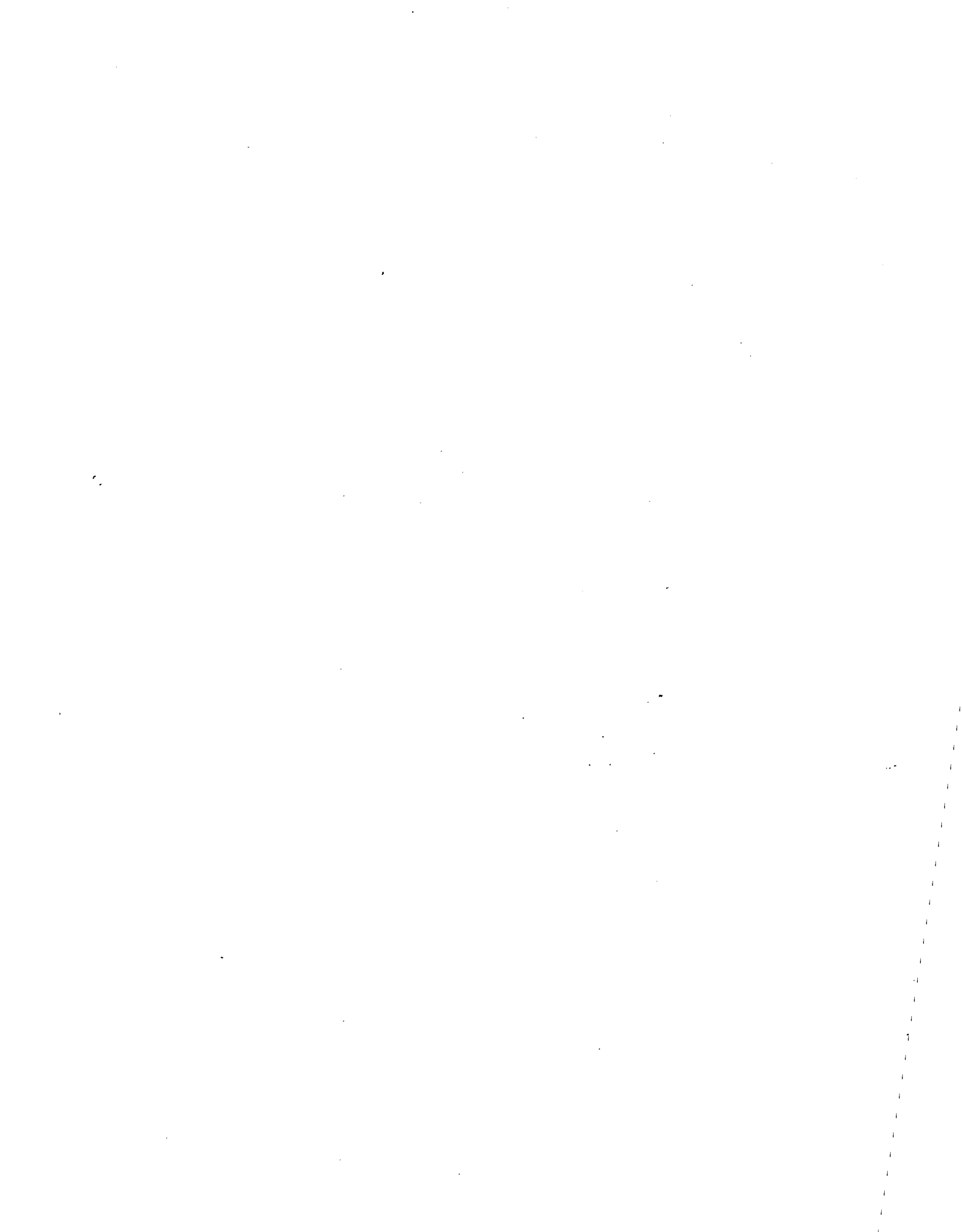
Reactor	Epithermal neutron fluence rate ( $10^9$ n/cm <sup>2</sup> ·s)	Fast neutron dose per epithermal neutron ( $10^{-13}$ Gy/n ·cm <sup>2</sup> )	Gamma dose per epithermal neutron ( $10^{-13}$ Gy/n·cm <sup>2</sup> )	Current/flux J/φ
BMRR, BNL	1.8	4.3	1.3	0.67
MITR-II, MIT	0.2	12.5	14.0	0.55
HFR, Petten	0.33	8.6	10.3	>0.8
MURR	9.5	2.9	0.4	0.82
MITR (with fission plate)	18.0	1.3	1.0	—
BMRR (with fission plate)	12.0	2.8	1.0	0.78
FiR 1 (TRIGA), Finland	3.5	2.6	1.0	—

Table 7.6

Neutron source	${}^7\text{Li}(p,n)$	${}^9\text{Be}(p,n)$	${}^9\text{Be}(p,n)$	${}^9\text{Be}(d,n)$	BMRR
Beam energy (MeV)	2.4	4.0	19	2.6	3 MW
Beam current (mA)	27	40-80	1.5 - 3	50 - 100	-
Moderator thickness (cm)	34	42	70	70	-
Eq. tumor dose (max.) (Gy-Eq)	66	61	53	54	62
Eq. tumor dose (5cm) (Gy-Eq)	51	44	38	39	39
Eq. tumor dose (8cm) (Gy-Eq)	22	20	16	16	15

Table 7.7

Particle type	Average number per $\pi^-$ capture in $^{16}\text{O}$	Kinetic energy per $\pi^-$ capture (MeV)
n	2.94	60.65
p	1.25	20.03
d	0.21	2.45
$^3\text{H}$	0.065	0.68
$^3\text{He}$	0.035	0.48
$^4\text{He}$	1.080	10.62
Heavier fragments	0.631	2.42
Excitation of nucleus		5.85



**ERNEST ORLANDO LAWRENCE BERKELEY NATIONAL LABORATORY  
ONE CYCLOTRON ROAD | BERKELEY, CALIFORNIA 94720**